Studies of Superfluid Stirling and Pulse Tube Refrigeration

by
Atsuhiko Watanabe

B.S., Engineering and Applied Science
California Institute of Technology, 1993

B.A., 3/2 Combined Degree
Occidental College, 1993

Submitted to the Department of
Mechanical Engineering in Partial Fulfillment of
the Requirements for the
Degree of

Master of Science
at the

Massachusetts Institute of Technology

June 1995

Signature of Author_____
Department of Mechanical Engineering
June 5, 1995

Certified by_____
John G. Brisson
Thesis Supervisor

Accepted by_____
Ain A. Sonin
Chairman, Department Committee on Graduate Degrees

Studies of Superfluid Stirling and Pulse Tube Refrigeration

by

Atsuhiko Watanabe

Submitted to the Department of Mechanical Engineering
on June 5, 1995
in Partial Fulfillment of the Requirements for the Degree of
Master of Science in Mechanical Engineering.

ABSTRACT

There is a niche for a sub-Kelvin cryogenic refrigeration unit that is simple, efficient, and does not require gravity. The superfluid Stirling refrigerator was developed in response to this demand. The refrigerator has cooled to 168 mK while exhausting heat at 383 mK, demonstrating the potential to cool to temperatures well below that attainable with a continuous ^{3}He evaporation refrigerator. The refrigerator has also been successfully operated with mixtures of up to 36% ^{3}He concentration with proportionately higher cooling powers, though we suspect that the flow exceeding the critical velocity poses a lower limit on the temperature attainable with high concentration mixtures. Superfluid pulse tube version of the refrigerator has been successfully operated, though the efficiency is found to be significantly lower than that of the Stirling refrigerator. Gravitational convection of fluid in the pulse tube necessitates the pulses be oriented cold side up, contrary to convention in cryostats. The gravity and the temperature gradient in the pulse tube dramatically thin down the viscous penetration depth, resulting in a slug flow in the pulse tube and hence making this an essentially ideal pulse tube.

Thesis Supervisor: John G. Brisson
Title: Assistant Professor of Mechanical Engineering

ACKNOWLEDGMENTS

This research has been supported by the Division of Materials Science in the U.S. Department of Energy's Office of Basic Energy Sciences.

I wish to thank professor John G. Brisson whose dedication has made possible my research in Los Alamos National Laboratory. He spent countless hours walking me through the experiment, and truly went above and beyond his duties.

I am also greatly indebted to Greg W. Swift of Los Alamos National Laboratory who provided a stimulating environment in which to carry out this research and whose guidance and support was essential to my practical and theoretical education. I would also like to thank Chris Espinoza, Kevin Graham, Tim Pierce, and Roy Rockage for their technical support and advice.

Finally, I would like to thank my friends and family who encouraged me throughout this project. I wouldn't have been able to finish this project without their patience and support.

Table of Contents

List of Figures

List of Tables

List of Symbols

A	Area
c	Mass fraction
C	Specific heat
C_p	Specific heat at constant pressure
C_v	Specific heat at constant volume
D	Diameter
f	Frequency, body force
g	Degeneracy, gravity
h	Enthalpy per mole, length scale
H	Enthalpy
I	Current
k	Boltzmann's gas constant
L	Latent heat, length
m	mass
M	Molecular mass
n	Number of moles
p	Pressure
P	Power
Q	Heat transfer, volume flow rate
Q_C	Heat absorbed by the fluid in the cold piston per cycle
r	Spatial variable
R	Universal gas constant, gas constant per mass, resistance, Rayleigh number
R_o	Resistive flow impedance of the orifice
t	Tube wall thickness, time
T	Temperature
T_C	Cold platform temperature
T_H	Hot platform temperature
u	Velocity
U	Internal energy
v	Molar volume, velocity
V	Volume, voltage
V_0	Time average of hot and cold piston volumes
V_r	Regenerator volume
W	Work transfer\

W_C Work done by the fluid on the cold piston per cycle

x Spatial variable

X Mole fraction

y Spatial variable

z Fugacity, spatial variable

Z Geometric factor for a flow impedance

β Thermal expansion coefficient

ε_s Ratio of specific heats

ϕ Phase

γ Ratio of specific heats

κ Isothermal compressibility, thermal conductivity

μ Viscosity

θ Temperature difference

ρ Mass density, molar density

σ Viscous shear stress

τ Period

ω Frequency

Chapter 1

Introduction

There is a niche for a sub-Kelvin cryogenic refrigeration unit that is simple, efficient, and does not require gravity. The superfluid Stirling refrigerator was developed in response to this demand. Kotsubo and Swift[9,10] built and successfully operated the first SSR in 1990, proving the feasibility of a sub-Kelvin Stirling refrigerator with a ^{3}He-^{4}He liquid mixture as a working fluid. Brisson and Swift[1-4] built the second generation SSR in 1992 that achieved a significantly lower temperature. However, the ultimate performance of the SSR will be limited by the thermodynamics of the ^{3}He solute as it approaches complete Fermi degeneracy below the Fermi temperature. These considerations led us to undertake the work presented here, to investigate the SSR's performance in the Fermi regime. We also explored the SSR's performance using mixtures of higher concentrations than in the previous SSR's in an effort to increase the SSR's cooling power proportionately. Pulse tube version of the refrigerator attempts to reduce the complexity by eliminating one of the two pistons of the Stirling cycle.

1.1 The Superfluid Stirling Refrigerator (SSR)

The need for cryogenic cooling in satellite applications has brought about a strong requirement for efficient and reliable refrigeration units. There are currently several techniques for cooling below 1 K. The ^{3}He-^{4}He dilution refrigerator utilizes the endothermic heat of mixing of ^{3}He into ^{4}He to reach temperatures below 10 mK. However, the dilution refrigerator typically has a power consumption rate of kilowatts, and relies on gravity to phase separate the less dense ^{3}He phase over the ^{3}He-^{4}He phase. The continuous ^{3}He evaporation refrigerator has the advantage of being relatively simple,

but can only reach a minimum temperature of around 0.3 K. It also consumes around a kilowatt of power and relies on gravity to maintain the free surface between the liquid phase and the gaseous phase. Adiabatic demagnetization of a paramagnetic salt often requires magnetic shielding between the refrigerator and the object to be cooled. In short, there is a niche for a low energy consumption cryogenic refrigeration unit that outperforms the ^{3}He evaporation refrigerator and does not require gravity or magnetic shielding. The superfluid Stirling refrigerator (SSR) was developed in response to this demand.

Kotsubo and Swift[9,10] built the first SSR in 1990 that cooled to 0.6 K with the heat rejected at 1.2 K, proving the feasibility of a sub-Kelvin Stirling refrigerator with a ^{3}He-^{4}He liquid mixture as a working fluid. Brisson and Swift[1-4] built the second generation SSR in 1992 that cooled to 0.3 K with the heat rejected also at 1.2 K, demonstrating the SSR's potential to outperform the continuous ^{3}He evaporation refrigerator. However, the ultimate performance of the SSR will be limited by the thermodynamics of the ^{3}He solute as it approaches complete Fermi degeneracy below the Fermi temperature. For example, in a 6% solution, a model based on an ideal Fermi gas suggests that the cooling power is about half that of a classical ideal gas refrigerator at 0.2 K and rapidly drops to zero at lower temperatures.

These considerations led us to undertake the work presented here, to investigate the SSR's performance in the Fermi regime. We also explored the SSR's performance using mixtures of higher concentrations than in the previous SSR's in an effort to increase the SSR's cooling power proportionately.

A schematic diagram of the four processes of a Stirling refrigerator is shown in Fig. 1.1. Two pistons, one at high temperature T_H and the other at low temperature T_C, are connected by an array of high heat capacity capillary tubes, the regenerator. We assume here that the working fluid is an ideal gas, that the piston clearance volumes and regenerator volumes are negligible, and that the regenerator has a linear temperature profile from one end to the other with negligible streamwise thermal conduction. Initially, the working fluid is entirely contained by the hot piston, as shown in Fig. 1.1(a). The refrigerator then goes through the following cycle, where (a)-(d) refer also to Fig. 1.2.

(a) The hot piston isothermally compresses the fluid. Conservation of energy for a closed system implies

$$dU = dQ - dW \tag{1.1.1}$$

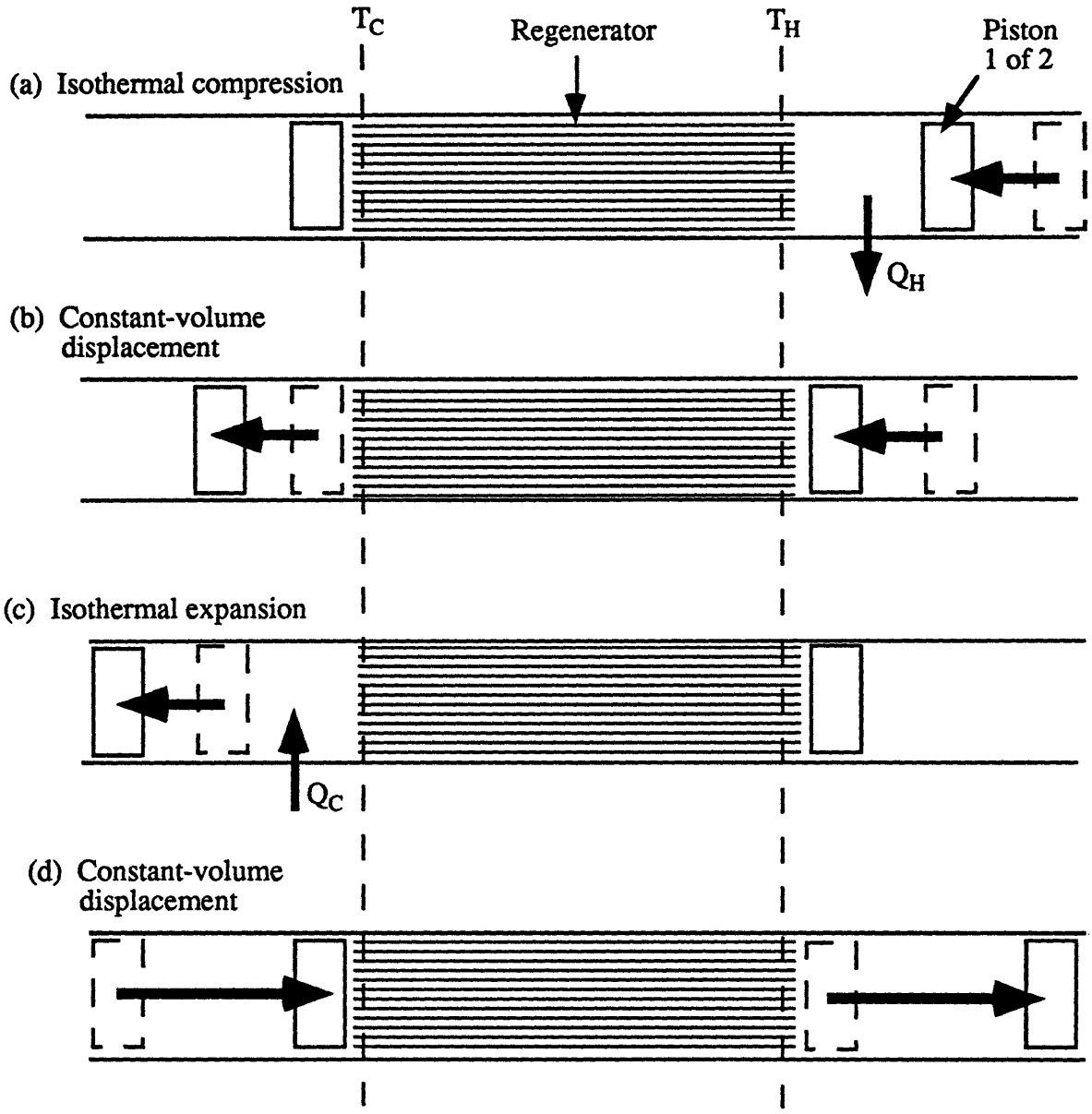

Figure 1.1. Four steps of a Stirling cycle refrigerator.

where U is the internal energy of the fluid, Q is the heat added to the fluid, and W is the work done by the fluid. Since dU = 0 for an isothermal process of an ideal gas, an amount of heat

$$-dQ = -dW = dW_{\text{hot piston}} \tag{1.1.2}$$

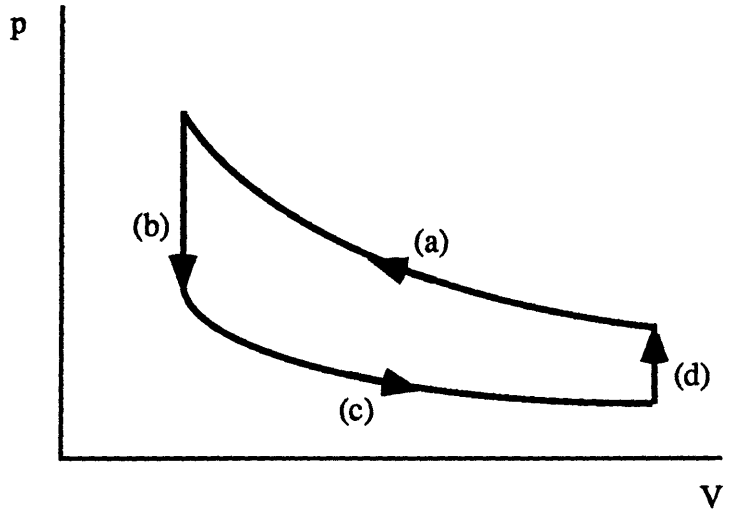

Figure 1.2. Representation of a Stirling cycle on a p-V diagram.

must be removed from the fluid, where $dW_{hot\ piston}$ is the work done by the hot piston on the fluid. This is the compression stroke. This process is represented by curve (a) in Fig. 1.2.

(b) Both the hot and the cold pistons move to the left and displace all of the fluid to the cold piston at constant volume. By virtue of the regenerator's high heat capacity and high thermal conduction with the fluid, the fluid is at T_C and a correspondingly lower pressure when it enters the cold piston This process is represented by line (b) in Fig. 1.2. Since there is no change in the fluid's volume,

$$dW = p \cdot dV = 0$$
$$dU = dQ$$
$$mC_v(T_C - T_H) = dQ \qquad (1.1.3)$$

where p and V are the fluid's pressure and volume, respectively, m is the mass of fluid in the refrigerator, and C_v is the fluid's specific heat at constant volume. The regenerator absorbs an amount of heat $mC_v(T_H - T_C)$ from the fluid during this process.

(c) The cold piston isothermally expands the fluid. Since $dU = 0$ for an isothermal process of an ideal gas, an amount of heat

$$dQ = dW = -dW_{cold\ piston} \qquad (1.1.4)$$

must be added to the fluid, where $dW_{cold\ piston}$ is the work done by the cold piston on the fluid. Note that dW is positive, as work has been done by the fluid on the piston. The fluid hence removes an amount of heat dQ from the surroundings of the cold piston. This is the refrigeration stroke. This process is represented by curve (c) in Fig. 1.2.
(d) Both the hot and the cold pistons move to the right and displace all of the fluid to the hot piston at constant volume. The fluid is at T_H and a correspondingly high pressure when it enters the hot piston because of the regenerator's high heat capacity and good thermal contact with the fluid. This process is represented by line (d) in Fig. 1.2. Since there is no change in the fluid's volume,

$$dW = p \cdot dV = 0$$
$$dU = dQ$$
$$mC_v(T_H - T_C) = dQ. \qquad (1.1.5)$$

The regenerator returns to the fluid the amount of heat it absorbed from the fluid in process (b). The net heat transferred from the fluid to the regenerator over a cycle is therefore zero. The regenerator simply maintains the same linear temperature profile from the hot end to the cold end during the refrigerator's cycle by virtue of its large heat capacity.

The cycle then repeats. Real Stirling refrigerators differ form the simplified model described above in several significant ways. The pistons execute harmonic motions rather than discontinuous motions in order to simplify the drive mechanism. The regenerator has a finite volume, and the heat transfer between it and the fluid is not complete, resulting in the fluid entering the pistons at temperatures different from T_H or T_C. The clearance volumes in the hot and cold pistons is not zero. The fluid in the pistons is often not isothermal owing to a limited heat transfer between the fluid and the surroundings. The working fluid may not behave as an ideal gas. Heat exchangers are placed between the pistons and the regenerator in order to enhance the heat transfer. Nevertheless, the essential principle of operation is as described above, with the net result being the cooling at the cold piston.

The superfluid Stirling refrigerator (SSR) uses a ^{3}He-^{4}He liquid mixture as a working fluid in the Stirling refrigeration cycle. Fig. 1.3 shows the phase diagram[14] of liquid ^{3}He-^{4}He mixtures. The mixture forms a homogeneous normal fluid above the λ line. A mixture of more than 6.4% ^{3}He phase separates and forms a two-phase mixture if

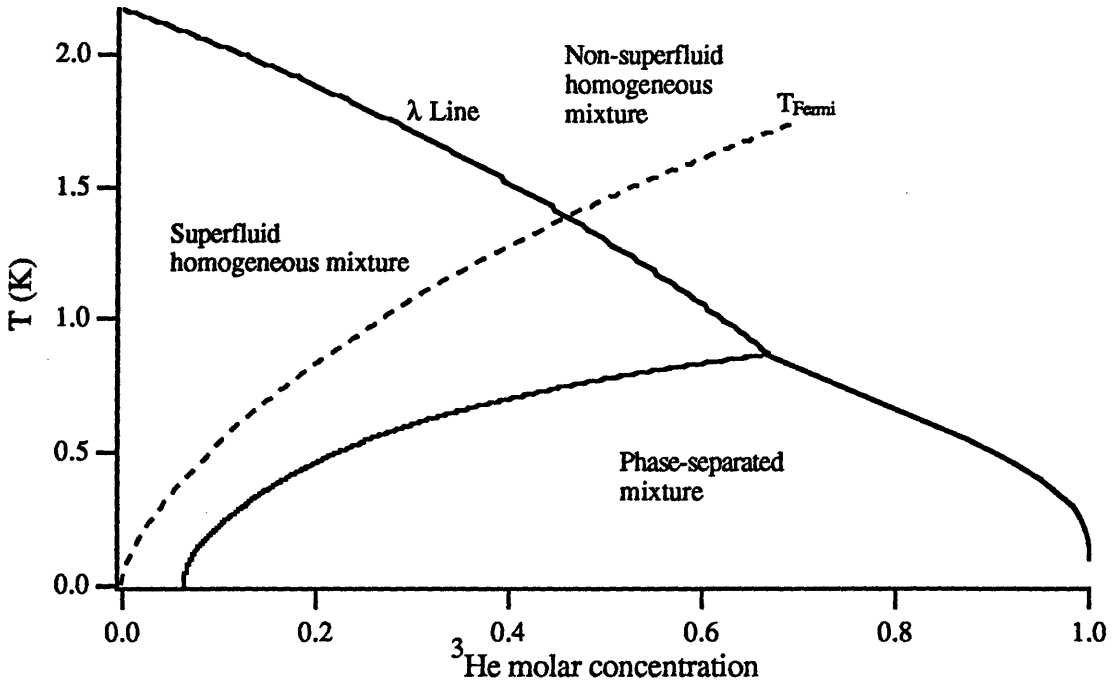

Figure 1.3. The ^{3}He-^{4}He phase diagram

cooled below the phase separation temperature, where a concentrated ^{3}He phase floats above a dilute phase. The SSR operates in the superfluid homogeneous mixture region between the λ line and the phase separation line where the ^{4}He component of the working fluid is superfluid. Fig. 1.3 also shows the Fermi temperature[7] as a function of the mixture's concentration. This is a measure of the temperature below which the fluid behaves as a Fermi gas. Fig 1.4 shows a superleak-equipped piston used in the SSR. On the left side of the piston is a mixture of ^{3}He and ^{4}He, and on the right side, pure ^{4}He. Superfluid ^{4}He can freely flow through the superleak by virtue of its zero viscosity, while the ^{3}He component which has a finite viscosity is confined to the left of the piston. Therefore, using pistons equipped with a superleak bypass, it is possible to compress and expand the ^{3}He component alone. Above the Fermi temperature and for low ^{3}He concentrations, the ^{3}He component of the working fluid, to first approximation, behaves thermodynamically as an ideal gas in the inert background of superfluid ^{4}He.[19] Osmotic pressure, which can be thought of as the ^{3}He component's pressure, is hence approximated by

$$\mathrm{Pos} = \frac{n_3 RT}{V} \tag{1.1.6}$$

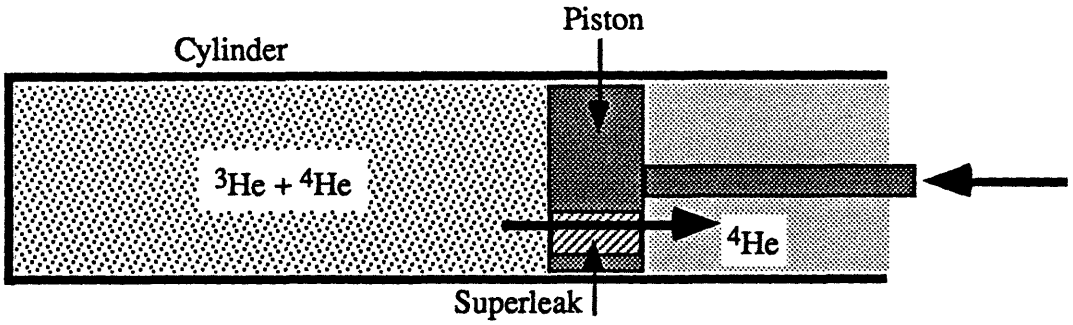

Figure 1.4. The superleak-equipped piston. The heavy arrow through the superleak indicates the direction of ^{4}He flow corresponding to the direction of piston motion shown.

where n_3 is the number of moles of ^{3}He particles, R is the universal gas constant, T is the temperature, and V is the volume. p_{os} is the difference in pressure between the fluid on the piston's left side and the fluid on the piston's right side. The ^{4}He component does not contribute significantly to the thermodynamics of the mixture, except at temperatures above 1 K.

The SSR is a Stirling machine equipped with these superleaked pistons to take advantage of the properties of the ^{3}He solute to cool below 1 K. The proof of principle was shown by Kotsubo and Swift[9,10] in 1990.

1.2 The Superfluid Orifice Pulse Tube Refrigerator (SOPTR)

The orifice pulse tube refrigerator replaces the Stirling refrigerator's cold piston with passive components consisting of a thermally insulating pulse tube and an orifice, thus reducing the refrigerator's complexity. The orifice pulse tube refrigerator is a relatively new technology, first developed by Mikulin *et al.* in 1983. They reached a low temperature of 105 K while exhausting waste heat at room temperature. More recently, Radebaugh *et al.*[15] has reached a temperature of 60 K under similar conditions. The orifice pulse tube refrigerator is not expected to surpass or even match the Stirling refrigerator in terms of efficiency or minimum temperature achieved. Its strength lies on its simplicity through the reduction in the number of moving parts.

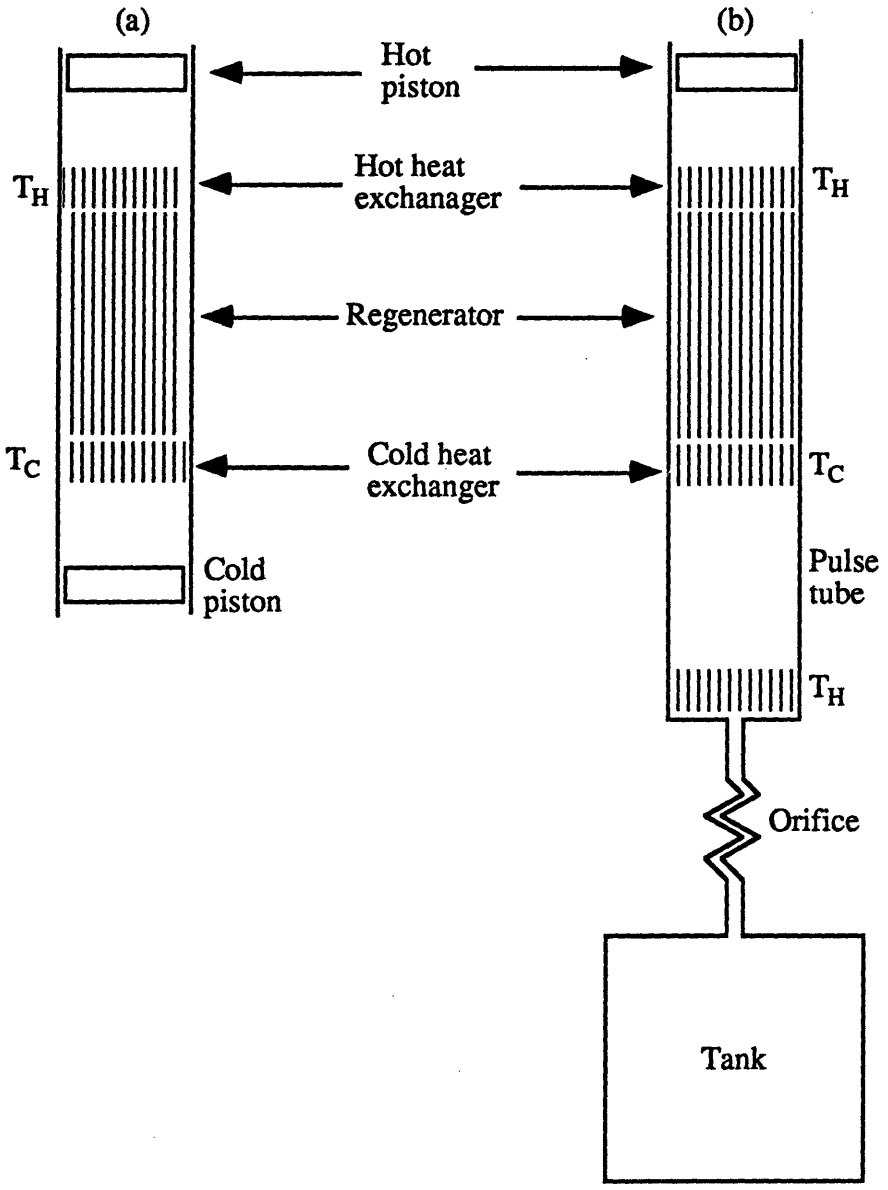

Figure 1.5. Schematics of (a) Stirling and (b) orifice pulse tube refrigerator, where the cold piston of the Stirling refrigerator is replaced by passive components.

In the Stirling cycle, the phasing of the cold piston's motion relative to the oscillating pressure is such that the cold piston expands the fluid while the pressure is high, and compresses the fluid while the pressure is low. The net effect averaged over a cycle is that the cold piston removes work from the fluid. The cold piston can therefore be replaced with a passive device with no external work input that maintains the same phasing between the pressure and the fluid flow. Fig. 1.5 shows the schematic of the orifice pulse tube refrigerator. Fluid in the pulse tube is connected via an orifice to a tank

that maintains a constant pressure. The orifice is a resistive flow impedance which passes oscillatory fluid flow in phase with the oscillatory pressure in the pulse tube. A heat exchanger near the orifice is thermally anchored at high temperature to dispose of this heat. The pulse tube is a simple tube full of the working fluid, connecting the cold heat exchanger to the orifice. It thermally isolates the orifice's dissipation from the cold end, while transmitting fluid motion. In other words, the fluid in the pulse tube can be thought of as an imaginary piston that duplicates the motion of the Stirling refrigerator's cold piston.

The orifice pulse tube refrigerator is less efficient than the Stirling refrigerator. Mechanical power is deliberately dissipated into heat in the orifice of the pulse tube refrigerator whereas it is efficiently recovered at the cold piston of the Stirling machine. This increases both the heat load on the hot platform and the amount of net mechanical power input required to give the same amount of cooling power as that of a Stirling refrigerator operating under similar conditions. The thermal conductance of fluid in the pulse tube exaggerates the loss mechanism. The reduction in the number of moving parts is a significant advantage, however, which may outweigh the disadvantages for some applications.

As discussed in Chapter 2, we modified our existing Stirling refrigerator, replacing the cold pistons with orifice pulse tube components, and operated the system with 17% and 6% mixtures. For simplicity, all numerical estimates of performance presented for the superfluid pulse tube refrigerator will model the ^{3}He in the mixture using the equation of state of a classical ideal gas.

1.3 Overview of Following Chapters

In Chapter 2, the design and instrumentation of both the SSR and the SOPTR as well as the surrounding equipment will be described in detail.

Chapter 3 will focus on the design and performance of mechanical actuators for the low temperature valves used to seal the fill lines into each of the two SSR's. They replaced the pneumatic actuators used previously in an effort to improve the refrigerator's efficiency. The operation of the refrigerator with the mechanical valves in place will be described, with an assessment of its advantages and disadvantages. Suggestions for future mechanical valve actuators will conclude this chapter.

In Chapter 4, we will discuss the SSR's "cooling power" operated at uniform temperature (heat exhaust temperature is equal to heat absorption temperature) in order to

simplify the analysis of the refrigerator. Detailed analytical models will predict the heat absorbed at the "cold" end and the work done by the fluid on the pistons. This will be followed by the experimental results, and their deviation from the analytical models will be discussed.

In Chapter 5, the SSR's cooling power as a function of the cold platform temperature will be presented. A simple model which assumes an ideal working fluid and isothermal compressions and expansions in the hot and cold pistons will give us the analytical framework. Deviation of the experimental results from the ideal behavior, including a loss mechanism, will be discussed.

In Chapter 6, the effect of the SOPTR's frequency on the cooling power will be investigated. The entire refrigerator will be held at a uniform temperature in order to simplify the analysis of the refrigerator's operation as much as possible. An analytic model based on a classical ideal gas will predict the cooling power. This will be followed by the experimental results, and their deviation from the analytic model will be discussed. This chapter will provide an insight into the pressure's phase lag from the piston motion, which is a key to the pulse tube's refrigerator's operation.

In Chapter 7, the effect of gravity on the fluid's oscillatory motion in the pulse tube will be investigated. The fluid's approximate velocity profile with and without gravity will be predicted, and the indicated cooling power with the cold platform held at a slightly lower temperature than the hot platform will provide an indirect evidence of the fluid's velocity profile in the pulse tube. A question of practical interest is how to set the piston displacement volume in order to maximize the cooling power.

In Chapter 8, the SOPTR's cooling power as a function of temperature will be presented. Results from the previous chapters will be used as a guideline to select the various parameters in order to maximize the SOPTR's cooling power. A simple model based on a classical ideal gas will predict the gross cooling power, which is the expected cooling power in the absence of losses, and the loss mechanism will be discussed.

Chapter 2

Experimental Equipment and Instrumentation

In this chapter, the design and instrumentation of both the SSR and SOPTR as well as the surrounding equipment will be described in detail.

2.1 The Superfluid Stirling Refrigerator

The first superfluid Stirling refrigerator was built by Kotsubo and Swift[9,10] in 1990. Brisson and Swift[1-4] built the second generation SSR in 1992 with several key improvements such as having two SSR's operating 180 degrees out of phase with each other. This design allows the use of a counterflow heat exchanger to serve as a regenerator by having the fluid in each half of the SSR regenerate each other. The design also takes advantage of both sides of the piston, eliminating the inert volume on the back side of each piston (shown in Fig. 1.4) that collects the ^{4}He that flows through the superleak. The apparatus used in this experiment is a slightly modified version of that built by Brisson and Swift. Improvements include a pumped ^{3}He evaporation refrigerator on the hot platform and improved shutoff valves on the fill lines.

Fig. 2.1 shows an overview of some of the equipment surrounding the SSR. The cryostat consists of three platforms: the platform cooled by a pumped ^{4}He pot which will also be called the 1 K platform, the platform cooled by a pumped ^{3}He pot which serves as the hot platform of the Stirling refrigerator, and the cold platform of the Stirling refrigerator. They are suspended inside a vacuum can for thermal insulation. The vacuum can is submerged in a liquid ^{4}He bath that is maintained at 4 K.

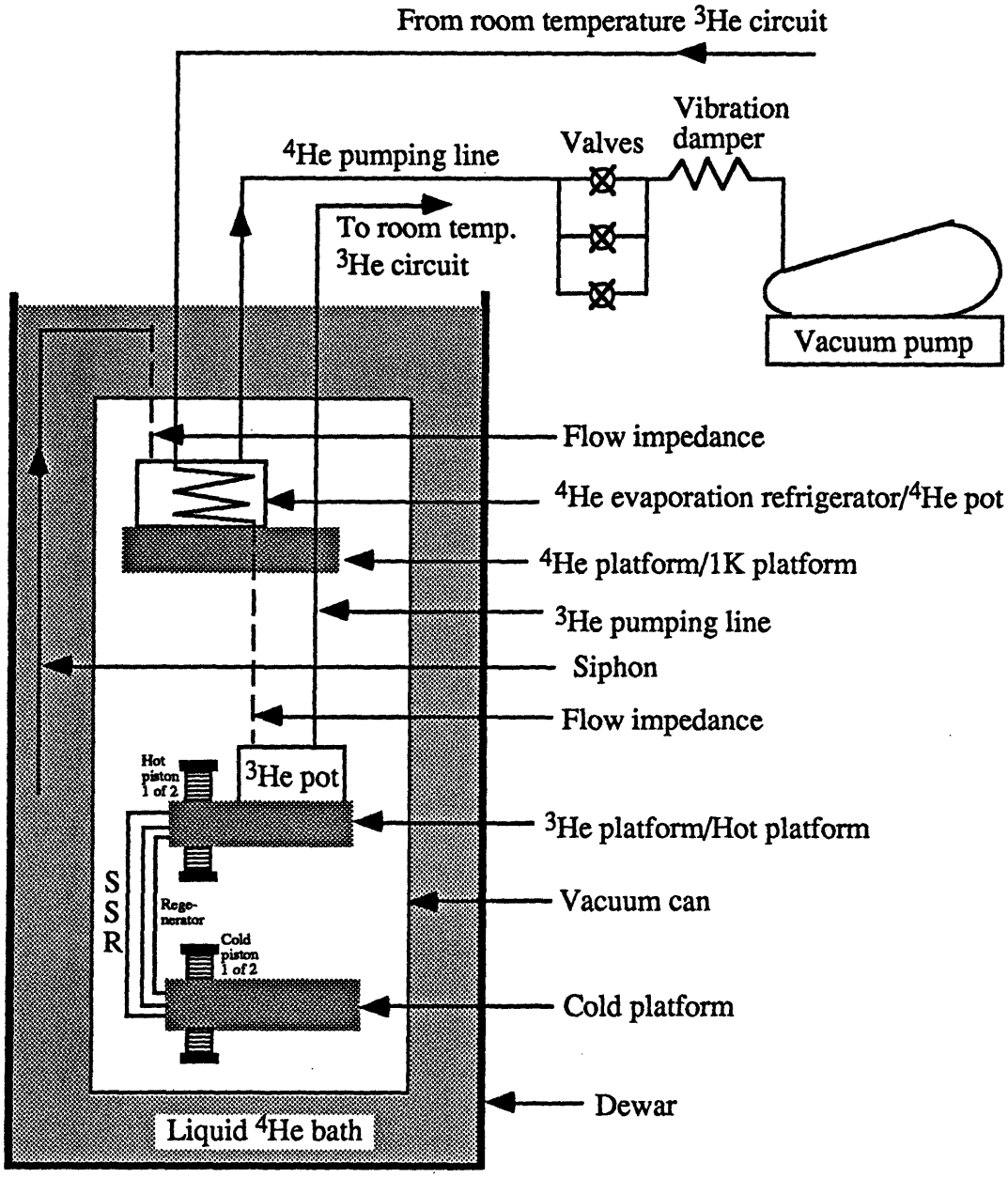

Figure 2.1. Schematic of the three platforms in the refrigerator and some of the surrounding equipment.

The ^{4}He platform, cooled by the ^{4}He evaporation refrigerator, serves as the first stage cooler of the cryostat. A five horsepower vacuum pump at room temperature pumps on the ^{4}He pot through the ^{4}He pumping line. The ^{4}He boils and lowers its temperature following the vapor pressure curve. There are a total of three valves placed in parallel, consisting of a large gate valve and two smaller valves, between the ^{4}He pot pumping line and the vacuum pump, all of which are closed before the ^{4}He pot is

depressurized. During startup, the pump is turned on and the smaller valves are slowly opened in order to prevent the liquid ^{4}He in the ^{4}He pot from foaming up and quickly evaporating. When the temperature falls below 2 K, the ^{4}He becomes superfluid and does not foam up by virtue of its high thermal conductivity. The large gate valve may then be opened. A vibration damper placed between the vacuum pump and the ^{4}He pumping line isolates the cryostat from the pump's mechanical vibration. The ^{4}He pot's source of liquid ^{4}He is the ^{4}He bath. A length of flow impedance is placed between the siphon and the ^{4}He pot in order to control the flow rate into the ^{4}He pot while maintaining a pressure gradient between the liquid ^{4}He bath and the ^{4}He pot. The length of flow impedance was made by inserting a thin SS wire inside a CuNi tube so as to block most of the cross sectional area inside the tube. The CuNi tube was then stretched in order to create a tight fit between the tube and the wire, thus maximizing the flow impedance. The ^{4}He platform maintains a temperature of slightly above 1 K and mounts several instruments and devices described subsequently, reducing the heat load on the ^{3}He platform.

Fig. 2.1 also shows the ^{3}He platform is cooled by a recirculating ^{3}He evaporation refrigerator. The recirculating ^{3}He is liquefied in the CuNi capillary inside the ^{4}He pot. A length of flow impedance is placed upstream of the ^{3}He pot in order to control the flow rate into the ^{3}He pot while maintaining a pressure gradient between the ^{3}He entering the cryostat and the ^{3}He pot. The amount of flow impedance for the ^{3}He pot and ^{4}He pot must be carefully balanced against each other through trial and error for reliable operation. The ^{3}He pot's flow impedance must be small enough to control the amount of ^{3}He flow so as not to overheat the ^{4}He pot, but large enough to provide enough cooling power for the ^{3}He pot; the ^{4}He pot's flow impedance must be chosen to provide the maximum cooling power under the given ^{3}He flow rate.

Fig. 2.2 shows the room temperature part of the ^{3}He circuit. A 1.5 horsepower vacuum pump pumps on the ^{3}He pot through the ^{3}He pumping line. A gate valve between the ^{3}He pumping line and the vacuum pump throttles the flow and controls the cooling power. A gate valve was chosen in order to minimize the flow impedance in the pumping line and hence maximize the cooling power at wide open throttle operation. A cold trap submerged in liquid Nitrogen and an oil trap, located downstream of the mechanical pump, filter out the elements that enter the circuit which would freeze and plug the capillaries in the cryostat. The length of flow impedance just upstream of the ^{3}He pot is especially susceptible to ice plugs due to the small cross sectional area. The in-line over pressure valve diverts the flow of ^{3}He downstream of the pump into the tank

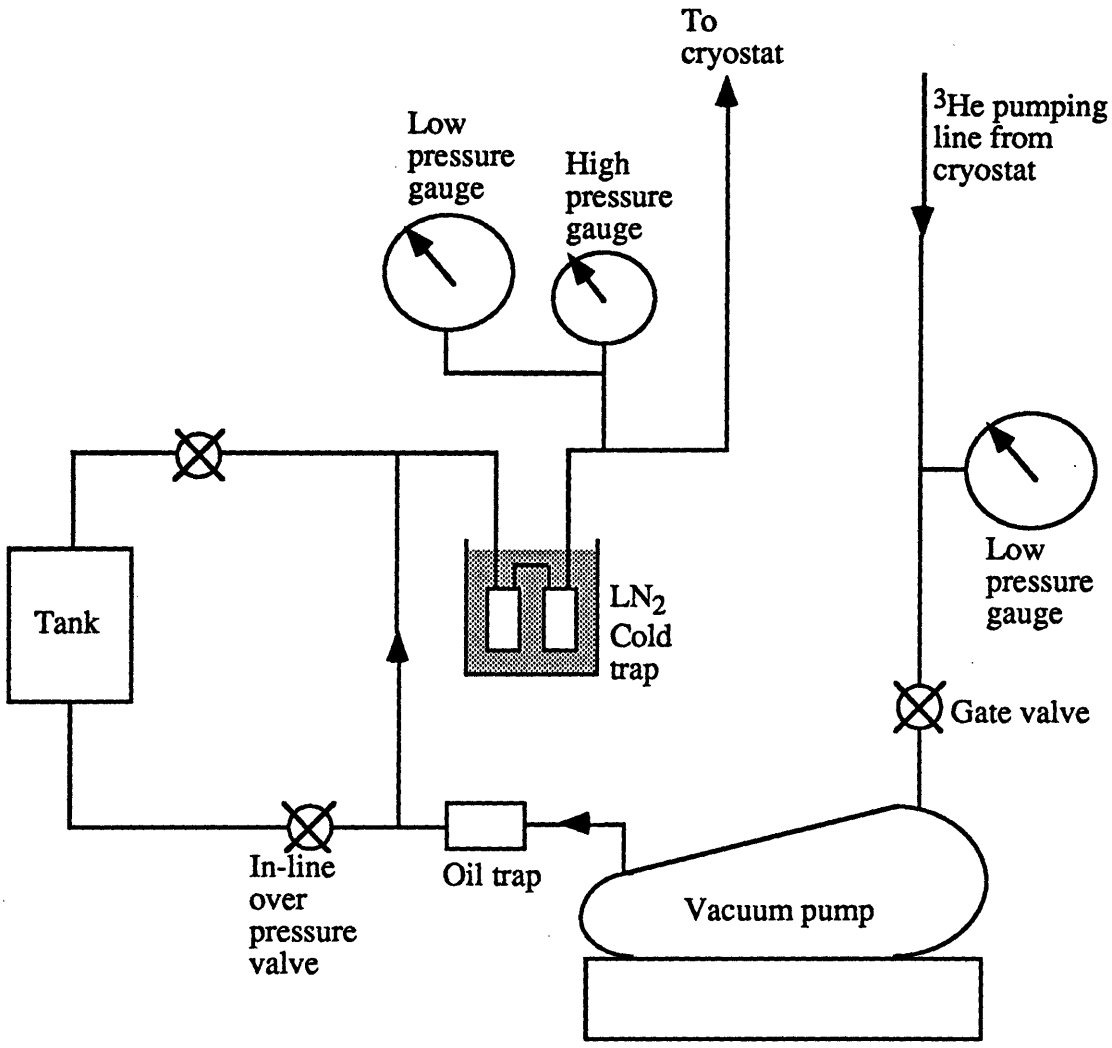

Figure 2.2. The room temperature part of the ^{3}He circuit

in case an ice plug formed in the capillary. The pump would otherwise build up a dangerously high pressure in the circuit. Pressure gauges at various locations monitor the pressure. The amount of ^{3}He in the circuit is approximately 0.3 mole.

Fig. 2.3 shows the SSR. It absorbs heat from the cold platform and rejects it to the hot platform. There are two refrigerators operating in parallel. The top refrigerator consists of the hot piston above the hot platform, the regenerator, and the cold piston above the cold platform. The bottom refrigerator consists of the hot piston below the hot platform, the regenerator, and the cold piston below the cold platform. The two refrigerators operate 180° out of phase with each other. The counterflow regenerator consists of a total of 238 0.305 mm O.D. CuNi tubes with 0.038 mm walls. These tubes are silver soldered in a hexagonally close packed array with alternating rows

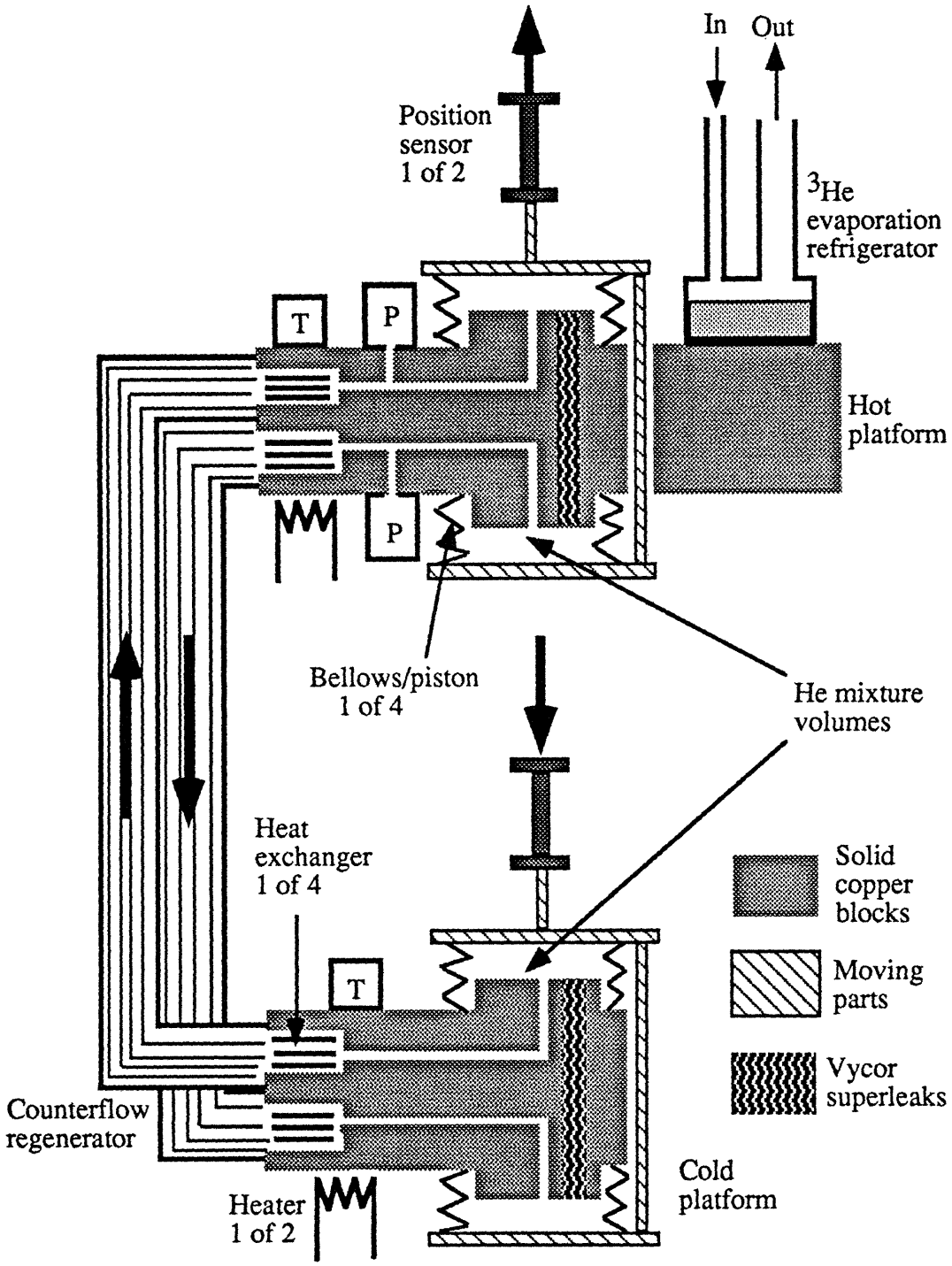

Figure 2.3. The SSR. Pressure gauges are delineated with a "P", thermometers with a "T". The pumped ^{4}He platform, which is located above the hot platform, is not shown. The arrows in the regenerator indicate the direction of fluid flow corresponding to the direction of piston motion shown.

corresponding to each half of the SSR. The fluid in one half of the refrigerator flows through the recuperator opposite to the fluid flow in other half and the two fluids regenerate each other. Silver solder was used to insure that the solder does not become a superconductor at the operating temperatures which would reduce the thermal conductivity between the tubes. The length of the regenerator is approximately 20 cm.

A Dayton model 4Z534A permanent magnet DC gearmotor drives a camshaft which has two cams with adjustable strokes and phase angles. The cams in turn drive the pistons' pushrods made of 6 mm O.D. SS tubes. A leather strap wrapped around a pulley at the end of the camshaft puts a brake on the camshaft in order to eliminate the slack in the driving mechanism; the camshaft would otherwise turn discontinuously during the cycle and put a significant heat load on the refrigerator.

The hot platform pistons are rigidly connected together and driven sinusoidally from room temperature by the pushrod. The cold platform pistons are similarly driven. The pistons are made with welded bellows which have convolutions that nest into one another. A large volume displacer press fit into the large copper block is placed inside each bellows to minimize the piston clearance volume. The effective cross sectional area of the bellows[16] is 3.16 cm^2.

The superleaks are cylinders of Vycor glass approximately 3.6 mm in diameter and 7.4 cm long epoxied into place. These allow the superfluid ^4He to freely flow between each half of the SSR while confining the ^3He.

The heat exchangers are copper cylinders press fit into the large copper blocks. The hot platform heat exchangers are 1.14 cm long with four 0.8 mm diameter holes drilled longitudinally through the cylinder. The cold platform heat exchangers are 1.14 cm long with 12 0.51 mm diameter holes.

The linear position sensors are mounted on the ^4He platform to monitor the positions of the pistons. They consist of two counter wound copper coils on a thin walled stainless steel tube. A pick-up coil wound on a ground stainless steel rod rides inside the counter wound coils. They are driven by a 1 mA 1 kHz signal and the output voltage of the pick-up coils is monitored as a measure of position by Princeton Applied Research model 5301A lock-in amplifiers. The resolution of the system is better than 0.025 mm. Each position sensor is calibrated using two electrical switches of known positions mounted on the large copper platforms.

The two fill lines into each of the SSR halves are sealed with low temperature mechanical valves mounted on the ^4He platform. Their purpose is to prevent the mixture from oscillating up and down the fill lines which puts a thermal load on the hot platform

and to create a well defined closed volume in the refrigerator. The construction and operation of the valves are described in more detail in Chapter 3.

Flexible diaphragm pressure gauges are connected to each half of the SSR on the hot platform. Their outputs are measured with Stanford Research System model SR530 lock-in amplifiers.

Calibrated germanium thermometers are mounted on each of the hot and cold platforms. Each thermometer is monitored by S.H.E. corporation model PCB potentiometric conductance bridge. Heaters controlled by Linear Research model LR-130 feedback controllers allow a precise control of the hot and cold platform temperatures.

Fig. 2.4 shows the ^{3}He-^{4}He mixture tanks and surrounding equipment at room temperature. Each tank contains a mixture of a known concentration. The SSR is filled with a mixture from one of these tanks. The liquid Nitrogen cold trap is used to filter out any contaminants present in the mixture that could plug the fill lines to the SSR in the cryostat. The concentrations of the mixtures are determined using an acoustic gauge[5,8] that measures the gas' speed of sound at 0°C. A Wallace and Tiernan model FA145 pressure gauge monitors the pressure downstream of the tanks.

An IBM PC monitors the outputs from various sensors.

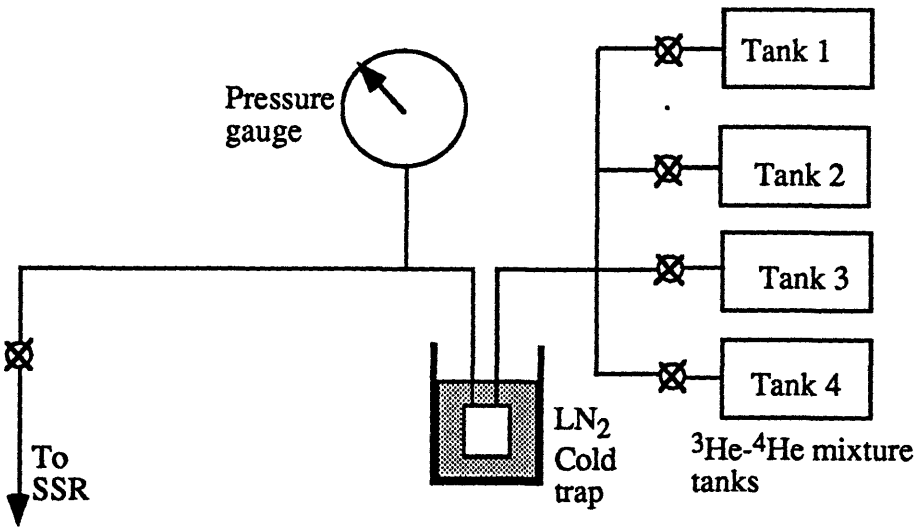

Figure 2.4. Room temperature ^{3}He-^{4}He mixture storage tanks and surrounding equipment

2.2 The Superfluid Orifice Pulse Tube Refrigerator

The superfluid orifice pulse tube refrigerator (SOPTR) is shown in Fig. 2.5. This refrigerator is a slightly modified version of the superfluid Stirling refrigerator. The bellows on the cold platform were replaced by pulse tubes, heat exchangers, and an orifice. Because of the 180° temporal phase shift between the two halves of the refrigerator, a single orifice linking the two halves of the refrigerator was used, so that each half of the refrigerator served as the tank of the other half. The heat exchangers at the hot ends of the pulse tubes, adjacent to the orifice, were thermally anchored to the hot platform. Other parts of the refrigerator are essentially identical to the superfluid Stirling refrigerator.

Stability against gravitational convection in ^{3}He-^{4}He mixtures requires that the cold end of the pulse tube be up, in contrast to convention in cryostats. Choice of dimensions of the pulse tubes was a rough compromise among several considerations. The total fluid volume in the pulse tube should be significantly larger than the fluid's volumetric displacement through the pulse tube, so that warm fluid that enters the pulse tube form the orifice does not enter the cold platform. The peak to peak volumetric displacement of each of our hot pistons was $V_{sw}<2$ cm^3, so we expected peak to peak volumetric displacements in the pulse tubes to be somewhat smaller than that. However, if the pulse tube volume is too large, the pressure amplitude will be reduced significantly for a given piston stroke, resulting in a correspondingly lower cooling power. Erroneously, we had believed that the pulse tube diameter should be significantly larger than the mixture's viscous thermal penetration depth

$$\delta_v = \sqrt{\frac{\mu}{\pi f (m^*/m)\rho}} \tag{2.2.1}$$

where μ is viscosity, f is operating frequency, m* and m are the effective and true mass of a ^{3}He atom, and ρ is the mass density of ^{3}He, so that the imaginary piston could move with a slug flow where the velocity is essentially independent of radial location within the pulse tube. The origin of Eq. 2.2.1 is discussed in Section 7.1. For the operating frequencies accessible with our drive motor (4 mHz<f <50 mHz), 0.5 mm< δ_v<1.6 mm for a 17% mixture at 1 K. The thermal load on the cold platform due to thermal conduction of fluid in the pulse tube, given approximately by

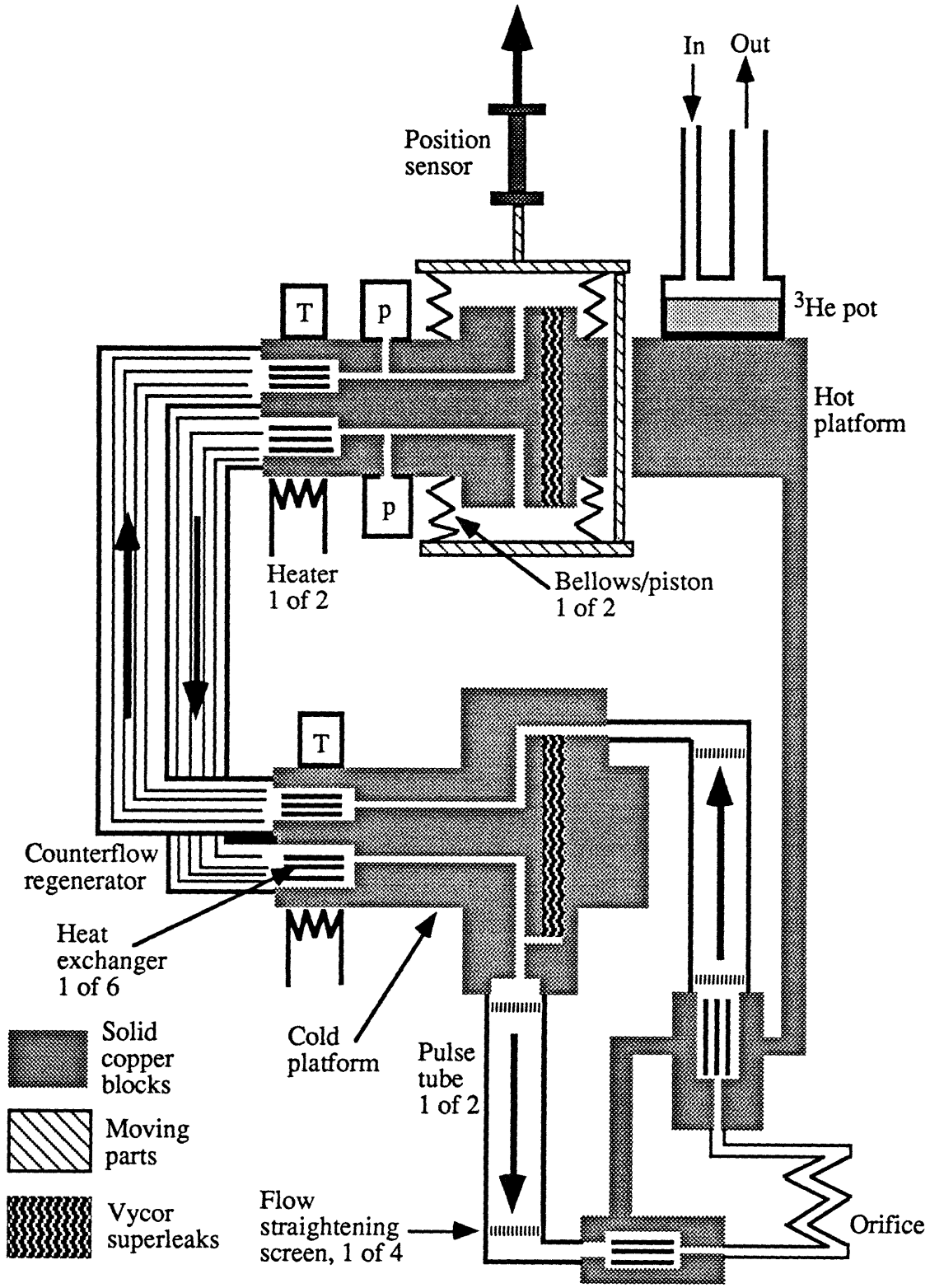

Figure 2.5. The SOPTR. Pressure gauges are delineated with a "P", thermometers with a "T". The pumped ^{4}He platform, which is located above the hot platform, is not shown. The arrows in the regenerator and the pulse tubes indicate the direction of fluid flow corresponding to the direction of piston motion shown.

$$\dot{Q}_{cond} = \kappa \frac{A}{L} \Delta T \tag{2.2.2}$$

where κ is the fluid's thermal conductivity, A and L are the cross sectional area and length of the pulse tube, and ΔT is the temperature difference across the pulse tube, should not be too large, so the area to length ratio of the pulse tube should be kept reasonably small. Finally, we were limited in the space below the existing cryostat, limiting the length of the pulse tube if major reconstruction of the refrigerator was to be avoided. We chose a 6.3 mm O.D. CuNi tube approximately 8 cm long with walls 0.15 mm thick.

4.8 mm O.D. Cu tubes were used to connect the cold platform or the heat exchanger to the pulse tubes. Their I.D. was approximately 3 mm, minimizing the connecting tube volume. Copper screens of approximately 25 mesh per cm at each end of each pulse tube served as flow straighteners in order to prevent possible flow separation of fluid as it entered the pulse tubes from the heat exchangers or 3 mm inner diameter connecting tubes, where the Reynolds number was of order 1000. The two pulse tubes are essentially identical. Details of the pulse tubes' geometry are found in Appendix J.

The approximate amount of flow impedance in the orifice was calculated as

$$Z = \frac{p_1 \tau}{V_1 \mu} \tag{2.2.3}$$

where p_1 is the fluid's pressure amplitude, τ is the refrigerator's period, V_1 is the volume amplitude of piston motion, and μ is the mixture's viscosity. The origin of Eq. 2.2.3 is discussed in Section 6.1. As a rough estimate, we assumed $p_1 = 0.25 \times 10^5$ Pa, $\tau = 15$ s, $V_1 = 1$ cm^3, and $\mu = 10^{-6}$ kg/m-s, which yielded $Z = 4 \times 10^{11}$/cm^3. Research orifice pulse tube refrigerators usually use needle valves as orifices so that the impedance can be varied during the course of the experiment. For our superfluid pulse tube refrigerator, with small displaced volume and low frequency, the required impedance was far higher than those of commonly available valves. Hence we used a fixed impedance. A length of flow impedance, the amount of which was adjusted at room temperature to match the value given by Eq. 2.2.3, was installed in the SOPTR and the refrigerator was cooled down. However, the flow rate through it was much lower than desired, possibly due to the difference in thermal contraction between the CuNi tube and the SS wire. The amount of flow impedance was therefore adjusted by trial and error. The orifice used to

measure most of the data presented in Chapters 6 through 8 was made by inserting a 0.15 mm diameter SS wire into a 2.7 cm long, approximately 0.2 mm inner diameter CuNi tube to block most of the area and achieve the desired flow impedance. We placed 16 such capillaries in parallel.

The hot heat exchangers at the ends of the pulse tubes are made of solid copper blocks with four 0.8 mm diameter holes 1.14 cm long drilled through the blocks. They are bolted on to the hot platform via brackets for thermal contact.

The SOPTR is otherwise identical to the SSR.

Chapter 3

Low Temperature Mechanical Valves

The fill lines into each half of the refrigerator are sealed with low temperature valves. Previous superfluid Stirling refrigerator used low temperature pneumatic valves activated by pressurized ^{4}He. While these were simple devices, they had several disadvantages, some of which would have been exaggerated by the addition of the ^{3}He pot on the hot platform. Mechanically actuated valves, though significantly more complex than pneumatic valves, improve the refrigerator's performance by reducing the heat load to the 1 K platform. Added complexities arose from the requirement that the valve drive mechanism fit into the existing cryostat without major modification, and a need to thermally disconnect the drive mechanism from the 1 K platform when not in use.

3.1 Design and Construction

Previous superfluid Stirling refrigerator used low temperature pneumatic valves, shown in Fig. 3.1, on the SSR's fill lines that used pressurized ^{4}He as the actuating fluid. The piston with a tip made of Teflon is attached to the seat via a bellows, and a cap attaches over the piston and the bellows. ^{3}He-^{4}He mixture flows through the seat. Pressurized ^{4}He under the cap presses down the piston, which makes a seal with the seat and closes the ^{3}He-^{4}He mixture's path. Part of the ^{3}He-^{4}He mixture that flows into the valve goes up into the gap between the seat and the piston, and occupies the space inside the bellows. This space, including the narrow gap between the seat and the piston, is 0.29 cm^3. The bellows acts as a spring to keep the piston open when not being pressed down, and separates the ^{3}He-^{4}He mixture from the actuating fluid. Note that it is the differential

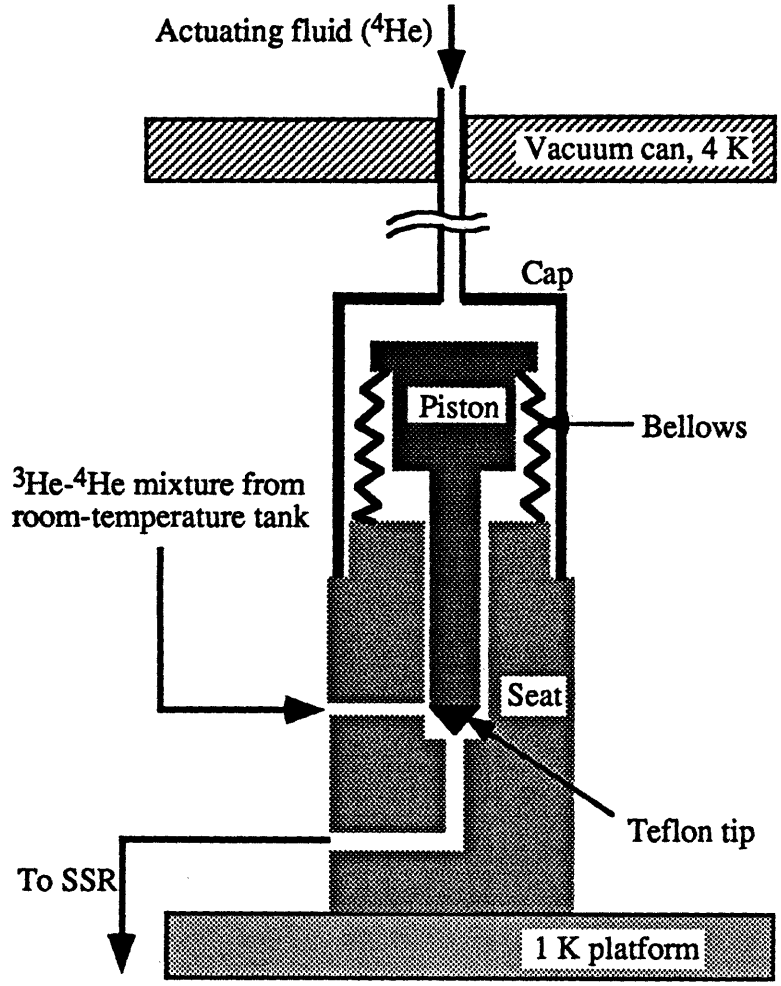

Figure 3.1. Schematic of the pneumatic valve and surrounding platforms

pressure between the ^{3}He-^{4}He mixture and the actuating fluid that pushes the piston down.

While this was a simple device, the actuating column of pure ^{4}He in the capillary between the vacuum can and the valve put a substantial thermal load on the 1 K platform due to superfluid counterflow; the effective thermal conductivity of superfluid ^{4}He is[19] above 4000 W/m-K, while the thermal conductivity of normal ^{4}He is around[19] 0.02 W/m-K. The addition of the ^{3}He evaporation refrigerator on the hot platform of the refrigerator put a significantly higher thermal demand on the 1 K platform over the demand of the previous refrigerator, since the ^{4}He pot has to liquefy the recirculating ^{3}He. The ^{4}He pot used in this apparatus is capable of handling either the ^{3}He pot's thermal load or the heat leak due to the column of actuating pure ^{4}He for the valve. However, the thermal load on the 1 K platform with both the ^{3}He pot and the pneumatic

valves in place has proven to be beyond the ^{4}He pot's capability. One option was to utilize pressurized ^{3}He in place of ^{4}He to actuate the valves, since the ^{3}He's thermal conductivity of around[17] 0.01 W/m-K is significantly lower than that of superfluid ^{4}He. However, this was not economically feasible. Additionally, the pneumatic valves did not seal reliably, even though a pressure of 100 psi was used to actuate them. It was necessary to press down the piston with a greater amount of force in order to achieve a tighter seal. Therefore, the means of sealing the valves was changed from pneumatic to mechanical. The cap was removed and the piston was exposed in order to allow a mechanical actuator to press down the piston directly.

Mechanical valves usually work as follows. A socket attached to the end of a shaft that runs down from room temperature turns a screw which pushes down the piston. The socket can be disconnected from the screw when not in use in order to minimize the thermal conduction. The shaft passes through rubber O-rings at room temperature which maintain the pressure difference between the vacuum can and the atmosphere. A knob attached to the end of the shaft is manually turned. Lifting the knob disengages the socket from the screw, thus thermally disconnecting the valve from the drive gear.

For this cryostat, however, there was another requirement. There was only room for one shaft to run from room temperature to the cryostat through the struts and flanges supporting the vacuum can, while there were two valves in the cryostat, one for each half of the refrigerator. They had to be actuated simultaneously with a single drive mechanism, as making room for another shaft would have resulted in a major reconstruction of the struts and flanges. The drive mechanism is shown in Fig. 3.2. A socket at the end of a shaft made of a 7.9 mm O.D. SS tube that comes down from room temperature turns the nut which is welded to the bolt. The socket is normally lifted from the nut in order to reduce the thermal conduction from the vacuum can, which is at 4 K, to the 1 K platform, but may be lowered to engage and turn the nut. The bolt pushes down a bridge which in turn pushes down and seals both of the valves. Universal joints were placed between the shaft and the socket, as the location of the shaft, which passed through a tube that had previously carried electrical wires only, did not match that of any of the existing holes in the top flange of the 1 K platform. A socket guide bolted to the vacuum can placed the socket in the correct location. This guide had to be attached to the vacuum can, as attaching it to the 1 K platform would have thermally loaded the 1 K platform by creating a thermal path between the vacuum can and the 1 K platform. The

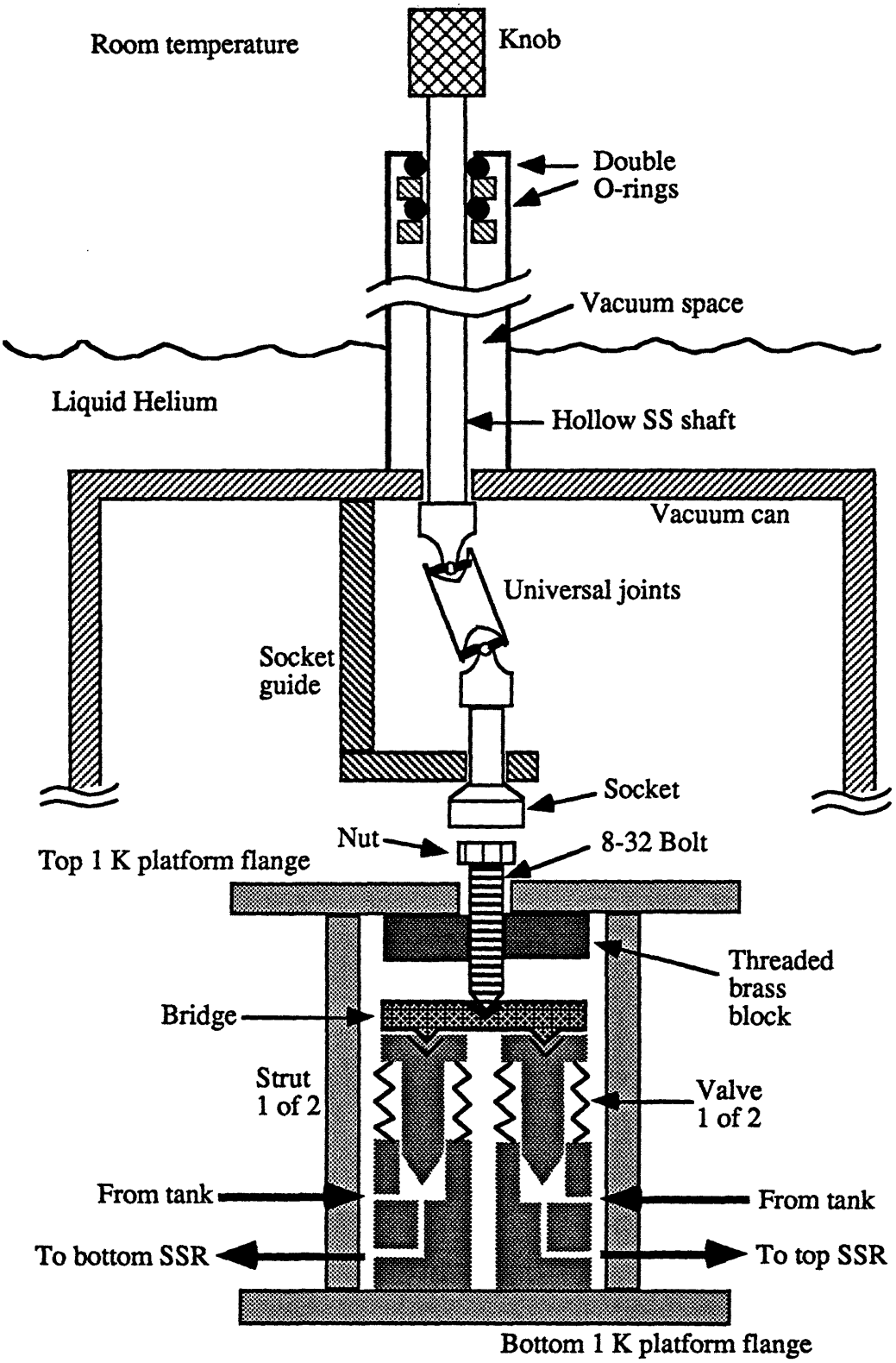

Figure 3.2. The mechanical valve assembly. The heavy arrows indicate the direction of ^{3}He-^{4}He mixture's flow into the SSR.

existing threads in the 6 mm thick copper flange, spaced out in a square matrix 12.7 mm apart from one another and tapped for 4-40 screws, were deemed insufficient to hold up the required load. We therefore attached a 12.7 mm thick block of brass underneath the copper flange to engage the bolt's threads and utilized an 8-32 bolt. One of the existing holes in the copper flange was enlarged so that the 8-32 bolt could pass through it. In order to keep the bridge in place, a dimple was machined on top of the bridge and the tip of the screw was pointed to fit into the dimple. Similarly, dimples were machined on top of the pistons and pointed tips on the bridge fit in them.

The tightness of the valves' seal relies on the correct spacing between the top and the bottom flanges of the 1 K platform. There were three struts connecting the top and the bottom 1 K platform flanges, one of which was next to the valves, but another one was placed on the other side of the valves in order to provide more rigidity between the two flanges in the vicinity of the valves. Without the additional strut, the top and bottom flanges of the 1 K platform may plastically deform and separate from each other over a period of time, compromising the tightness of the seal.

3.2 Operation of the Mechanical Valves

The valves sealed more tightly when mechanically actuated. The pressure oscillation observed by the Wallace and Tiernan gauge at room temperature during the SSR's operation when pneumatic valves were used was no longer present.

The reduction in thermal load on the 1 K platform due to the absence of the column of ^{4}He may be estimated as:

$$\dot{Q} = 2\kappa A \frac{dT}{dx} \tag{3.2.1}$$

where κ is the effective thermal conduction due to thermal counterflow[19] and A is the cross sectional area of the capillary. The factor of two comes from the fact that there were two pressurizing capillaries. Assuming a κ of 4000 W/m-K, a 0.2 mm diameter capillary, and a thermal gradient of 5 K/m, Eq. 3.2.1 yields 1.3 mW.

One operational idiosyncrasy that was discovered while operating the cryostat was that closing the valves would temporarily surge the 1 K platform's temperature. The temperature would rise by a fraction of a degree and come back down in a few minutes. This may be due to the compression of the ^{3}He component of the mixture between the

piston and the bellows. As the valve is closed, the volume between the piston and the bellows decreases, forcing the mixture in the volume to flow out through the gap between the piston and the seat. ^{4}He would easily flow out by virtue of its lack of viscosity while ^{3}He would initially be confined to the volume. The resultant compression of ^{3}He would result in the warming of the 1 K platform. Another possibility for the temporary temperature rise is the friction generated by the threads.

Thermal conduction between the vacuum can and the 1 K platform through the bolt and the socket was almost negligible. The refrigerator was operated at times with the socket unintentionally engaging the nut and thus creating a thermal path between the vacuum can and the 1 K platform. However, the additional heat load on the 1 K platform, estimated to be of the order of 200 μW, was so small that it was usually unnoticed. The poor thermal conduction may have resulted from thermal boundary resistance among the various moving parts in the complex drive mechanism.

3.3 Conclusions and Suggestions

Mechanically actuated valves seal more tightly than pneumatic valves, helping to create a well defined closed volume for the SSR. Another advantage of the mechanical valves over the pneumatic valves is the reduced heat load on the 1 K platform due to the elimination of the capillary between the vacuum can and the 1 K platform that carries the fluid, usually ^{4}He, that actuates the valves.

A secondary advantage would be the reduced thermal load on the 1 K platform when closing the valves. In pneumatic valves, the incoming ^{4}He that presses down the piston would liquefy, rejecting heat to the 1 K platform. Though the mechanical actuators also generate some heat when closing the valves, it is suspected to be small in comparison.

The primary disadvantage of the mechanically actuated valves is the added complexity, especially if two or more valves are to be actuated with a single drive mechanism. This particular conversion from pneumatic to mechanical actuators took about a week to design and assemble, excluding the amount of time spent waiting for the parts to be machined and the universal joints to arrive. It also requires a path for the drive shaft through the struts supporting the cryostat. A conversion from pneumatic to mechanical valves is virtually impossible without a preexisting path. However, future mechanical valves may be significantly simplified as stated below.

It would be worthwhile to consider in the future a simple mechanical drive system where the bolt is permanently attached to the hollow SS shaft. Such a design should have as much of the shaft between the vacuum can and the 1 K platform made from SS tubes as possible to minimize thermal conduction. In designing future cryostats, paying attention to the alignment between the shaft that runs down from room temperature and the bolt used to press down the valve would eliminate the need for universal joints in the drive mechanism.

This particular design demands a high structural rigidity between the top and the bottom 1 K platforms flanges, but such a requirement may not be necessary in a design in which a bolt attaches directly to the valve as opposed to the top 1K platform flange. Such a design, however, would make it difficult to actuate two valves with a single shaft, as there would be two bolts to turn.

Chapter 4

The SSR Uniform Temperature Measurements

The ultimate performance of the SSR is limited by the thermodynamics of the ^{3}He as it becomes Fermi degenerate. A model based on an ideal Fermi gas suggests that the SSR's cooling power rapidly drops to a fraction of that of a classical, ideal gas refrigerator below the Fermi temperature. In order to explore this phenomenon, the SSR was operated with the cold platform held at the same temperature as the hot platform so that the temperature was essentially constant throughout the apparatus. This greatly simplified the analysis of the operation and allowed us to analytically predict the cooling power and the work done by the fluid on the "hot" and "cold" pistons. Both the thermodynamic table of ^{3}He-^{4}He mixtures by Radebaugh[14] and an ideal Fermi gas model were used as the equations of state. The refrigerator was operated with a 5.9%, 17%, and 36% mixtures, and the results support different predictions at different regimes.

4.1 Theory

We will first present the formula by Brisson and Swift, which accounts for both the ^{3}He and the ^{4}He components' contribution to the cooling power and is hence a thermodynamically accurate expression throughout a wide range of temperatures. Radebaugh's tables of thermodynamic data[14] will be used to evaluate this expression. We will then derive a different model that assumes that the ^{4}He component does not contribute to the thermodynamics of the mixture. The latter model was derived in order to simplify the expression for the cooling power and enable us to use the equation of state of an ideal Fermi gas.

We will assume throughout this chapter that V_H,the hot piston volume, and V_C, the cold piston volume, are:

$$V_H = V_0 + \frac{V_{sw}}{2}\cos \omega t = V_0 + V_1 \cos \omega t$$
$$V_C = V_0 - \frac{V_{sw}}{2}\sin \omega t = V_0 - V_1 \sin \omega t \qquad (4.1.1)$$

where V_0 is the average piston volume, V_{sw} is the piston swept volume, and V_1 is half of the piston swept volume. Brisson and Swift[3] have shown that, for isothermal operation, the heat absorbed by the fluid in the cold piston per cycle is given by

$$Q_C = W_C + H_C = \left[\frac{1}{\rho RT}\left(\frac{\partial p}{\partial c}\right)_{T,\mu_4} - \frac{c_0}{RT}\left(\frac{\partial h_{os}}{\partial c}\right)_{T,\mu_4}\right]\frac{\pi m R T V_1^2}{(2V_0 + V_r)^2} \qquad (4.1.2)$$

where W_C is the work done by the fluid on the cold piston per cycle, H_C is the enthalpy that flows out from the cold piston through the regenerator per cycle, ρ is the mixture's total mass density, R is the gas constant per mass of ^{3}He, T is the temperature, p is the pressure, c is the mass concentration of the mixture, μ_4 is the chemical potential of ^{4}He, c_0 is the average mass density of the mixture in the refrigerator, h_{os} is the osmotic enthalpy of the mixture, m is the mass of ^{3}He in each half of the refrigerator, and V_r is the volume of the regenerator. Eq. 4.1.2 accounts for both the ^{3}He and ^{4}He components' contribution to the cooling power and is hence a thermodynamically accurate expression throughout a wide range of temperatures. The heat divided by the work is

$$\frac{Q_C}{W_C} = 1 - \rho c_0 \left(\frac{\partial h_{os}}{\partial p_{os}}\right)_{T,\mu_4} = -\rho c_0 \frac{(\partial h_{os}/\partial c)_{T,p}}{(\partial p_{os}/\partial c)_{T,p}} - \rho(1-c_0)\frac{(\partial \mu_4/\partial c)_{T,p}}{(\partial p_{os}/\partial c)_{T,p}} \qquad (4.1.3)$$

which can be evaluated by taking differences between entries in tables[14] of thermodynamic data. For a reversible operation with the hot and cold platforms held at an equal temperature, the work done by the fluid on the hot piston is the negative of the work done by the fluid on the cold piston. For an ideal gas, the first quantity in the square brackets in Eq. 4.1.2 is unity and the second quantity is zero, and Eq. 4.1.3 is unity. In other words, in a reversible ideal gas refrigerator operating at uniform

temperature, the heat absorbed at the cold end is equal to the work done by the fluid on the cold piston.

We will now derive an expression for the cooling power in which we assume a monatomic ^{3}He gas as a working fluid in a Stirling refrigerator operating isothermally. We will ignore the contribution of ^{4}He to the thermodynamics of the mixture in order to simplify the expression and enable us to use an ideal Fermi gas model to predict the cooling power. In cyclic operation, conservation of energy of fluid in the cold piston implies that $Q_C=W_C+H_C$, where Q_C is the heat absorbed by the fluid per cycle, W_C is the work done by the fluid on the piston per cycle, and H_C is the enthalpy that flows out through the regenerator per cycle. Our approach will be to find Q_C by adding W_C and H_C.

We can find W_C from the integral $\oint p \cdot dV_C$. Eq. 4.1.1 implies that the total volume of the refrigerator is

$$V_{tot} = 2V_0+V_r+V_1(\cos \omega t-\sin \omega t) = (2V_0+V_r)+\sqrt{2}\, V_1\cos(\omega t+\pi/4). \qquad (4.1.4)$$

Since the fluid's viscous dissipation and inertial forces are negligible, the pressure throughout the refrigerator is

$$p = p_0+\left(\frac{\partial p}{\partial V}\right)_T \left(V_{tot} - \overline{V}_{tot}\right) = p_0+\frac{\sqrt{2}V_1}{\kappa(2V_0 + V_r)}\cos(\omega t + \pi / 4) \qquad (4.1.5)$$

where p_0 is the average pressure, $\overline{V}_{tot}$ is the average total volume of the refrigerator, and κ is the isothermal compressibility. Using Eqs. 4.1.1 and 4.1.5, we find that the work done by the fluid on the cold piston per cycle is

$$W_C = \oint p \cdot dV_C = \frac{\pi V_1^2}{\kappa(2V_0 + V_r)}. \qquad (4.1.6)$$

H_C is calculated as follows:

$$H_C = -\oint h\frac{dn_C}{dt}dt \qquad (4.1.7)$$

where h is the enthalpy per mole and n_C is the number of moles of fluid in the cold piston. h and n_C are given by

$$h = h_0 + \left(\frac{\partial h}{\partial v}\right)_T \left[\frac{V_{tot}}{n} - \frac{\bar{V}_{tot}}{n}\right] = h_0 + \left(\frac{\partial h}{\partial v}\right)_T \frac{\sqrt{2}V_1}{n}\cos(\omega t + \pi/4) \tag{4.1.8a}$$

$$n_C = \rho V_C = \frac{n}{V_{tot}} V_C \tag{4.1.8b}$$

where h_0 is the average enthalpy per mole, v is the molar volume, n is the number of moles of working fluid in the refrigerator, and ρ is the fluid's mole density. Expanding Eq. 4.1.8b to first order in $\frac{V_1}{2V_0 + V_r}$ and substituting into Eq. 4.1.7, we obtain

$$H_C = \frac{\pi V_1^2}{(2V_0 + V_r)}\left(\frac{\partial h}{\partial v}\right)_T. \tag{4.1.9}$$

To find $\left(\frac{\partial h}{\partial v}\right)_T$, we use the thermodynamic relations[6]

$$dh = Tds + vdp$$
$$Tds = C_v dT + \frac{T\beta}{\kappa} dv \tag{4.1.10}$$

where s is the fluid's entropy per mole, C_v is the specific heat at constant volume, and β is the thermal expansion coefficient. We obtain, after some manipulation,

$$\left(\frac{\partial h}{\partial v}\right)_T = \frac{T\beta - 1}{\kappa}. \tag{4.1.11}$$

Combining Eqs. 4.1.6, 4.1.9, and 4.1.11, we find

$$Q_C = W_C + H_C = \frac{T\beta}{\kappa}\frac{\pi V_1^2}{(2V_0 + V_r)}$$
$$\frac{Q_C}{W_C} = T\beta. \tag{4.1.12}$$

4.2 Procedure and Results

The SSR was operated at a constant speed with the cold platform temperature held equal to the hot platform temperature, and the heat absorbed at the cold end and the work done by the fluid on the pistons were measured as a function of the temperature.

As the mixture approaches the λ line, the critical velocity of ^{4}He in the superleaks decreases rapidly. Exceeding the critical velocity in the superleaks results in the compression of ^{4}He in each half of the refrigerator and a rapid warming of the fluid; therefore, the critical velocity limits the maximum temperature at which the SSR is able to operate. The relatively long 300 second period for the 36% measurements was chosen in order to keep the ^{4}He below the critical velocity at high temperatures.

The SSR's period, the time necessary to complete one cycle, was manually controlled by varying the current passing through the drive motor. The period was found by measuring the time required for the camshaft to make one or more turns with a stopwatch. The period could be controlled to within ±1%.

T_C was actively controlled by a feedback temperature controller that delivered a voltage to the heater mounted on the cold platform. The circuit used to measure the amount of heat is shown in Fig. 4.1. R_1 is the resistance of the heater in the cold platform of the cryostat, and R_2 is a resistance of known value, either 1 kΩ or 10 kΩ. The power dissipated in the heater is

$$P = V_1 I_1 = \frac{V_1 V_2}{R_2}. \tag{4.2.1}$$

P was averaged over five to ten periods to give $\dot{Q}$, the cooling power of the SSR. The results are shown in Figs. 4.2 through 4.5.

T_H was controlled by a combination of the ^{3}He pot and the heater mounted on the hot platform. The ^{3}He pumping line was throttled at high temperatures with the gate valve upstream of the vacuum pump in order to prevent the excessive boiling of ^{3}He. The heater mounted on the hot platform controlled by a feedback temperature controller similar to that used for the cold platform precisely maintained T_H. The amplitude of oscillation of T_H and T_C during the refrigerator's cycle was a few mK.

The work done by the fluid on the hot and cold pistons shown in Figs. 4.2 through 4.5 were calculated from

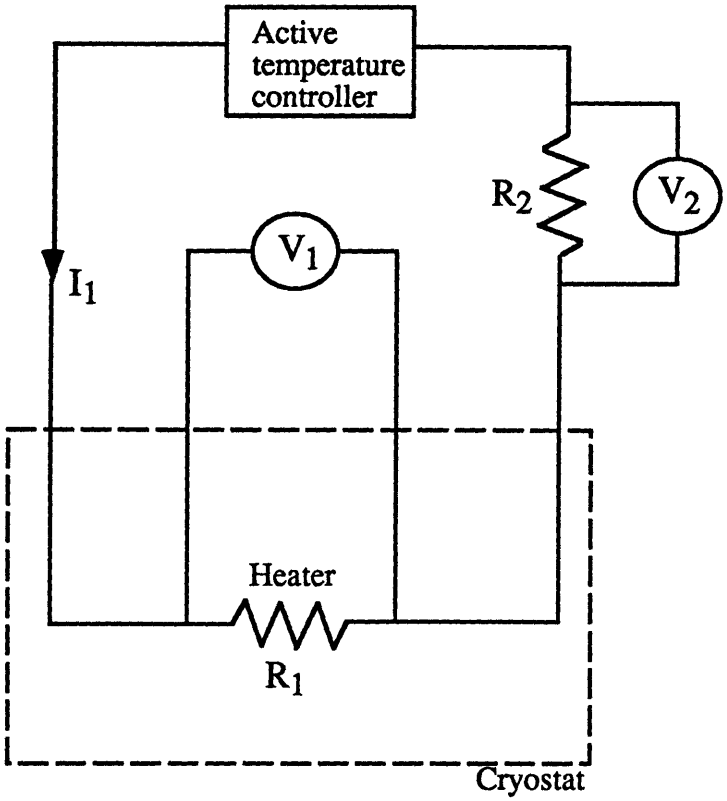

Figure 4.1. The circuit used to measure the cooling power.

$$\dot{W}_H = \frac{1}{n\tau}\int_0^{n\tau} \Delta p \cdot dV_H$$
$$\dot{W}_C = \frac{1}{n\tau}\int_0^{n\tau} \Delta p \cdot dV_C \qquad (4.2.2)$$

where n is an integer between five and ten, Δp is the difference between the pressure in the top refrigerator and the bottom refrigerator, and τ is the refrigerator's period. V_H and V_C were measured using the linear transducers mounted on the 1 K platform. Fig. 4.6 shows an example of p-V diagram from which the piston powers were calculated.

The compressions and expansions of fluid in the refrigerator in reality are not isothermal. This enhanced the amplitude of the pressure oscillation and the cooling power above the values predicted for isothermal operation. We have adjusted the theoretical cooling power and piston powers for this phenomenon by substituting the effective volume for the geometric volume in Eq. 4.1.2. We define as effective volume the volume of fluid that would yield the same amount of pressure rise in isothermal

compression as that of the compression of the actual volume of fluid. For instance, for an ideal gas, the relative changes in pressure for a small adiabatic compression and a small isothermal compression are

$$\left(\frac{dp}{p}\right)_{Adiabatic} \approx -\gamma\frac{dV}{V_{eff}} \tag{4.2.3a}$$

$$\left(\frac{dp}{p}\right)_{Isothermal} \approx -\frac{dV}{V_{actual}} \tag{4.2.3b}$$

where γ is the ratio of specific heats and V_{eff} and V_{actual} are the effective and actual volumes of the fluid. Equating Eqs. 4.2.3a and 4.2.3b, we obtain

$$V_{eff} = \frac{V_{actual}}{\gamma}, \tag{4.2.4}$$

so the effective volume for a small adiabatic compression of an ideal monatomic gas is 3/5 of the actual volume. The effective volume of the refrigerator was found from the measured pressure amplitude as follows. We assume that a volume of $(2V_0+V_r)_{eff}$, or V_{eff}, experiences isothermal compressions and expansions to yield the observed pressure oscillation. The pressure in the top and bottom refrigerators is therefore

$$p_{top}(t) = \frac{1}{\rho RT}\left(\frac{\partial p}{\partial c}\right)_{T,\mu_4}\frac{mRT}{V_{eff}+\sqrt{2}V_1\cos(\omega t+\pi/4)}$$

$$p_{bot}(t) = \frac{1}{\rho RT}\left(\frac{\partial p}{\partial c}\right)_{T,\mu_4}\frac{mRT}{V_{eff}-\sqrt{2}V_1\cos(\omega t+\pi/4)} \tag{4.2.5}$$

where ρ is the mixture's total mass density, R is the gas constant per mass of ^{3}He, c is the mass concentration of the mixture, μ_4 is the chemical potential of ^{4}He, and m is the mass of ^{3}He in each half of the refrigerator. The normalized isothermal compressibility may be evaluated using tables of thermodynamic data by Radebaugh.[14] We use $\Delta p = p_{top} - p_{bot}$ to find the amplitude of pressure oscillation. This may be understood as follows. The total volume of the two halves of the refrigerator changes slightly during the cycle because the effective cross sectional areas of the four bellows are slightly different from one another. This results in the compression of the total liquid ^{3}He-^{4}He mixture which distorts the pressure of the mixture from that of Eq. 4.2.5. However, Δp, the difference between the two, is unaffected since the compression affects p_{top} and p_{bot} equally. Fig. 4.7 is a plot of

the measured p_{top}, p_{bot}, and Δp, as a function of time. Note that Δp is a clean harmonic function while p_{top} and p_{bot} are somewhat distorted due to the compression of the liquid ^{3}He-^{4}He mixture. We will therefore use only Δp when finding the amplitude of the pressure:

$$\begin{aligned}\Delta p &= p_{top} - p_{bot} \\ &= \frac{1}{\rho RT}\left(\frac{\partial p}{\partial c}\right)_{T,\mu_4}\left[\frac{mRT}{V_{eff}+\sqrt{2}V_1\cos(\omega t+\pi/4)} - \frac{MRT}{V_{eff}-\sqrt{2}V_1\cos(\omega t+\pi/4)}\right].\end{aligned} \tag{4.2.6}$$

The maximum Δp occurs at $\omega t = 3\pi/4$ and the minimum Δp at $\omega t = 7\pi/4$, so

$$\begin{aligned}\Delta p_{max} &= \frac{1}{\rho RT}\left(\frac{\partial p}{\partial c}\right)_{T,\mu_4} mRT\left[\frac{1}{V_{eff}-\sqrt{2}V_1} - \frac{1}{V_{eff}+\sqrt{2}V_1}\right] \\ \Delta p_{min} &= \frac{1}{\rho RT}\left(\frac{\partial p}{\partial c}\right)_{T,\mu_4} mRT\left[\frac{1}{V_{eff}+\sqrt{2}V_1} - \frac{1}{V_{eff}-\sqrt{2}V_1}\right].\end{aligned} \tag{4.2.7}$$

Solving for V_{eff} using Eq. 4.2.7,

$$V_{eff} = \left[\frac{1}{\rho RT}\left(\frac{\partial p}{\partial c}\right)_{T,\mu_4}\frac{4\sqrt{2}mRTV_1}{\Delta p_{max}-\Delta p_{min}} + 2V_1^2\right]^{\frac{1}{2}} \tag{4.2.8}$$

where Δp_{max} and Δp_{min} were obtained directly from the readings of pressure gauges. V_{eff} as a function of temperature for the 5.9% and 17% measurements are shown in Figs. 4.8 and 4.9. The "theoretical" piston power and cooling power were then calculated, where V_{eff} was substituted for $(2V_0+V_r)$ in Eq. 4.1.2. Radebaugh's tables[14] of thermodynamic data were used to evaluate the various quantities in Eqs. 4.1.2 and 4.1.3. Details of evaluation are found in Appendix E. The solid and broken lines in Figs. 4.2 through 4.4 are thus a hybrid of theory and experiment, where experimentally determined effective volumes are used in a theory to predict the piston powers and cooling power in order to compensate for the non-isothermal operation of the refrigerator. Eq. 4.1.2 was not evaluated for Fig. 4.5 due to the lack of thermodynamic data for 36% mixtures.

In an attempt to account for the dissipation represented by $\dot{W}_{tot}$, we have added $|\dot{W}_{tot}|/2$ to both the measured $\dot{Q}_C$ and the measured $\dot{W}_C$ in calculating $\left(\dot{Q}_C/\dot{W}_C\right)_{rev}$, the

cooling power divided by the power extracted by the cold piston in a reversible cycle. This may be understood as follows. We imagine a Stirling refrigerator with both the hot and cold pistons held at approximately the same temperature T undergoing four discontinuous movements similar to that described in Section 1.1. The refrigerator goes through a compression stroke at the hot end, a displacement stroke to the cold end, an expansion stroke at the cold end, and a displacement stroke to the hot end. We assume that the piston clearance volume and the regenerator volume are zero. During process (a) which is the compression stroke, we assume that the hot piston changes its volume from V_1 to V_2 and that the temperature is somewhat higher than T due to imperfect heat transfer between the fluid in the piston and the surroundings. The work done by the fluid on the hot piston is

$$W_H^{(a)} = \int_{V_1}^{V_2} p \cdot dV = nR(T+\Delta T)\int_{V_1}^{V_2} \frac{dV}{V} = nR(T+\Delta T)\ln\frac{V_2}{V_1} \tag{4.2.9}$$

where we assume an ideal gas as the working fluid for simplicity. The temperature returns to T at the end of the compression process so dU=0 and

$$Q_H^{(a)} = W_H^{(a)} = nR(T+\Delta T)\ln\frac{V_2}{V_1} \tag{4.2.10}$$

where Q_H is the heat added to the fluid in the hot piston. During process (b) which is the displacement stroke to the cold end, we assume that the hot piston changes its volume form V_2 to 0 and the cold piston form 0 to V_2, all under temperature T. The work done by the fluid on the hot and the cold pistons are

$$W_H^{(b)} = p\Delta V = \frac{nRT}{V_2}(-V_2) = -nRT$$
$$W_C^{(b)} = -W_H^{(b)} = nRT. \tag{4.2.11}$$

During process (c) which is the compression stroke, we assume that the cold piston changes its volume from V_2 to V_1. We further assume that the temperature is somewhat lower than T due to imperfect heat transfer between the fluid in the piston and the surroundings, so the work done by the fluid on the piston is

$$W_C^{(c)} = \int_{V_2}^{V_1} p \cdot dV = nR(T-\Delta T)\int_{V_2}^{V_1} \frac{dV}{V} = nR(T-\Delta T)\ln\frac{V_1}{V_2}. \tag{4.2.12}$$

The temperature returns to T at the end of the expansion process so dU=0 and

$$Q_C^{(c)} = W_C^{(c)} = nR(T-\Delta T)\ln\frac{V_1}{V_2}. \tag{4.2.13}$$

where Q_C is the heat added to the fluid in the cold piston. During process (d) which is the displacement stroke to the hot end, we assume that the hot piston changes its volume form 0 to V_1 and the cold piston form V_1 to 0, all under temperature T. The work done by the fluid on the hot and cold pistons are

$$W_H^{(d)} = \text{nRT}$$
$$W_C^{(d)} = \text{-nRT}. \tag{4.2.14}$$

The total work done by the fluid on the hot piston over a cycle is

$$W_H = -nRT\ln\frac{V_1}{V_2} - nR\Delta T\ln\frac{V_1}{V_2}. \tag{4.2.15}$$

The first term is the work if the refrigerator operated reversibly. The second term is a correction for the irreversible heat transfer in the refrigerator. Similarly, the fluid's work on the cold piston is

$$W_C = nRT\ln\frac{V_1}{V_2} - nR\Delta T\ln\frac{V_1}{V_2}. \tag{4.2.16}$$

The total work done by the fluid on the pistons is therefore

$$W_{tot} = -2nR\Delta T\ln\frac{V_1}{V_2}. \tag{4.2.17}$$

Comparing Eqs. 4.2.16 and 4.2.17, we find

$$W_{C,rev} = W_C + |W_{tot}|/2 \tag{4.2.18}$$

where the subscript "rev" refers to the work in the reversible cycle. The total heat absorbed by the fluid at the cold end is

$$Q_C = nR(T-\Delta T)\ln\frac{V_1}{V_2} = Q_{C,rev} - nR\Delta T\ln\frac{V_1}{V_2} \tag{4.2.19}$$

so the heat absorbed in the reversible cycle is

$$Q_{C,rev} = Q_C + |W_{tot}|/2. \tag{4.2.20}$$

The heat divided by work in the reversible cycle is

$$\frac{Q_{C,rev}}{W_{C,rev}} = \frac{Q_C + |W_{tot}|/2}{W_C + |W_{tot}|/2}. \tag{4.2.21}$$

Note that Q_C, W_C, and W_{tot} may be replaced by $\dot{Q}_C$, $\dot{W}_C$, and $\dot{W}_{tot}$.

Finally, we must account for the heat generated in the background in order to find the total heat absorbed by the fluid in the cold pistons. Eq. C.5 gives an expression for the background heat due to friction generated by the bellows, which was added to the measured cooling power in calculating $\left(\dot{Q}_C/\dot{W}_C\right)_{rev}$ shown in Figs. 4.10 through 4.12:

$$\left(\frac{\dot{Q}_C}{\dot{W}_C}\right)_{rev} = \frac{\dot{Q}_{C,measured} + \dot{Q}_{background} + \left|\dot{W}_{tot}\right|/2}{\dot{W}_{C,measured} + \left|\dot{W}_{tot}\right|/2} \tag{4.2.22}$$

where $\dot{Q}_{C,measured}$ and $\dot{W}_{C,measured}$ are the measured cooling power and cold piston power.

The error bars in Figs. 4.9 and 4.10 are two standard deviations calculated from

$$\Delta\left(\frac{\dot{Q}_C}{\dot{W}_C}\right) = \sqrt{\left(\frac{\Delta\dot{Q}_C}{\dot{Q}_C}\right)^2 + \left(\frac{\Delta\dot{W}_C}{\dot{W}_C}\right)^2} \tag{4.2.23}$$

where Eq. C.5 gives the uncertainty in the background heat and Eq. F.3 gives the uncertainty in $\dot{W}_C$. Error bars calculated for Fig. 4.12 in a similar manner were so small that they were omitted.

The solid curves in Figs. 4.10 through 4.12 were calculated from Eq. 4.1.3 using tables of thermodynamic data by Radebaugh. The broken curves were calculated from Eq. 4.1.12 using approximate values of $p_3(\rho,T)$, which may be obtained by using the ideal Fermi gas equation of state. Details are found in Appendix E.

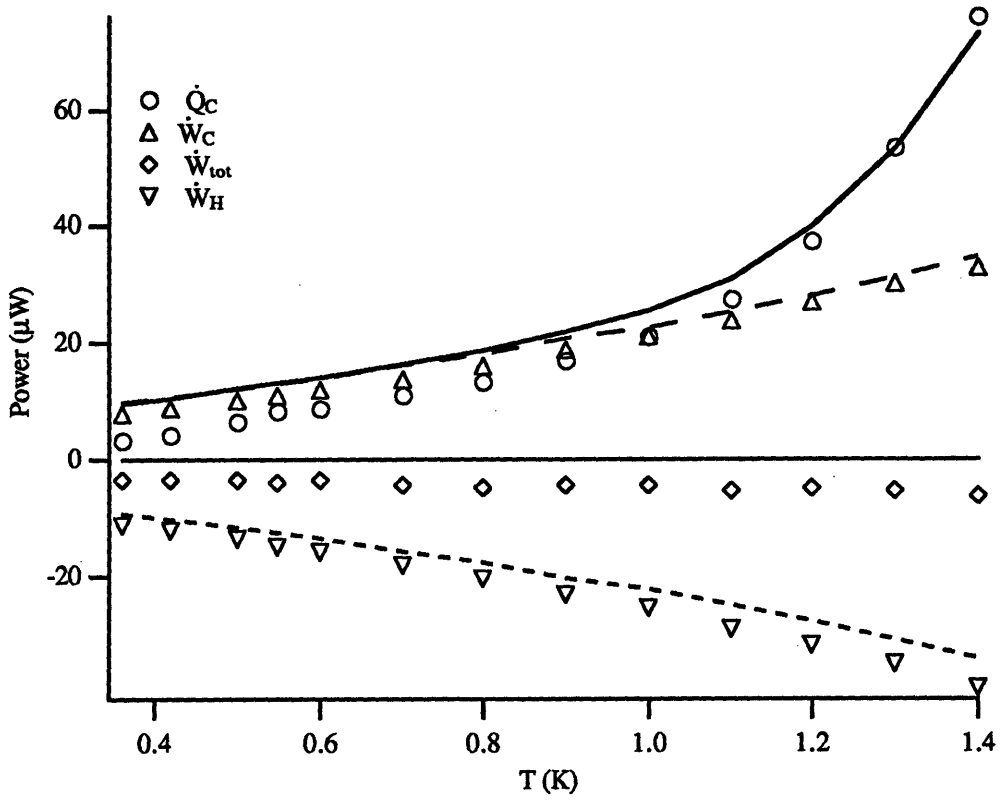

Figure 4.2. Cooling power and piston powers for a 5.9% mixture and a period of 100 s as a function of the common temperature T of the hot and cold platforms. Symbols are measured values. $\dot{Q}_C$ is the heat absorbed at the cold end per unit time, $\dot{W}_C$ is the work done by the fluid on the cold piston per unit time, $\dot{W}_{tot}$ is the total work done by the fluid on the pistons per unit time, and $\dot{W}_H$ is the work done by the fluid on the hot piston per unit time. The hot and cold piston swept volumes were both 0.78 cm^3. The solid curve and the broken lines are the theoretical cooling power and piston powers, respectively, calculated from Eq. 4.1.2 using Radebaugh's tables. Eq. 4.1.2 is multiplied by twice the operating frequency because our apparatus consists of two Stirling refrigerators operating in parallel.

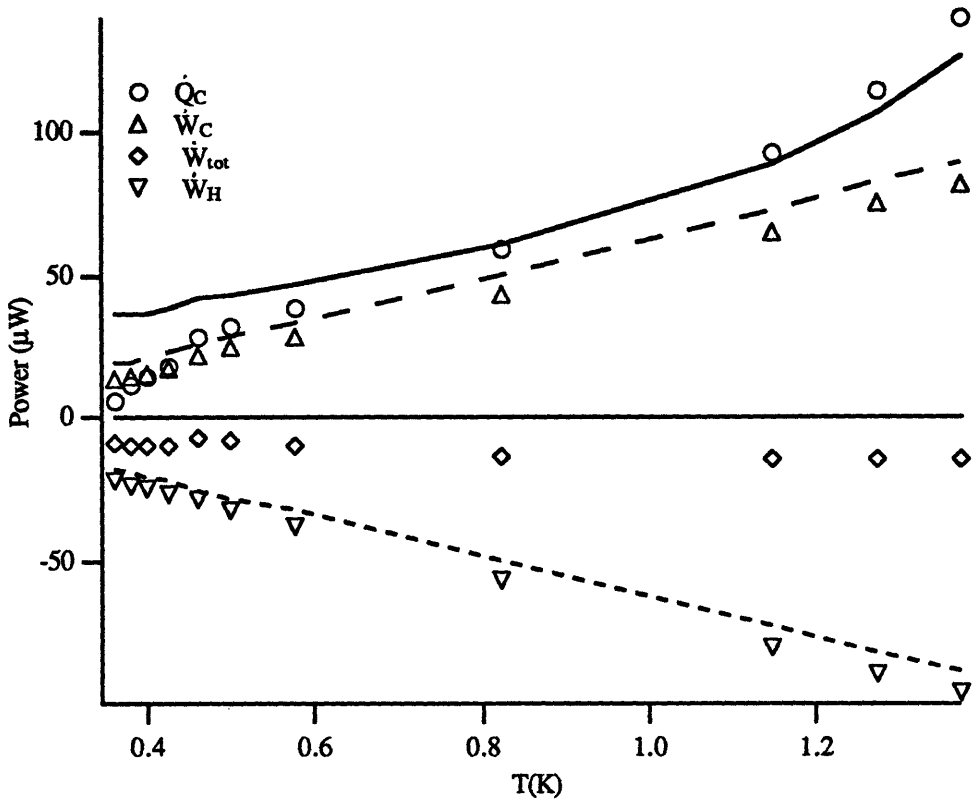

Figure 4.3. Cooling power and piston powers of the SSR for a 17% mixture and a period of 100 s as a function of the common temperature T of the hot and cold platforms. Symbols are measured values. $\dot{Q}_C$ is the heat absorbed at the cold end per unit time, $\dot{W}_C$ is the work done by the fluid on the cold piston per unit time, $\dot{W}_{tot}$ is the total work done by the fluid on the pistons per unit time, and $\dot{W}_H$ is the work done by the fluid on the hot piston per unit time. The hot and cold piston swept volumes were 0.76 cm^3 and 0.82 cm^3, respectively. The solid curve and the broken lines are the theoretical cooling power and piston powers, respectively, calculated from Eq. 4.1.2 using Radebaugh's tables. Eq. 4.1.2 is multiplied by twice the operating frequency because our apparatus consists of two Stirling refrigerators operating in parallel.

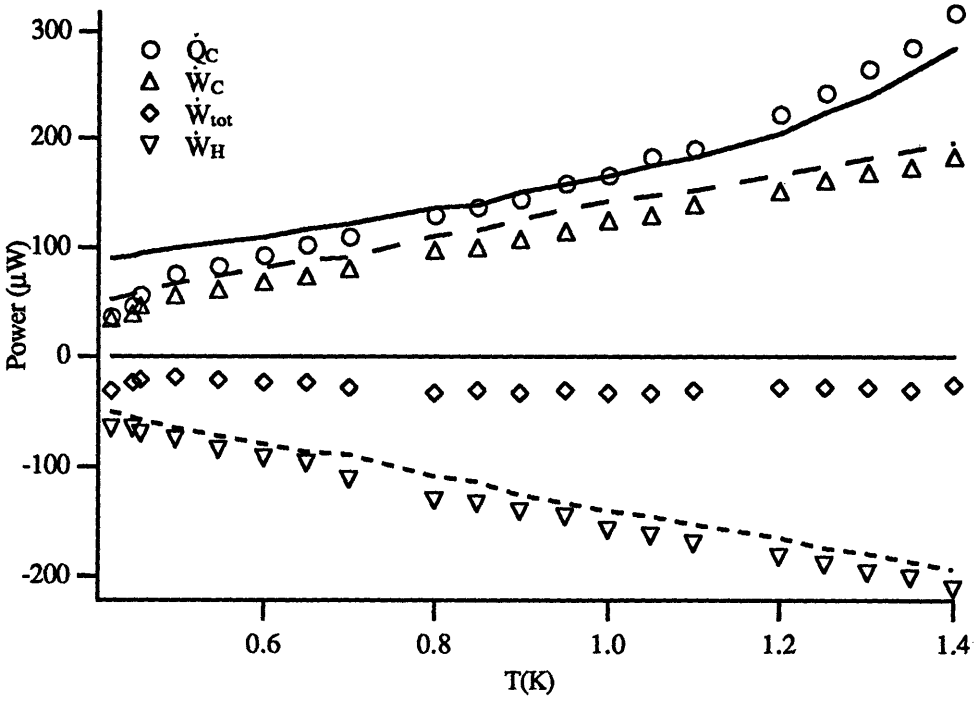

Figure 4.4. Cooling power and piston powers of the SSR for a 17% mixture and a period of 80 s as a function of the common temperature T of the hot and cold platforms. Symbols are measured values. $\dot{Q}_C$ is the heat absorbed at the cold end per unit time, $\dot{W}_C$ is the work done by the fluid on the cold piston per unit time, $\dot{W}_{tot}$ is the total work done by the fluid on the pistons per unit time, and $\dot{W}_H$ is the work done by the fluid on the hot piston per unit time. The hot and cold piston swept volumes were 1.02 cm^3 and 0.98 cm^3, respectively. The solid curve and the broken lines are the theoretical cooling power and piston powers, respectively, calculated from Eq. 4.1.2 using Radebaugh's tables. Eq. 4.1.2 is multiplied by twice the operating frequency because our apparatus consists of two Stirling refrigerators operating in parallel.

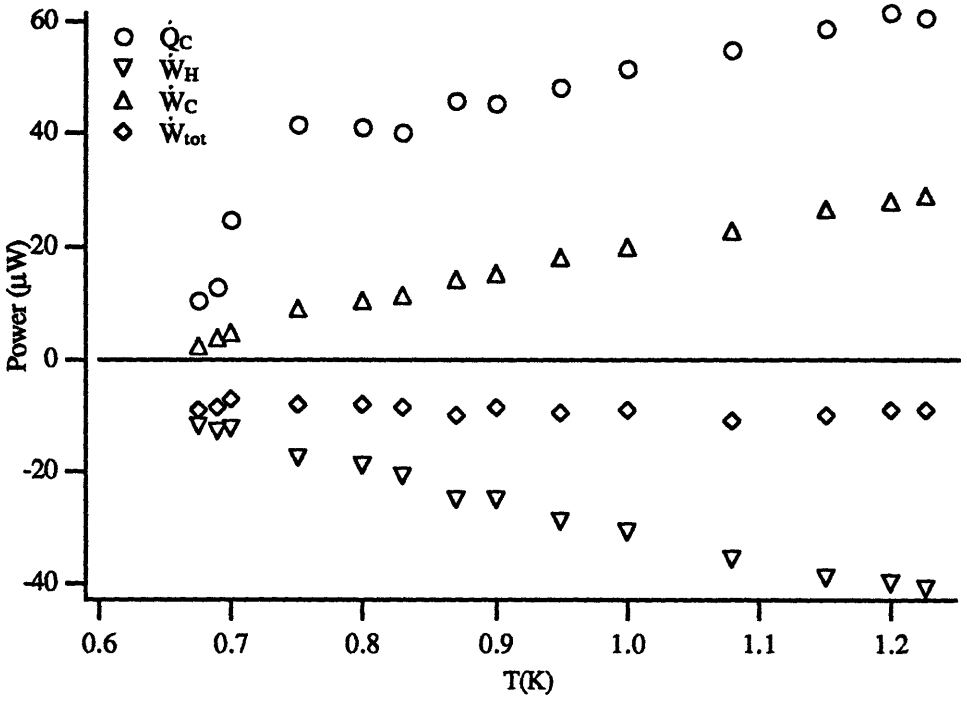

Figure 4.5. Measured cooling power and piston powers of the SSR for a 36% mixture and a period of 300 s as a function of the common temperature T of the hot and cold platforms. Symbols are measured values. $\dot{Q}_C$ is the heat absorbed at the cold end per unit time, $\dot{W}_C$ is the work done by the fluid on the cold piston per unit time, $\dot{W}_{tot}$ is the total work done by the fluid on the pistons per unit time, and $\dot{W}_H$ is the work done by the fluid on the hot piston per unit time. The hot and cold piston swept volumes were 0.76 cm^3 and 0.80 cm^3, respectively.

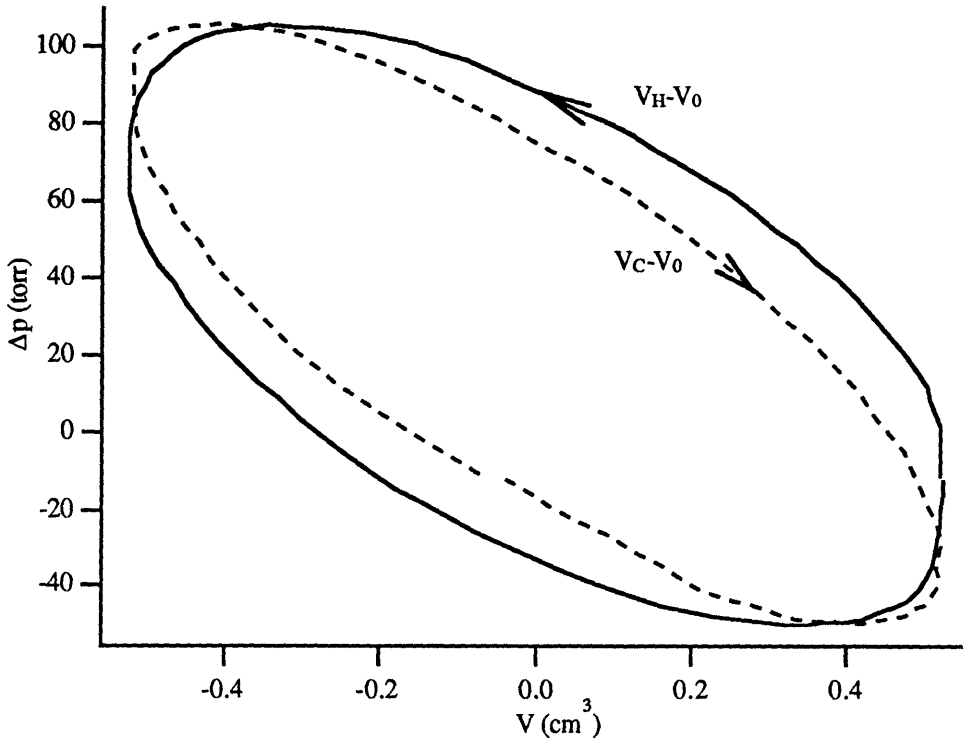

Figure 4.6. Indicator diagrams of the hot and cold platform pistons for a 17% mixture at 1 K. The pressure difference in Fig. 4.2 is plotted as a function of the hot and cold piston displacement volumes. The arrows show the direction in which the diagrams are traced during the operation of the SSR. The pressure difference is not centered around zero due to a shift in the pressure gauge's calibration.

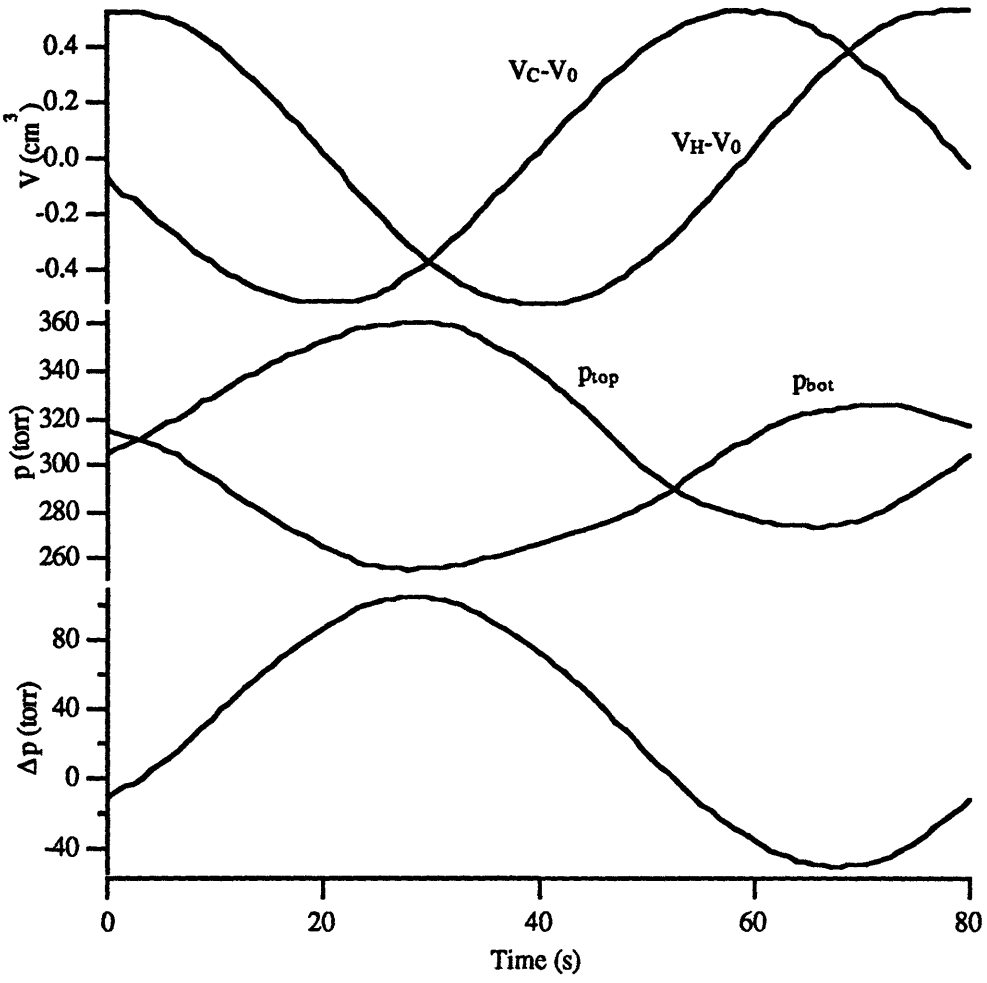

Figure 4.7. The pressures and piston volumes during the cycle. This is for a 17% mixture at 1 K. The top figure shows the hot and cold piston displacement volumes, where V_0 is the time average of the volume in the piston. The center figure shows the readout of the pressure gauges for the top and bottom refrigerators and the bottom figure shows p_{top}-p_{bot}. The pressure difference is not centered around zero due to a shift in the pressure gauge's calibration.

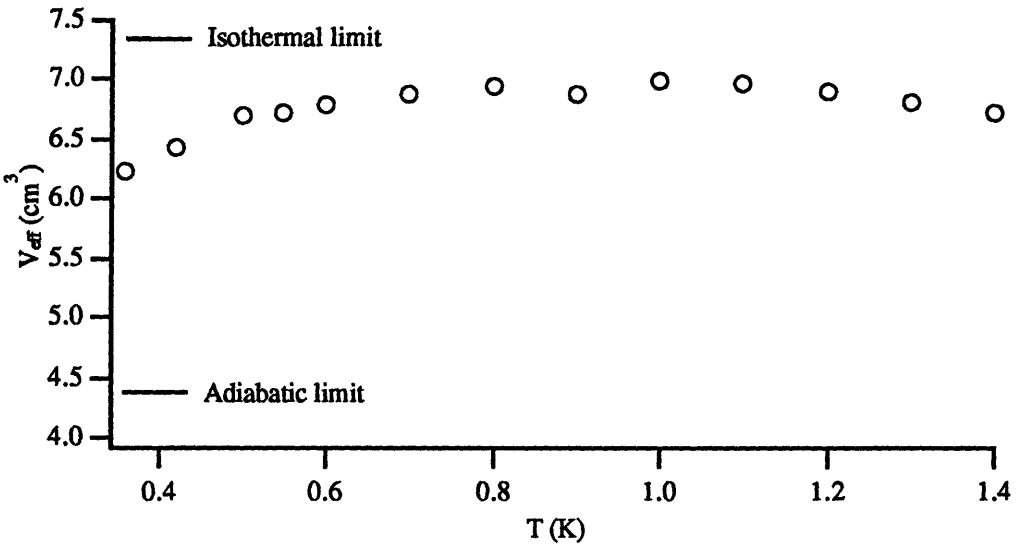

Figure 4.8. The effective volume for the 5.9% measurements, calculated using Eq. 4.2.8, as a function of the common temperature T of the hot and cold platform temperatures.

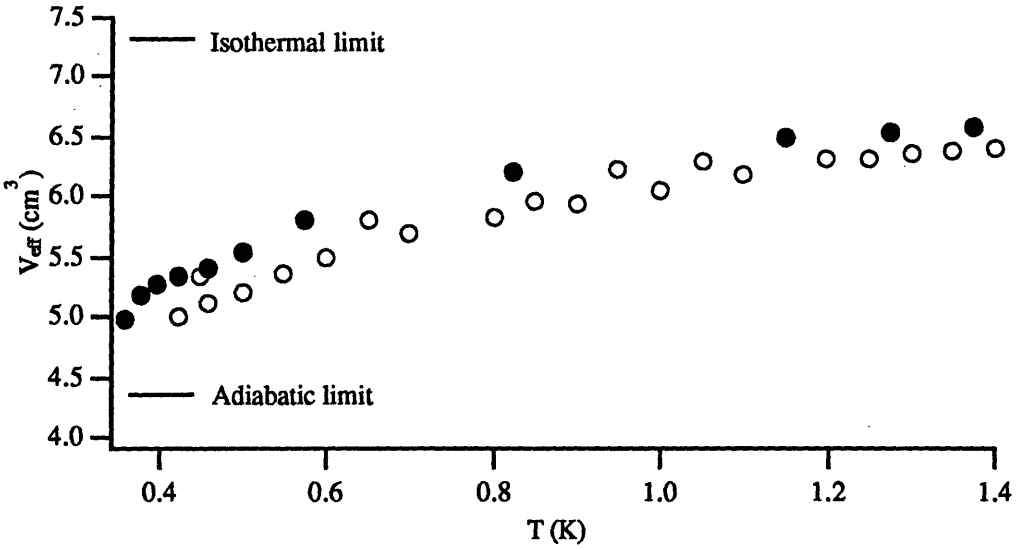

Figure 4.9. The effective volume for the 17% measurements, calculated using Eq. 4.2.8, as a function of the common temperature T of the hot and cold platform temperatures. The black and the white symbols correspond to the measurements of Figs. 4.3 and 4.4, respectively, which differ only in the piston swept volumes.

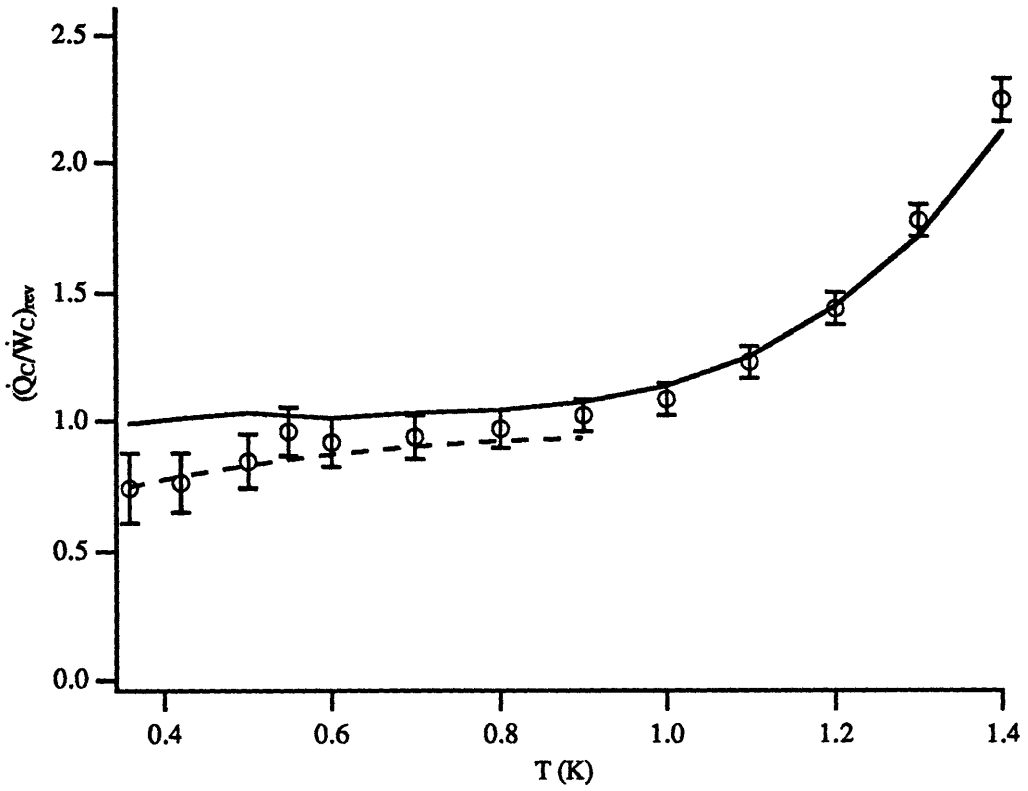

Figure 4.10. Ratio of reversible cooling power to reversible mechanical power extracted by the cold piston for the 5.9% measurements. The circles are calculated from Eq. 4.2.22 using measured values. Fermi Temperature for this concentration is 0.34 K. The solid line is Eq. 4.1.3 using Radebaugh's tables and the dashed line is Eq. 4.1.12 using an ideal Fermi gas. Error bars are two standard deviations.

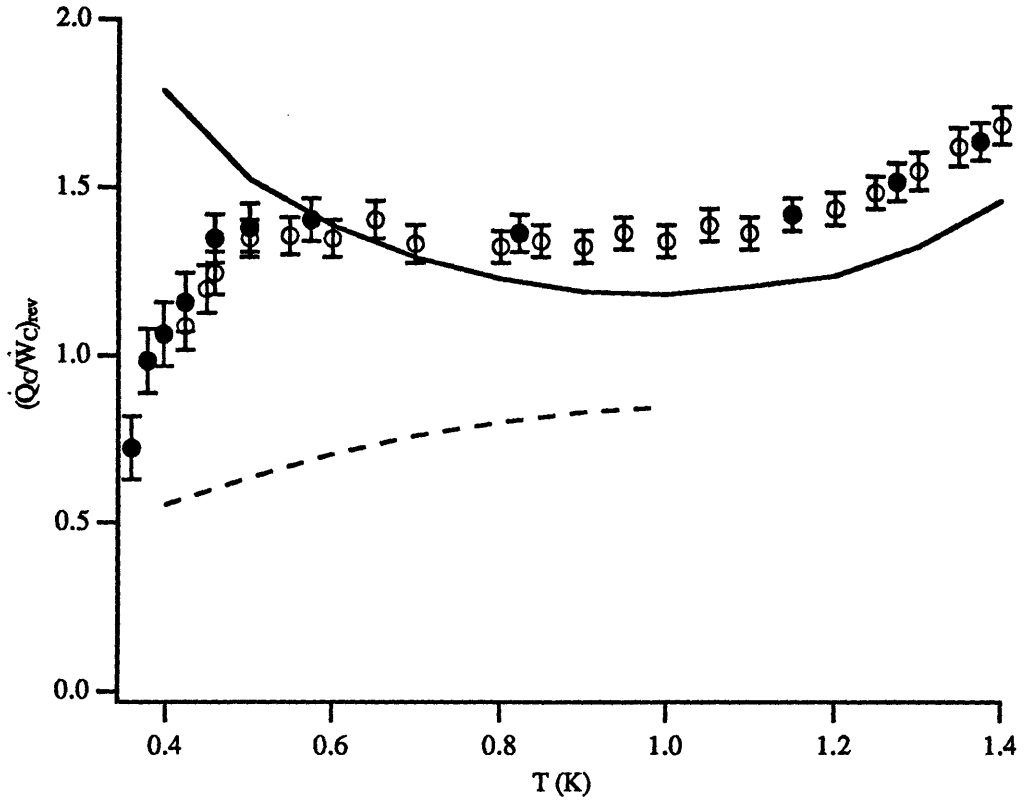

Figure 4.11. Ratio of reversible cooling power to reversible mechanical power extracted by the cold piston for the 17% measurements. The symbols are calculated from Eq. 4.2.22 using measured values. The black and the white symbols correspond to the measurements of Figs. 4.3 and 4.4, respectively. They differ only in the piston swept volumes. The solid line is Eq. 4.1.3 using Radebaugh's tables and the dashed line is Eq. 4.1.12 using an ideal Fermi gas. Error bars are two standard deviations. Fermi temperature for this concentration is 0.74 K. The effective phase separation temperature discussed in Section 4.3 is 0.45 K.

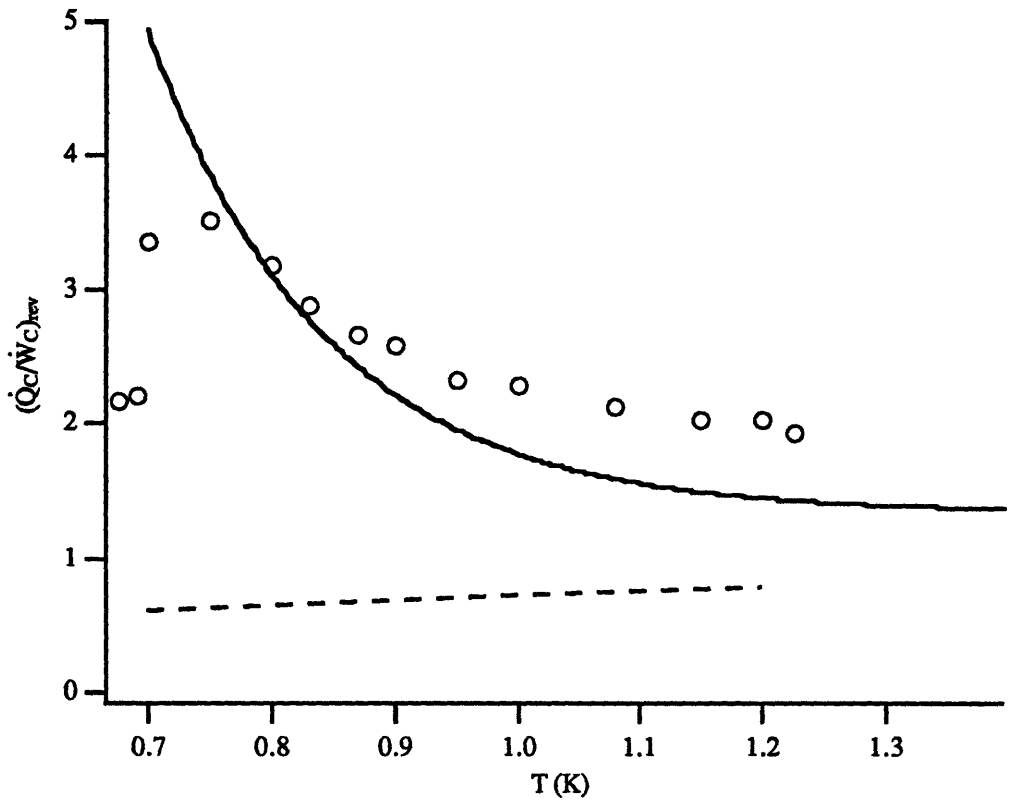

Figure 4.12. Ratio of reversible cooling power to reversible mechanical power extracted by the cold piston for the 36% measurements. The symbols are calculated from Eq. 4.2.22 using measured values. The solid line is Eq. 4.1.3 using Radebaugh's tables and the dashed line is Eq. 4.1.12 using an ideal Fermi gas. Fermi temperature for this concentration is 1.19 K. The effective phase separation temperature discussed in Section 4.3 is 0.71 K.

4.3 Discussion

Fig. 4.2 shows a good agreement between the "theoretical" and the measured cooling power and the piston powers at the highest temperatures, where we put the word theoretical in quotation marks because the lines are, as stated in Section 4.2, hybrids of theory and experiment.

The negative total power is due to the irreversible pressure oscillations experienced by the fluid. This phenomenon is analytically treated in the previous section, but we will seek a physical interpretation of it here. In a piston with a constant mass of fluid in which the fluid behaves perfectly isothermally or adiabatically, the fluid acts as a reversible spring. It removes a certain amount of work from the piston when the piston compresses the gas, and gives the same amount of work back to the piston when the piston expands

the gas. The net work done by the piston is therefore zero. In a piston in which the fluid behaves neither isothermally nor adiabatically, however, the fluid heats up when the piston compresses the gas because the compression is not isothermal. Some of this heat is released to the surroundings because the compression is not adiabatic, thereby lowering the fluid's pressure. Thus, the fluid's pressure when the piston expands the gas is somewhat lower than the fluid's pressure when the piston compresses the gas, and the net work done by the piston on the fluid is positive. The fluid in the regenerator is essentially isothermal, so its pressure oscillations are reversible. In contrast, fluid in the pistons about a thermal penetration depth δ_κ from the nearest massive solid surface experiences irreversible pressure oscillations, absorbing work and releasing it to the surroundings as heat.

In Fig. 4.2, the measured cooling power at lower temperatures is well below the values predicted by Eq. 4.1.2 using Radebaugh's tables[14] for the equations of state, even though the piston powers show a good agreement with the prediction. Some of the reasons are the background heat generated by the friction in the bellows and the entropy created by irreversibility. The data above 1 K, on the other hand, show an excellent agreement with the theory. The cooling power is significantly enhanced above the values predicted based on an ideal working fluid due to the phonon and roton excitations of ^{4}He.

Fig. 4.10 shows the ratio of the cooling power and the piston power corrected for those two phenomena. It becomes apparent below 0.6 K that the cooling power agrees better with the prediction using the ideal Fermi gas as the equation of state, although there is a considerable amount of uncertainty due to the 1 μW uncertainty in the background heat. Fermi temperature[7] for a 4.9% concentration is 0.34 K, which is only slightly below the lowest data point for this set of measurements. Note that $(\dot{Q}_C / \dot{W}_C)_{rev}$ predicted by Eq. 4.1.12 is valid only at low temperatures where the contribution of ^{4}He to the thermodynamics of the mixture is negligible.

Fig. 4.11 shows the reversible gross cooling power divided by the reversible piston power for the 17% mixture. The measurements show a fair qualitative agreement with the prediction based on the equation of state using Radebaugh's tables for temperatures over 0.9 K, although they are about 20% higher than the prediction. The measurements start deviating at lower temperatures, however, where $(\dot{Q}_C / \dot{W}_C)_{rev}$ does not increase with decreasing temperature as the solid curve suggests. $(\dot{Q}_C / \dot{W}_C)_{rev}$ remains flat at around 1.35 until near the phase separation temperature, where it exhibits a sharp drop. $(\dot{Q}_C / \dot{W}_C)_{rev}$ does not resemble that predicted using either Radebaugh's tables or the ideal Fermi gas. It is somewhere between the two, although it is closer to the former than

to the latter. Fermi temperature[7] for a 17% mixture is 0.74 K, so some of the data points are well into the Fermi regime.

Fig. 4.12 shows the $(\dot{Q}_C / \dot{W}_C)_{rev}$ for 36% mixture. Radebaugh's tables only give the mixture's properties up to a molar concentration of 30%, so $(\dot{Q}_C / \dot{W}_C)_{rev}$ was extrapolated linearly based on the values at 25% and 29%. The extrapolated $(\dot{Q}_C / \dot{W}_C)_{rev}$, given at discrete temperatures in increments of 0.1 K, was curve fitted using an exponential function, yielding the curve shown in Fig. 4.12. The measured $(\dot{Q}_C / \dot{W}_C)_{rev}$ show a fair agreement with the values predicted using Radebaugh's tables at all temperatures except near and below the phase separation temperature, though they are about 20% higher than the predicted values at temperatures above 1 K. Fermi temperature for a 36% mixture is 1.19 K, so virtually all of the data points are in the Fermi regime.

The effective volume in each half of the refrigerator for the 5.9% measurements shown in Fig. 4.8 is uniformly lower than the geometric volume of 7.3 cm^3, implying that the compressions and expansions of the fluid are not isothermal. This is due to both the thermal resistance in the fluid itself and the thermal boundary resistance between the copper block and the fluid. The former effect may be understood by considering the thermal penetration depth of the ^{3}He-^{4}He mixture

$$\delta_\kappa = \sqrt{\frac{\kappa}{\pi \rho C_p f}} \tag{4.3.1}$$

where κ is the thermal conductivity of the mixture, ρ and C_p are the density and heat capacity of the total mixture, and f is the frequency of the refrigerator. Using published figures[12,14] for C_p and κ, δ_κ is found to stay essentially constant at around 7 mm below 0.9 K. However, it decreases sharply above 1 K due to the rapidly increasing heat capacity of the ^{4}He component of the mixture, to 3.8 mm at 1.4 K. Since the fluid in the convolutions in the bellows is as much as 6 mm away from massive solid surfaces, some of the fluid is farther away from massive solid surfaces than the thermal penetration depth at temperatures above 1 K. The compressions and expansions therefore become more adiabatic above 1 K and lower the effective volume. We do not understand the decrease of the effective volume below 0.8 K.

The effective volume for the 17% measurements shown in Fig. 4.9 is significantly lower than that for the 5.9% measurements. In fact, it is closer to the adiabatic limit than the isothermal limit at the lowest temperatures. This is partly due to the shorter thermal

penetration depth of about 4 mm below 1 K that results from the 17% mixture's higher heat capacity[14] and lower thermal conductance.[12]

It is apparent from some of the figures in the previous section that the cooling power exhibits a sharp drop as the temperature approaches the phase separation temperature. We will take a closer look at this phenomenon.

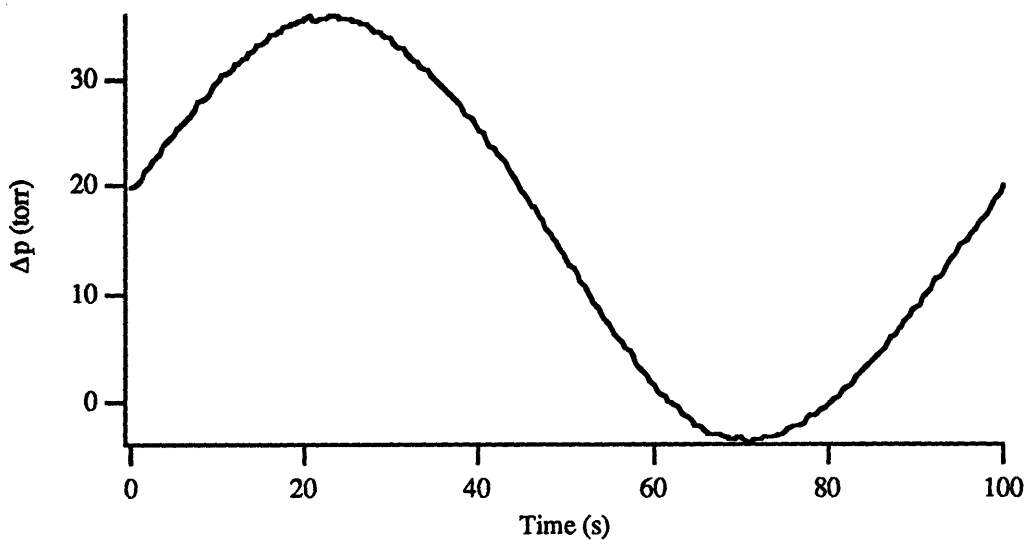

Figure 4.15. Pressure difference between the top and bottom refrigerators as a function of time in the phase separated regime. The refrigerator's period was 100 s, the hot and cold platform temperatures were both 0.425 K, the mixture was 17%, and the hot and cold piston swept volumes were 0.76 cm^3 and 0.82 cm^3, respectively. The effective phase separation temperature, explained in Section 4.3, is 0.45 K. The pressure difference is not centered around zero due to a shift in the pressure gauge's calibration.

Fig. 4.15 shows the pressure as a function of time in the phase separated regime. We can gain an insight into the dynamics of phase separation in the SSR from Fig. 4.15. If the time constant for the phase change were much shorter than the SSR's period, some of the phase separated pure ^{3}He would "evaporate" into the mixture as the pistons expand the fluid and "condense" into pure ^{3}He as the pistons compress the fluid. Since the mass of ^{3}He in the dilute phase would decrease when the pistons compress the gas, we would expect the pressure's peaks to be flattened if this were the case. If, on the other hand, the time constant for the phase change were much longer than the SSR's period, the amount of phase separated pure ^{3}He would remain approximately constant throughout the SSR's cycle, resulting in an undersaturated mixture in the cold piston through most of the cycle. The pressure's peaks would not show any flattening if this were the case. The time constant for the phase change may be estimated using the following model. We assume a

^{3}He-^{4}He mixture in a vertical cylinder of cross section A of 3 cm^2, with a puddle of pure ^{3}He in the top whose thickness is h. The concentration of the dilute phase[14] at this temperature is around 14%, while the concentration of the concentrated phase is close to 100%. Assuming that one mole of 17% mixture has phase separated into α mole of 14% mixture and (1-α) mole of 100% mixture, the amount of ^{3}He before and after the separation are equal, which means

$$1 \text{ mol} \times 17\% = \alpha \text{ mol} \times 14\% + (1-\alpha)\text{mol} \times 100\%, \tag{4.3.2}$$

yielding α=0.97 mol. This results in 0.03 mol of 100% mixture. In other words, 3% of the mixture is in the concentrated phase. The cold piston contains 3.2 cm^3 of mixture, so we have approximately 0.1 cm^3 of 100% mixture in the cold piston. This corresponds to a thickness h of 0.03 cm. In order for this pure ^{3}He to dissolve into the mixture, an amount of heat

$$\dot{Q} = -LA\, dh/dt \approx -LA\, h/\tau = -\kappa A\, dT/dx \approx -\kappa A\, dT/h \tag{4.3.3}$$

must flow into the puddle of pure ^{3}He, where L is the latent heat of phase change, t is time, τ is the time constant for the pure ^{3}He to dissolve into the mixture, κ is the thermal conductivity of ^{3}He, T is the temperature, and x is the vertical coordinate. Solving Eq. 4.3.3 for τ, we obtain

$$\tau \approx -Lh^2/\kappa dT. \tag{4.3.4}$$

This is the amount of time it takes for the puddle of pure ^{3}He to completely dissolve into the dilute phase. We assume that the thermal boundary resistance is negligible. L is 0.9 MJ/m^3 at this temperature, and κ is 0.04 W/m-K.[12] We assume that dT is 10 mK, which is the order of magnitude of a temperature difference we can expect in the refrigerator. The above expression yields a time constant of 800 s, which is much longer than the SSR's period of 80 s. This suggests that the amount of pure, phase separated ^{3}He in the refrigerator does not change significantly during the cycle, and that consequently the pressure's peaks would not show a significant amount of flattening. This explanation is consistent with the observed pressure oscillations on Fig. 4.15.

Figs. 4.3 through 4.5, 4.11, and 4.12 show that the cooling powers drop sharply when the SSR approaches the phase separation temperature. However, several

phenomena imply that the drop in Q/W is not caused by phase separation of the ^{3}He-^{4}He mixture. First, Eq. 4.1.4 implies that the volume of the SSR is

$$V(t) = (2V_0+V_r)+\sqrt{2}\,V_1\cos(\omega t+\pi/4). \qquad (4.3.5)$$

The minimum volume during the cycle for the conditions of Fig. 4.11 is therefore 6.6 to 6.7 cm^3, which is approximately 10% lower than the time average volume of 7.3 cm^3. The maximum ^{3}He concentration during the cycle is therefore approximately $1.1\times 17\% = 19\%$, corresponding to a phase separation temperature[14] of 0.45 K. However, Fig. 4.11 indicates that Q/W for the 17% mixture starts dropping at around 0.47 to 0.48 K, which is somewhat higher than the phase separation temperature appropriate to the refrigerator. This effect is also seen on the 36% data. The maximum concentration in the refrigerator for the measurements with the 36% average concentration is $1.1\times 36\% = 40\%$, corresponding to a phase separation temperature of 0.71 K, while Fig. 4.12 indicates that Q/W starts dropping at around 0.73 to 0.74 K. Further, phase separation of the mixture would result in the decrease of the effective concentration of the working fluid, lowering both the cooling power and the piston power and thus preserving Q/W to first approximation. The decrease in the effective concentration of the working fluid that results form phase separation is inadequate to explain the drop in Q/W in the vicinity of the phase separation temperature. The above two phenomena imply that the drop in Q/W is not caused by phase separation of the mixture, but by some other sudden change in the fluid's properties.

This transition may be caused by the critical velocity. We suspect that the critical velocity decreases as the mixture approaches the phase separation temperature, causing the mixture to exceed the critical velocity and lower the cooling power. For a saturated mixture below 100 mK, Zeegers *et al.*[20] empirically found a critical velocity of

$$v_c = (K/d)\ln(d/d_0) \qquad (4.3.6)$$

where $K=0.05$ cm^2/s, d is the diameter of the capillary, and $d_0=15$ μm. Although both the temperature and the concentration used to find Eq. 4.3.6 are significantly lower than those used in our refrigerator, we are unaware of any other published figure for the critical velocity of superfluid ^{3}He-^{4}He mixtures. This formula would nevertheless allow us to compare the critical velocities calculated at various locations. Three possible locations were chosen: the capillary that connects the heat exchanger to the piston, the holes in the cold heat exchanger, and the regenerator. The maximum ^{3}He velocity, which is the

maximum velocity the normal component of the fluid would attain during the refrigerator's cycle, was numerically estimated from the formula[3]

$$Av_n = \frac{V_C\dot{V}_H - (V_H + V_r)\dot{V}_C}{V_C + V_r + V_H} \tag{4.3.7}$$

where A is the cross sectional area of a path between the cold piston and the regenerator. Eq. 4.3.7 gives the instantaneous volume flow rate of the normal component of the mixture averaged over the cross section of the path. The results are shown in Table 4.1. Having both the highest maximum ^{3}He velocity during the cycle and the lowest critical velocity given by Eq. 4.3.6, it appears that the capillary connecting the heat exchanger and the piston is the most likely place where the flow is exceeding the critical velocity.

Location	Path between piston and heat exchanger	Cold heat exchanger	Regenerator
Diameter	0.8 mm	0.51 mm	0.229 mm
Max. v_n	4.3 cm/s	0.9 cm/s	0.23 cm/s
v_c	2.5 cm/s	3.5 cm/s	6.0 cm/s

Table 4.1. The maximum ^{3}He velocity and the critical velocities at various points in the refrigerator The maximum v_n during the refrigerator's cycle was calculated for the conditions of Fig. 4.15 using Eq. 4.3.7. The critical velocity is calculated from Eq. 4.3.6 using the diameters shown.

Note in Figs. 4.8, 4.9, and 4.11 that the magnitude of the total work done by the fluid on the piston increases very slightly when the SSR cools below the phase separation temperature. It has been indicated above that the amount of phase separated, concentrated ^{3}He does not change significantly during the cycle, but some phase change still occurs. Some of the mixture in the dilute phase "condenses" and increases slightly the amount of pure ^{3}He during compression, which increases the mixture's temperature. Some of the pure ^{3}He "evaporates" and dissolves into the dilute phase during expansion, which decreases the mixture's temperature. The presence of phase separated pure ^{3}He in the refrigerator thus exaggerates the temperature oscillation of the mixture during the cycle. This increases the entropy created by irreversibility and consequently the magnitude of the total work done by the fluid on the piston. This slight increase in magnitude of the total piston power may be used as an indication that the mixture in the refrigerator has phase separated.

4.5 Conclusion

The cooling powers for the 5.9% and 17% mixtures above 1 K are significantly enhanced above the values predicted based on an ideal working fluid due to the phonon and roton excitations of ^{4}He.

The cooling power for the 5.9% mixture near the Fermi temperature is lower than the values predicted based on an ideal working fluid due to Fermi degeneracy. For the 17% and 36% mixture measurements, on the other hand, the cooling power below the Fermi temperature is higher than the ideal gas values and does not resemble the predictions based on the ideal Fermi gas, casting doubt on the validity of the Fermi gas approximation. They resemble instead the predictions based on the equation of state of Radebaugh's tables.

Further observations include the following. The compressions and expansions of fluid in the refrigerator are found to be non-isothermal due to imperfect heat transfer between the copper platform and the fluid. The mixture exceeding the critical velocity is suspected be the cause of the drop in the measured cooling power near or below the phase separation temperature.

Chapter 5

The SSR Cooling Power Measurements

Using a 6.6% mixture, Brisson and Swift achieved a temperature of 0.3 K with the SSR with the heat rejected at 1.2 K. In this chapter we investigate the SSR's operation with the heat rejected at around 0.4 K, which would allow a significantly lower temperature. We also investigate the cooling power with high concentration mixtures which would increase the cooling power proportionately. We use Schmidt analysis in order to gain a rough analytic estimate of the cooling power with the cold platform temperature different form the hot platform temperature. This model assumes an ideal working fluid and isothermal compressions and expansions in the pistons.

5.1 Theory

Professor Gustav Schmidt of the German Polytechnic Institute published in 1871 his analysis of the Stirling cycle.[18] The principal assumption of his analysis is that the gas in the hot piston is at a constant hot temperature and that the gas in the cold piston is at a constant cold temperature. Assuming an ideal gas, this isothermal assumption makes it possible to generate a simple expression for the working gas pressure as a function of the volume variations. He also assumed a linear temperature profile in the regenerator.

We assume identical average volumes V_0 and swept volumes V_{sw} for the hot and cold pistons with a 90° phase between the pistons so that the hot and cold piston volumes (V_H, V_C) are:

$$V_H = V_0 + \frac{V_{sw}}{2} \sin \omega t$$

$$V_C = V_0 + \frac{V_{sw}}{2}\cos \omega t. \tag{5.1.1}$$

Under these circumstances, cooling power, which is the amount of heat absorbed at the cold platform per unit time, is found to be

$$\dot{Q}_{\text{Schmidt}} = \frac{f\frac{\pi}{2}\left(\frac{V_{sw}}{V_0}\right)^2 nRT_H\left[\frac{\alpha}{1+\alpha}\right]^2}{\left[1-\frac{V_r}{V_0}\frac{\alpha \ln \alpha}{1-\alpha^2}\right]^2} \tag{5.1.2}$$

to lowest order in (V_{sw}/V_0), where f is the refrigerator's operating frequency, n is the number of moles of working fluid in the refrigerator, R is the universal gas constant, T_H is the hot platform temperature α is T_C/T_H, T_C is the cold platform temperature, and V_r is the volume of the regenerator. We have multiplied the standard Schmidt result by twice the operating frequency because our refrigerator consists of two Stirling refrigerators operating in parallel. Details of derivation are found in Appendix H.

5.2 Procedure and Results

The SSR's cooling power was measured as a function of the mixture's average concentration, hot platform temperature, cold platform temperature, and the operating speed. T_C was actively controlled by a feedback controller that delivered current to the heater mounted on the cold platform, and the heat delivered averaged over five to ten periods determined the cooling power. With the exception of the 4.9% mixture, T_H was actively controlled by a combination of the ^{3}He evaporation refrigerator and a feedback controller delivering current to the heater mounted on the hot platform. For the 4.9% mixture, T_H was kept as cold as the ^{3}He evaporation refrigerator allowed. This was done in order to find the performance of the ^{3}He evaporation refrigerator-SSR system as a whole. The maximum frequency of SSR operation was limited by the ^{3}He refrigerator's cooling power in all of the runs. Running the SSR too fast put too large a heat load on the hot platform and resulted in the ^{3}He pot quickly running dry. The methods used to measure the cooling power of the SSR here are analogous to the methods used for the uniform temperature SSR measurements described in detail in Chapter 4. The results are shown in Figs. 5.1 through 5.4.

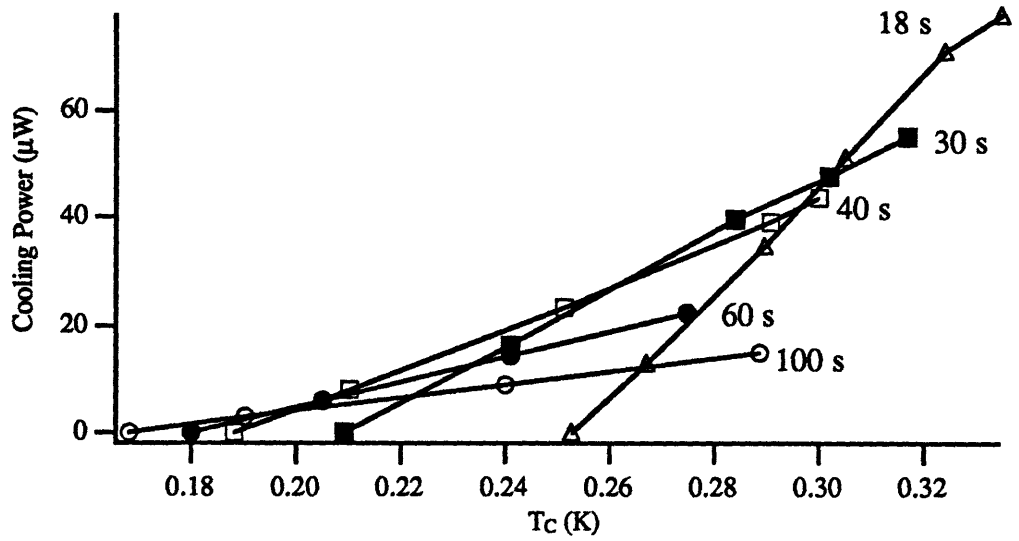

Figure 5.1. The SSR's cooling power versus T_C for a 4.9% mixture. Here and in the following figures, each set is labeled with the SSR's period, and the lines are only guides to the eye. The hot and cold piston swept volumes were 1.53 cm^3 and 1.56 cm^3, respectively. The hot platform temperature was approximately 0.450 K, 0.417 K, 0.407 K, 0.400 K, and 0.387 K for the period of 18, 30, 40, 60, and 100 seconds, respectively.

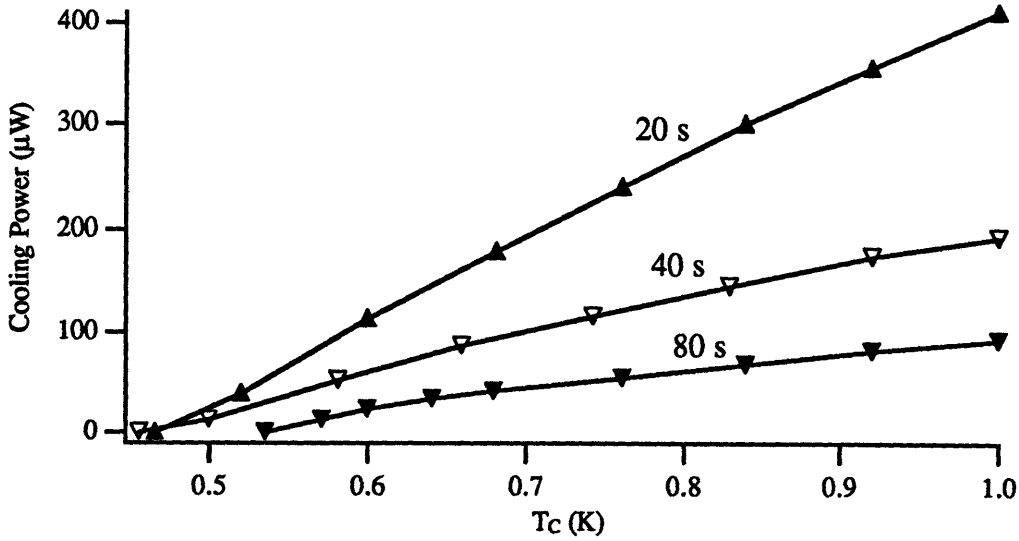

Figure 5.2. The SSR's cooling power versus T_C for a 17% mixture and a hot platform temperature of 1 K. The hot and cold piston swept volumes were 0.763 cm^3 and 0.811 cm^3, respectively.

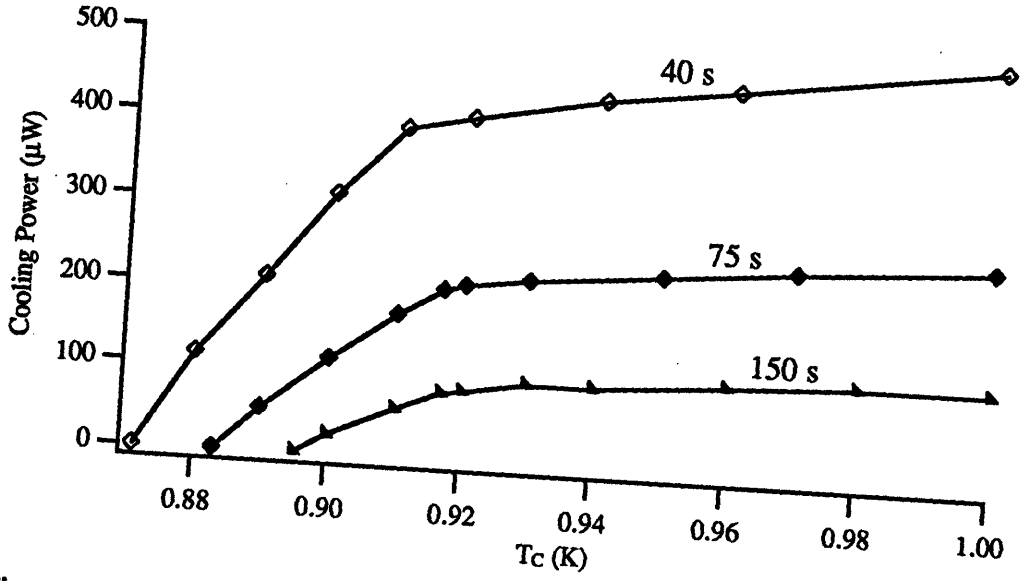

Figure 5.3. The SSR's cooling power versus T_C for a 36% mixture and a hot platform temperature of 1 K. The hot and cold piston swept volumes were 0.767 cm^3 and 0.811 cm^3, respectively.

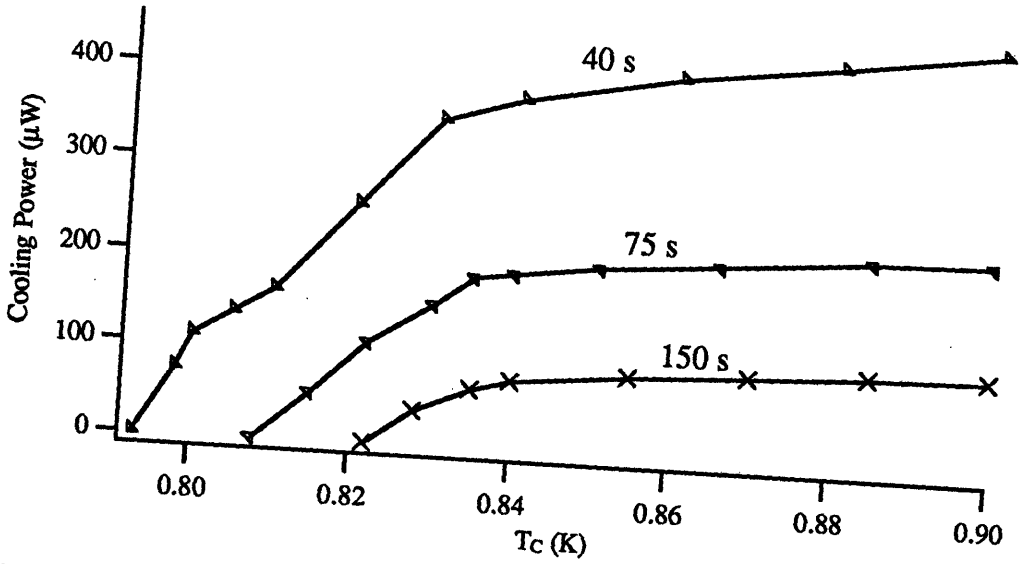

Figure 5.4. The SSR's cooling power versus T_C for a 36% mixture and a hot platform temperature of 0.9 K. The hot and cold piston swept volumes were 0.767 cm^3 and 0.811 cm^3, respectively.

5.3 Discussion

Fig. 5.1 shows the SSR's cooling power at various speeds as a function of the cold platform temperature for a 4.9% mixture. With no external heat load, the SSR reached a minimum temperature of 168 mK with a period of 100 seconds and hot platform temperature of 383 mK. Fig. 5.1 also shows that there is an optimum operating speed at each temperature to maximize the cooling power. The upper envelope of the lines defines the SSR's maximum cooling power as a function of temperature.

Note that the SSR has achieved its lowest temperature with a relatively long period. This may be understood as follows. The net, or measured, cooling power is the difference between the gross cooling power and the various losses. Most of the losses arise from the inefficiency of the regenerator. During the displacement stroke to the cold end, fluid slightly warmer than T_C enters the cold platform from the regenerator, thus thermally loading the cold platform. Brisson and Swift[4] made an estimate of the loss in cooling power due to imperfect thermal contact in the regenerator. One model assumes Schmidt flow through the regenerator with a constant thermal gradient on the regenerator walls and the hot and cold pistons operating 180 degrees out of phase. This model predicts a heat load on the cold platform of

$$\dot{Q}_{\text{regen}} = \left[\frac{T_H - T_C}{2US}\right](\rho\pi C_p V_{sw})^2 f^2 \qquad (5.3.1)$$

where U is the heat transfer coefficient between the fluids in each half of the refrigerator, S is the surface area in the regenerator, and ρ and C_p are the fluid's density and specific heat. Experiments have shown the actual heating rate to be an order of magnitude greater than that predicted by this analytic model, but Eq. 5.3.1 nevertheless implies that the frequency dependence of the loss in the cooling power due to imperfect heat transfer in the regenerator is proportional to the square of the frequency. Eq. 5.1.2, on the other hand, shows that the gross cooling power, which is the expected cooling power in the absence of loss mechanisms, is proportional to frequency. The net cooling power can therefore be expressed as

$$\dot{Q}_{\text{measured}} \approx \dot{Q}_{\text{Schmidt}} - \dot{Q}_{\text{regen}} = Af - Bf^2 \qquad (5.3.2)$$

where A and B are the proportionality constants for the gross cooling power and the regenerator heat loss, respectively. The frequency at which the maximum net cooling power is delivered is determined by setting to zero the derivative of Eq. 5.3.2 with respect to frequency. There exists, then, an optimum frequency where the net cooling power is maximized, a frequency where the gross cooling power and the heat loss are properly balanced out.

It is of interest to model the mixture's concentration as a function of position in the refrigerator corresponding to the experimental conditions measured above. Because of the temperature difference, the concentration in the cold platform pistons is higher than the "nominal" concentration, and that in the hot platform pistons is lower. For low concentrations of ^{3}He, the mixture should obey[1]

$$P_3(\rho,T)+P_f = \text{constant} \tag{5.3.3}$$

throughout the refrigerator, where P_3 is the osmotic pressure of ^{3}He, ρ is the mixture's ^{3}He density, T is the temperature, and P_f is the fountain pressure. Approximate values of $P_3(\rho,T)$ can be obtained by using the ideal Fermi gas equation of state described in Appendix E. It was assumed that the hot piston volume and the cold piston volume are 3.2 cm^3. The regenerator, which has a volume of 1.0 cm^3, was modeled as six discrete volumes with a linear temperature profile. The number of ^{3}He particles in the refrigerator is constant, which means

$$\Sigma\, \rho(T)_i\, V_i = \rho_{avg}\, V_{tot} \tag{5.3.4}$$

where $\rho(T)_i$ and V_i are the ^{3}He density and volume at various points in the refrigerator, ρ_{avg} is the average ^{3}He density in the refrigerator, and V_{tot} is the total volume of the refrigerator. With Eq. 5.3.4 as a constraint, we can solve iteratively for the mixture's concentration as a function of position in the refrigerator, given the hot and cold platform temperatures and average concentration. Fig. 5.6 shows the results of the calculation for four sets of operating conditions, superimposed on a ^{3}He-^{4}He phase diagram. The top point in each curve is the state of the mixture in the hot piston, the bottom point is the state of the mixture in the cold piston, and the six intermediate points represent the mixture states in the regenerator.

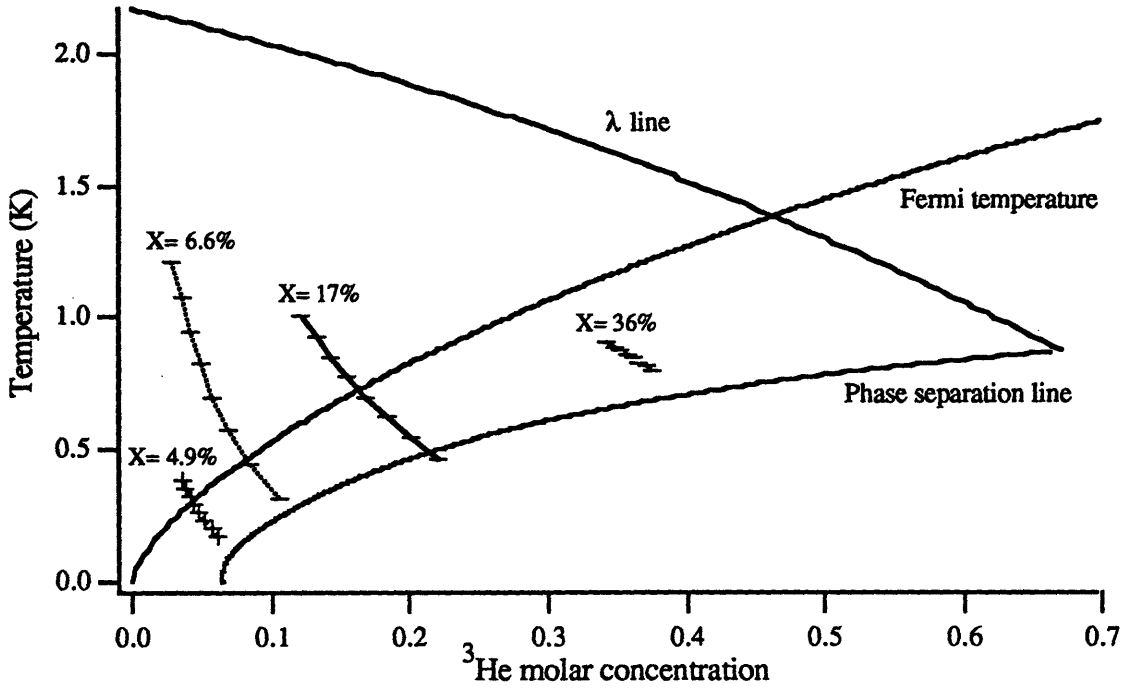

Figure 5.5. The mixture's state as a function of position in the refrigerator; for four different average concentrations superimposed on a phase diagram. Each curve is labeled with the mixture's average concentration. Three of the curves are for operating conditions of this paper. The 6.6% curve is for the conditions of Ref. 2. The ^{3}He Fermi temperature as a function of concentration is also shown. The top point in each curve is the state of the mixture in the hot piston, the bottom point is the state of the mixture in the cold piston, and the six points in-between these points represent the mixture states in the regenerator.

We can make several observations using Fig. 5.5. The first is that for all the conditions modeled the state of the ^{3}He in the cold piston is in the Fermi regime. In addition, when the SSR was loaded with an average concentration of 36%, the entire refrigerator was operated below the Fermi temperature.

Fig. 5.5 also indicates that there is a small amount of phase separated mixture in the cold piston for the run with the 17% mixture. Based on the analysis of the refrigerator's operation with a phase separated mixture in Section 4.3, we would expect the cooling power to drop and the total piston power to increase slightly in magnitude when the mixture is phase separated. However, the cooling power where the mixture is suspected to have phase separated is so low in this case that a drop in the cooling power would be undetectable. Further, the piston powers were not recorded for the runs with no external heat load. We therefore cannot infer from the available data whether the mixture has phase separated or not in the 17% data run shown in Fig. 5.5.

The experimental cooling power results for the 36% mixture, shown in Figs. 5.3 and 5.4, show a "cutoff" temperature where the cooling power drops off sharply as a function of temperature. Clearly, this is not due to phase separation of the mixture, as a ^{3}He-^{4}He mixture does not phase separate at 0.92 K regardless of the concentration.[14] Yet the sharpness of the transition suggests that it is caused by an abrupt transition in fluid properties, such as the critical velocity. Based on the analysis of critical velocity in Section 4.3, we suspect that the mixture is exceeding the critical velocity in the 0.8 mm diameter capillary connecting the piston to the heat exchanger.

Except for this unusual behavior at 36% concentration, cooling power exhibits remarkable linearity in T_C. This linearity may be understood as follows. For a given T_H and $V_r/V_0 \ll 1$, the temperature dependence of Eq. 5.1.2 is

$$\dot{Q}_{Schmidt} \sim [\alpha/(1+\alpha)]^2 \tag{5.3.5}$$

where α is T_C/T_H. This expression is very nearly linear in α for $\alpha > 0.2$. We can write

$$\dot{Q}_{measured} = \dot{Q}_{Schmidt} - \dot{Q}_{losses} \tag{5.3.6}$$

where $\dot{Q}_{measured}$ is the measured cooling power and $\dot{Q}_{losses}$ accounts for thermal loads on the cold platform due to thermal conduction from the hot platform, imperfect thermal contact in the regenerator, and other, smaller losses. Eq. 5.3.1 suggests that the heat loss due to the regenerator losses is proportional to T_H-T_C, and thermal conduction is also approximately proportional to T_H-T_C. Since $\dot{Q}_{Schmidt}$ and $\dot{Q}_{losses}$ are both approximately linear in T_C, Eq. 5.3.6 predicts that $\dot{Q}_{measured}$ will also be approximately linear in T_C.

The measured cooling powers normalized by those given by Schmidt analysis are plotted in Fig. 5.6. The normalized cooling powers extrapolate to between 1.1 and 1.6 near T_H=T_C, where the regenerator losses are predicted to be negligible. If the ^{3}He behaved as an isothermal ideal gas with no regenerator losses, the normalized cooling power would be 1. The deviation from this value can be attributed, in part, to the deviation of the working fluid's thermodynamic behavior from that of an ideal Boltzmann gas. The deviation is enhanced further by the non-isothermal compression and expansion in the real refrigerator. The latter effect can be estimated by considering the thermal penetration depth in the ^{3}He-^{4}He mixture, given by

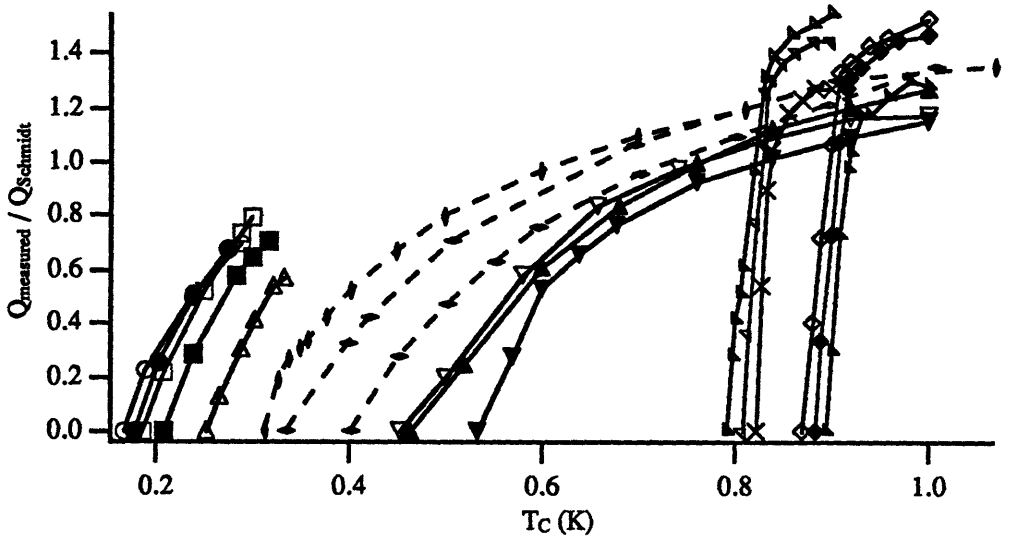

Figure 5.6. The measured cooling powers normalized by the cooling power calculated from Schmidt analysis. The measured cooling powers are not adjusted to give the reversible values, in contrast to some values presented in Chapter 4. The symbols correspond to those shown in Figs. 5.1 through 5.4. The dashed lines represent the normalized cooling power of data of Brisson and Swift.[2]

$$\delta_\kappa = \sqrt{\frac{\kappa}{\pi \rho C_p f}} \tag{5.3.7}$$

where κ is the thermal conductivity of the mixture and ρ and C_p are the density and heat capacity of ^{3}He. We assume that C_p=5R/2=20.8 J/mol-K. This is a good assumption below 1 K where phonon and roton excitations of ^{4}He are negligible. Using published figures[12] for κ, we calculate $\delta_{\kappa min}$ corresponding to the minimum period τ_{min} and $\delta_{\kappa max}$ corresponding to the maximum period τ_{max} for the conditions of each concentration. The results, shown in Table 5.1, shows that δ_κ varies between 1.3 mm and 4.2 mm for our operating conditions at 1 K. Since the fluid is as much as 6 mm away from isothermal solid surfaces, part of the fluid behaves more adiabatically than isothermally. This increases the pressure amplitude above that predicted by the Schmidt model, leading to a significant cooling power enhancement.

The normalized cooling power for the 36% mixture extrapolates to a higher number than those for the 6.6% and 17% mixtures near T_H=T_C, even though δ_κ does not appear to be much shorter than those for the latter concentrations. This may be due to the uncertainty in δ_κ, as κ(X) is interpolated from the values at X=1.3%, 5%, and 100%, resulting in a significant amount of uncertainty. Other possible reasons include the stronger deviation from ideal gas behavior and higher Kapitza boundary resistance at

X	4.9%	6.6%	17%	36%
κ	0.06 W/m-K	0.06 W/m-K	0.04 W/m-K	0.03 W/m-K
ρ	1750 mol/m^3	2350 mol/m^3	5900 mol/m^3	11800 mol/m^3
τ_{min}/τ_{max}	18 s / 100 s	19 s / 45 s	20 s / 80 s	40 s / 150 s
$\delta_{\kappa min}/\delta_{\kappa max}$	3.1 mm/7.3 mm	2.7 mm/4.2 mm	1.5 mm/2.9 mm	1.3 mm/4.2 mm

Table 5.1. Thermal penetration depths at various operating conditions calculated from Eq. 5.3.7. Minimum and maximum thermal penetration depths for each concentration corresponding to the maximum and minimum periods were calculated using the variables shown.

higher concentrations. No reliable data for liquid ^{3}He-^{4}He mixture's thermodynamic properties or boundary resistance at high concentrations exists to verify these claims. Fig. 5.6 nevertheless indicates that the cooling power is roughly proportional to the concentration of the working fluid.

5.4 Conclusion

The SSR has cooled to 168 mK with the hot platform being held at 383 mK, demonstrating the potential to cool to temperatures well below that attainable with a ^{3}He evaporation refrigerator. The cooling power at a fixed operating speed is linear to the cold platform temperature. The SSR has also been successfully operated with mixtures of up to 36% concentration with proportionately higher cooling powers, though we suspect that the flow exceeding the critical velocity poses a lower limit on the temperature attainable.

Chapter 6

The SOPTR's Frequency Response at Uniform Temperature

We will derive a simple model for the superfluid orifice pulse tube refrigerator and compare the model with data. Of particular interest is the pressure's phase lag from piston motion, which is the key to a pulse tube's refrigerator's operation. To that effect, we regulated both the hot and the cold platform temperatures to 1 K so that the temperature was essentially uniform throughout the apparatus, and operated the refrigerator with a 17% mixture. This greatly simplified the analysis of the operation and allowed us to analytically predict the pressure's phase lag and the cooling power as a function of the operating frequency. The working fluid was assumed to behave as an ideal gas to model the operation of the refrigerator.

6.1 Theory

We will derive a simple model based on an ideal working fluid for the pulse tube refrigerator operating with the hot platform temperature equal to the cold platform temperature. This will enable us to gain a rough understanding of the effects of various parameters such as the pulse tube's volume, the flow resistance through the orifice, and the operating frequency on the cooling power.

We first model the flow of gas through the orifice using the model shown in Fig. 6.1. The pressure drop for a steady state flow in a capillary is given by

$$\frac{dp}{dx} = -\frac{\mu Z Q}{L} \qquad (6.1.1)$$

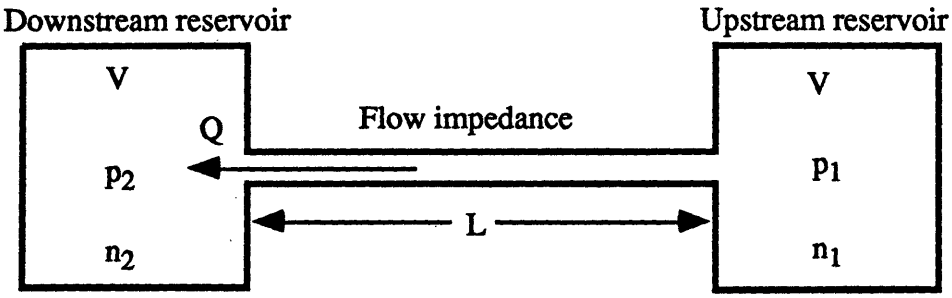

Figure 6.1. The flow of gas across a flow impedance

where μ is the fluid's viscosity, Z is the geometric factor of the capillary, Q is the volume flow rate, and L is the length of the capillary. Assuming an incompressible flow and a volume flow rate that is constant throughout the capillary's length, Eq. 6.1.1 becomes

$$\Delta p = -\mu Z Q \tag{6.1.2}$$

where Δp is the pressure drop across the capillary. However, the volumetric flow rate for a steady isothermal compressible flow through a capillary varies from one point to another as the fluid's density varies with pressure. We will therefore express the pressure drop across a capillary for an isothermal compressible flow as a function of the molar flow rate, which is constant throughout the capillary's length. Using the ideal gas law and the relation $Q=\rho \dot{n}$ where ρ is the molar density and $\dot{n}$ is the molar flow rate, we can rewrite Eq. 6.1.1 as

$$\frac{dp}{p} = -\left[\frac{\mu Z \dot{n}}{LRT}\right] dx. \tag{6.1.3}$$

where R is the universal gas constant and T is the temperature. The quantity in square brackets is constant, so we can integrate Eq. 6.1.3 over the length of the capillary and obtain

$$\dot{n} = \frac{RT}{\mu Z} \ln \frac{p_1}{p_2} \tag{6.1.4}$$

where p_1 is the upstream pressure and p_2 is the downstream pressure. We must now find the relationship between p_1 and p_2 appropriate to the SOPTR. We assume that the gas flows isothermally from an upstream reservoir with volume V, pressure p_1, and n_1 moles of gas, to a downstream reservoir with volume V, pressure p_2, and n_2 moles of gas. V corresponds to the volume in each half of the refrigerator. Neglecting the volume of capillary, the ideal gas law requires

$$(p_1+p_2) = \frac{RT}{V}(n_1+n_2). \tag{6.1.5}$$

Then p_1+p_2 is constant because T and n_1+n_2 are constant. We therefore let

$$\begin{aligned} p_1 &= p_0+dp \\ p_2 &= p_0-dp \end{aligned} \tag{6.1.6}$$

where p_0 is the average pressure of the gas. Substitution into Eq. 6.1.4 yields

$$\dot{n} = \frac{RT}{\mu Z}\ln\frac{p_0+dp}{p_0-dp} = \frac{RT}{\mu Z}\left[2\frac{dp}{p_0}+\frac{2}{3}\left(\frac{dp}{p_0}\right)^3+.....\right]. \tag{6.1.7}$$

The molar flow rate responds linearly to small pressure differences across the capillary, even though the fluid is compressible. Therefore, in the following model for the SOPTR, we assume a linear mass flow rate.

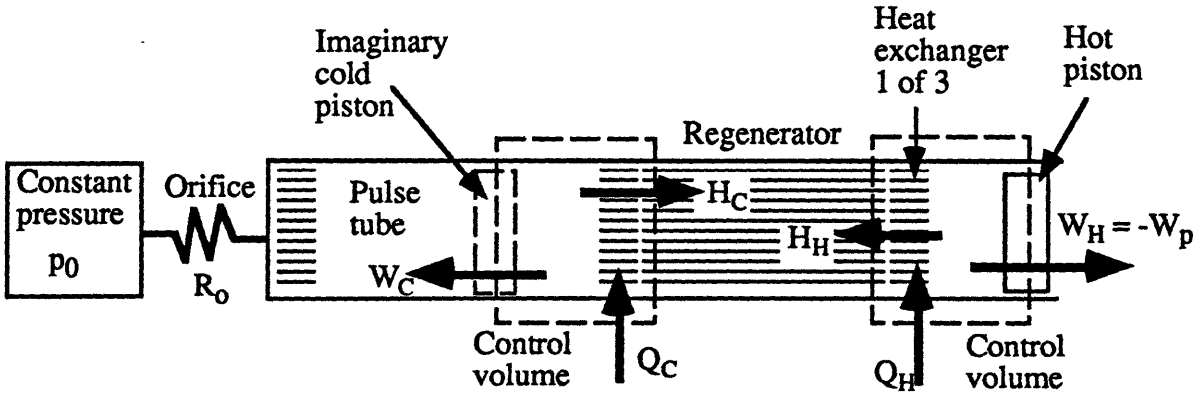

Figure 6.2. Schematic diagram of pulse tube refrigerator with an imaginary piston in the cold end. Heavy arrows indicate the net energy flow per cycle.

We now estimate the refrigerator's cooling power using the schematic diagram of pulse tube refrigerator shown in Fig. 6.2. Part of the fluid in the refrigerator behaves isothermally and part of it behaves adiabatically. However, we can model the entire fluid in the refrigerator as an isothermal volume of fluid and then use the effective volume discussed in Chapter 4 for the purposes of calculating the fluid's approximate pressure as a function of volume. This model, which is a linearized model for small compressions and expansions, will enable us to analytically estimate the pressure amplitude and phase with a minimum of mathematical tedium. We hence assume an isothermal oscillating volume

$$V(t) = V_0 - V_1 \cos\omega t \tag{6.1.8}$$

of gas is weakly linked by a resistive impedance R_0 to a location of constant pressure p_0, where V_0 is the effective volume of the refrigerator and V_1 is the geometric volume amplitude of the hot piston. For our refrigerator, the point of constant pressure p_0 is approximately the midpoint of the capillary, or orifice. Viscous pressure drops outside the orifice and inertial forces are negligible, so that p(t) is spatially uniform. Assuming an ideal gas, the number of moles of gas in a volume is proportional to pV, so assuming a mass flow rate response to a pressure we find

$$\frac{d(pV)}{dt} = -\frac{p - p_0}{R_o} \tag{6.1.9}$$

where R_0 is the resistive flow impedance of the orifice. Using $p = p_0 + |p_1|\cos(\omega t+\phi)$ and the ideal gas law, we find

$$|p_1| = p_0 \frac{V_1}{V_0} \frac{1}{\sqrt{1+\left(\frac{1}{\omega R_o V_0}\right)^2}} \tag{6.1.10a}$$

$$\phi = \tan^{-1}\left(\frac{1}{\omega R_o V_0}\right) \tag{6.1.10b}$$

to first order in (V_1/V_0). $\dot{W}_p$, the work done by the piston on the fluid per unit time, is the negative of the work done by the fluid on the piston per unit time:

$$\dot{W}_p = -\frac{d}{dt} W_H \tag{6.1.11}$$

This is an expression for average work hence

$$\dot{W}_p = -\frac{1}{\tau}\int_0^\tau p \cdot dV = \frac{(V_1/V_0)^2}{1+(1/\omega R_o V_0)^2}\frac{p_0}{2R} = \pi f V_1 |p_1| \sin\phi \tag{6.1.12}$$

where τ is the refrigerator's period and f is the frequency. Details of the derivation are shown in Appendix I.

We can find the refrigerator's cooling power from the piston power using an energy balance. Assuming no streamwise heat transfer in the fluid in the pulse tube, the only energy flow out of the cold end of the refrigerator through the fluid in the pulse tube is mechanical work W_C. The fluid in the pulse tube can then be treated as an imaginary piston. We draw a control volume around the cold end of the refrigerator as shown in Fig. 6.2. During each cycle, heat Q_C is absorbed by the fluid, work W_C is done by the fluid on the imaginary cold piston, and enthalpy H_C flows out through the regenerator. In cyclic operation, conservation of energy implies $Q_C = W_C + H_C$. Neglecting kinetic energy, the total energy flow in a fluid is the enthalpy flow, so

$$H_C = A\oint \rho v h \cdot dt \tag{6.1.13}$$

where A is the cross-sectional area of the gas in the regenerator, ρ is the mole density, v is the gas velocity, and h is the gas enthalpy per mole. For ideal gases, h depends only on temperature, so in an isothermal location, such as the left end of the regenerator, h is independent of time. Thus

$$H_C = h\oint A\rho v \cdot dt. \tag{6.1.14}$$

But $A\rho v$ is the instantaneous mass flow rate; its integral over one cycle must be zero, because the mass of gas in the control volume returns to its original value after each cycle. Hence $H_C = 0$ and

$$Q_C = W_C \tag{6.1.15}$$

for a classical ideal gas. A similar relationship holds at the hot end. Further, entropy balance in an ideal cycle requires

$$\frac{Q_C}{T_C}+\frac{Q_H}{T_H}=0. \tag{6.1.16}$$

Combining Eqs. 6.1.15 and 6.1.16, and taking the time derivative, we obtain

$$\dot{Q}_C=\frac{T_C}{T_H}\dot{W}_p \tag{6.1.17}$$

where $\dot{Q}_C$ is the heat absorbed at the cold end per unit time and $\dot{W}_p$ is the work done by the hot piston on the fluid per unit time. Hence $\dot{Q}_C=\dot{W}_p$ in reversible operation with $T_H=T_C$.

6.2 Procedure and Results

The SOPTR was operated with a 17% mixture with both the hot and the cold platform temperatures maintained at 1 K. $|p_1|$ was measured directly from the readouts of pressure gauges. The maximum and minimum values of $\Delta p = p_{top} - p_{bot}$ during the refrigerator's cycle were recorded, and the difference between the two divided by two gave the pressure amplitude, since $|p_1|$ is half of the peak to peak amplitude.

The phase between p_1 and V_1 was calculated from the data using the Fourier transform. We first calculated ϕ_p, the pressure's phase, as follows:

$$p_1(t) \propto \cos(\omega t+\phi_p)$$
$$\phi_p=-\tan^{-1}\left[\frac{\int_0^\tau p_1(t)\sin\omega t dt}{\int_0^\tau p_1(t)\cos\omega t dt}\right] \tag{6.2.1}$$

where τ is the refrigerator's period. Details of derivation of Eq. 6.2.1 are shown in Appendix I. We calculated ϕ_V, the phase of the piston displacement volume, in a similar fashion and then found

$$\phi=\phi_p-\phi_V. \tag{6.2.2}$$

T_C was actively controlled at 1 K by a feedback controller that delivered current to the heater mounted on the cold platform, and the heat delivered averaged over five to ten periods determined the cooling power $\dot{Q}_C$. $\dot{W}_p$, the average work done by the piston on the fluid per unit time, was calculated from $-\frac{1}{\tau}\int_0^\tau \Delta p \cdot dV$. The methods used to measure the cooling power and piston power of the SOPTR here are analogous to the methods used for the uniform temperature SSR measurements described in detail in Chapter 4. The results of the measurements are shown by the symbols in Fig. 6.3.

We can easily estimate the parameters in Eqs. 6.1.10 and 6.1.12 used to predict the pressure and piston power. First, we use the ideal gas law to find $p_0 = 366$ torr, the pressure of a classical ideal gas at 1 K with number density equal to that of a 17% mixture. The total effective volume of the refrigerator is

$$V_0 = V_{\text{eff piston}} + V_{\text{eff regenerator}} + V_{\text{eff pulse tube}} + V_{\text{eff connecting tubes}} \qquad (6.2.3)$$

where $V_{\text{eff piston}}$, $V_{\text{eff regenerator}}$, $V_{\text{eff pulse tube}}$, and $V_{\text{eff connecting tubes}}$ are the effective volumes of the piston, regenerator, pulse tube, and connecting tubes, respectively. The regenerator tubes' diameter is much shorter than the fluid's thermal penetration depth, so the fluid in the regenerator behaves isothermally. The regenerator's effective volume is hence equal to the geometric volume of 1.0 cm^3. In Chapter 4, the effective volume of the SSR with a 17% mixture at 1 K was found to be around 6 cm^3. This implies that $V_{\text{eff piston}}$ is 2.5 cm^3, which is somewhat smaller than the geometric volume of 3.2 cm^3. Geometric volumes of the piston and regenerator are found in Appendix B.

The fluid in the pulse tube and connecting tubes behaves adiabatically since the heat capacity of the tubes can be neglected. This can be shown by comparing the heat capacities between the ^{3}He-^{4}He mixture and the solid walls in the pulse tube and connecting tube wall:

$$\varepsilon_s = \frac{\frac{\pi D^2}{4}\rho C_p}{\pi D t C} \qquad (6.2.4)$$

where D is the tube's diameter, ρ and C_p are the fluid's total density and specific heat at constant pressure, t is the thickness of the wall, and C is the solid's specific heat. Based on published figures,[12,14] this quantity is 2×10^4 for the pulse tube and 2000 for the copper connecting tubes, indicating that the heat capacity of the solid walls is negligible

compared to that of the fluid. The fluid in the pulse tube and connecting tubes is therefore assumed to be adiabatic. Eq. 4.2.4 suggests that $V_{\text{eff pulse tube}}$ and $V_{\text{eff connecting tubes}}$ are 1.20 cm^3 and 0.33 cm^3, respectively, for small adiabatic compressions. The geometric volumes of the pulse tube and connecting tubes are found in Appendix J.

Using Eq. 6.2.3, the total effective volume of the refrigerator, V_0, is 5.0 cm^3, even though the comparable geometric volume of the refrigerator is 6.8 cm^3. V_1, which is half of the piston swept volume, is 0.56 cm^3. Finally, we estimate R_0 from the pressure decay time constant:

$$R_0 = \tau_0/V_0 = 11 \text{ s}/5.0 \text{ cm}^3 = 2.2 \text{ s/cm}. \qquad (6.2.5)$$

τ_0, the pressure decay time constant after an abrupt change in piston position as the fluid flows out through the orifice, is 11 s based on measurements. We use the refrigerator's effective volume in Eq. 6.2.5 in order to account for the fact that part of the fluid in the refrigerator behaves adiabatically. Details of derivation of Eq. 6.2.5 and the measurements for the pressure decay time constant are found in Appendix K.

With these values for p_0, V_0, V_1, and R_0, Eqs. 6.1.10a, 6.1.10b, and 6.1.12 yield the solid curves in Fig. 6.3. $|p_1|$ and $\dot{W}_p$ were multiplied by two since our apparatus consists of two refrigerators operating in parallel.

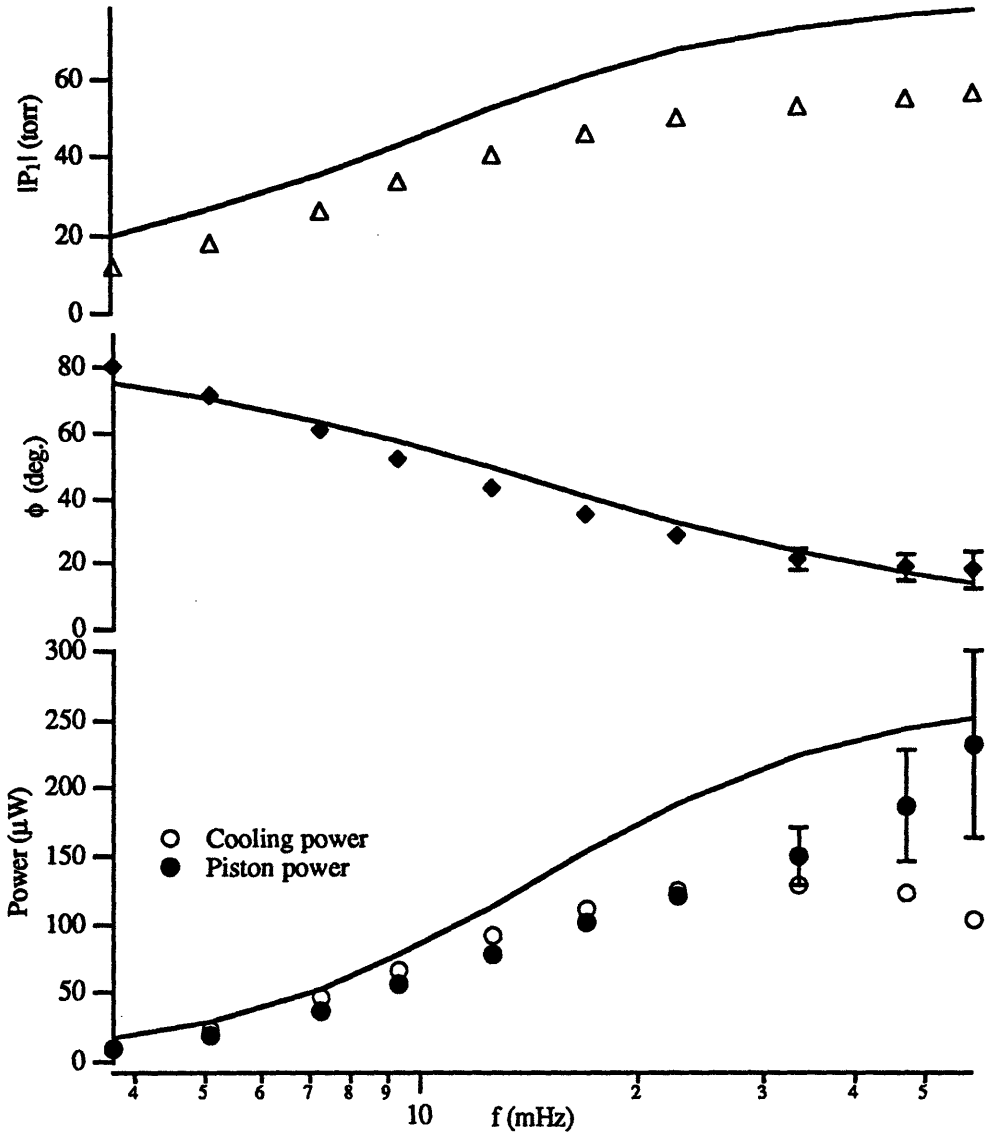

Figure 6.3. The SOPTR's frequency response with a 17% mixture. The hot and the cold platform temperatures were both 1 K, and the piston swept volume was 1.12 cm^3. Symbols are measured values. The solid lines indicate the theoretical values calculated from Eqs. 6.1.10 and 6.1.11. Error bars are one standard deviation calculated from Eqs. F.2 and F.3, where measured values were used for ϕ and $\dot{W}$ in Eq. F.3.

6.3 Discussion

Fig. 6.3 shows a good qualitative agreement between theory and measurements, supporting the validity of the calculations presented above.

The observed pressure amplitude shows a good agreement with the theory except for the fact that it is somewhat lower than predicted. It is suspected that most of the difference between the theory and the measurements is due to our use of ideal gas approximation in the theory. Assuming for the moment that the refrigerator has a geometrical volume of 5.0 cm^3 and undergoes isothermal compressions and expansions, we can rewrite Eq. 6.1.10a as

$$|p_1| = p_0' \left[\frac{1}{\rho RT} \left(\frac{\partial p}{\partial c} \right)_{T,\mu_4} \right] \frac{V_1}{V_0} \frac{1}{\sqrt{1 + \left(\frac{1}{\omega R_0 V_0} \right)^2}} \tag{6.3.1}$$

where p_0' is the actual osmotic pressure of ^3He and the expression in square brackets is the normalized isothermal compressibility, which is unity for an ideal gas. This expression differs from Eq. 6.1.10a by a factor of

$$\frac{|p_1|_{Eq.6.3.1}}{|p_1|_{Eq.6.1.10a}} = \frac{p_0'}{p_0} \frac{1}{\rho RT} \left(\frac{\partial p}{\partial c} \right)_{T,\mu_4} = 0.67. \tag{6.3.2}$$

Radebaugh's tables[14] were used to evaluate Eq. 6.3.2. On average, the observed pressure amplitude is smaller than the theoretical pressure amplitude based on an ideal gas by a factor of 0.72, which is close the value calculated in Eq. 6.3.2. However, as stated earlier, Eq. 6.3.1 is an isothermal approximation, whereas part of the fluid in the refrigerator behaves adiabatically and not isothermally. A better understanding of the pressure amplitude would require a more detailed cycle analysis.

Phase to first approximation is unaffected by the fact that the working fluid is non-ideal, and Fig. 6.3 shows an excellent agreement between theory and experiment .

According to Eqs. 6.1.12 and 6.2.5, maximum heat is absorbed at the cold end per cycle when the refrigerator's period is

$$\tau = 2\pi\tau_0 \tag{6.3.3}$$

where τ_o is the pressure decay time constant after an abrupt change in piston position as the fluid flows out through the orifice. We will label this quantity as τ_n, the SOPTR's natural period. Eq. 6.1.10b suggests that phase between the piston motion and the pressure is 45° at this frequency, which is identical to the prediction based on Schmidt analysis with a 90° phase between the hot and the cold pistons. The pulse tube refrigerator therefore mimics the Stirling refrigerator's operation at this frequency. This is one measure of the pulse tube refrigerator's optimum frequency, the natural frequency based on how the Stirling refrigerator works. However, in a pulse tube refrigerator with a fixed flow impedance at the orifice, the cooling power keeps rising beyond the natural frequency because cooling power is also proportional to frequency. In fact, according to Eq. 6.1.12, the cooling power is a strictly increasing function of frequency, and asymptotes to a maximum value of $(V_1/V_0)^2 p_0/2R_o$ at the limit of infinite frequency. Numerical substitution into Eq. 6.3.3 yields τ_n = 69 s, corresponding to a natural frequency of 15 mHz. The measured cooling power, contrary to prediction, reaches a maximum at around 30 mHz, which is about twice the natural frequency, and decreases at higher frequencies. The behavior of piston power at high frequencies is obscured by the uncertainty.

We do not fully understand the observed decrease of the measured cooling power at the highest frequencies. One candidate is irreversible pressure oscillation of fluid. The fluid in the regenerator is essentially isothermal, so its pressure oscillations are reversible. The fluid in the center of the pulse tube experiences essentially adiabatic pressure oscillations, which are also reversible. In contrast, fluid about a thermal penetration depth δ_κ from the nearest massive solid surface experiences irreversible pressure oscillations, absorbing work and releasing it to the surroundings as heat. It is possible that the heat transfer between the fluid and the refrigerator has been negatively affected due to high frequency, thus thermally decoupling more of the fluid in the piston.

We devise the following model in order to estimate roughly the decrease in the cooling power due to irreversible pressure oscillation. We assume that the piston shown in Fig. 6.4 undergoes a harmonic motion, where W is the work done by the piston on the fluid per cycle and Q is the heat released to the surroundings per cycle. W is given by $W = \Delta p \cdot V$, where Δp is the difference between the fluid's pressure during the compression stroke and the expansion stroke and V is the piston swept volume. Ideal gas relation implies $\Delta p/p = \Delta T/T$, where ΔT is the difference between the fluid's temperature during the compression stroke and the expansion stroke. In cyclic operation, conservation of energy implies Q=W. Using the above results and multiplying Q by twice the frequency because the apparatus consists of two Stirling refrigerators operating in parallel, we find

that the heat released to the surroundings per unit time is $2fVp\Delta T/T$. We can subtract this value from the reversible cooling power in order to account for the irreversible pressure oscillation in the refrigerator. Assuming a ΔT of 10 mK, this expression yields 50 μW for the conditions of Fig. 6.3 at the highest frequency, which suffices to explain the decrease in the measured cooling power. Because of the extremely complicated fluid/solid geometry in the bellows, heat exchangers, and connecting tubes, this should be regarded as only a rough estimate showing plausibility of this explanation.

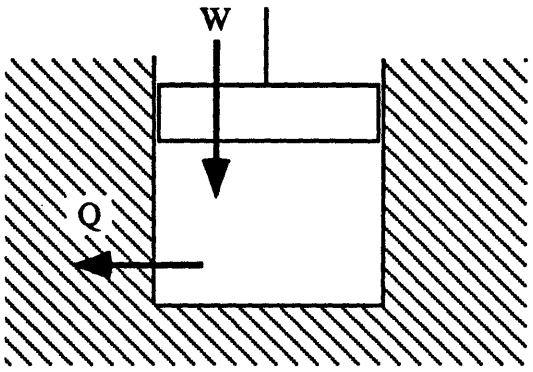

Figure 6.4. Work and heat flow in an irreversible oscillatory motion

Another possibility responsible for the observed decrease of the measured cooling power is non-linear flow of fluid in the orifice. In fact, in one measurement with a different orifice geometry than the one used in this set of measurements, pressure relaxation time constant for the orifice varied between 56 s and 14 s depending on the magnitude of the pressure difference across the orifice. Such non-linear flow may increase the effective flow impedance of the orifice at high frequencies and result in the decrease of the measured cooling power.

A combination of the above two phenomena would also lead to a decrease in the cooling power.

6.4 Conclusion

A model that assumes an ideal gas working fluid, a linear mass flow rate through the orifice, and perfect heat transfer in the piston and the regenerator suggests that the cooling power of a pulse tube refrigerator with a fixed flow impedance through the orifice

is a strictly increasing function of frequency that asymptotes to a limit as frequency approaches infinity. Measurements taken with the refrigerator shows, however, that cooling power drops at high frequencies. Suspected reasons for the drop in the cooling power include imperfect heat transfer between the solid walls and the fluid and non-linear flow of fluid in the orifice.

Chapter 7

Effects of Gravity in the Pulse Tube

A question of practical interest is when, if ever, the imaginary piston, the insulating column of fluid in the pulse tube that does not leave the pulse tube during the cycle, would disappear. When this happens, fluid in the pulse tube thermally loads the cold platform and reduces the measured cooling power. It will be shown that gravity coupled with thermal gradient has a profound effect on fluid flow in the pulse tube, affecting the length of the imaginary piston. The results from this chapter give us a guideline on how to set the piston displacement volume in order to maximize the cooling power.

7.1 Theory

Imaginary piston is the slug of fluid that executes a harmonic motion near the middle of the pulse tube. It does not contact either the hot or the cold heat exchanger as it oscillates in the pulse tube. It can be thought of as a long, thermally insulating piston, and we will derive an analytic expression for its approximate length in order to find when it would disappear.

Due to the fluid's compressibility, the magnitude and phase of the fluid's oscillatory motion are different near the pulse tube's hot end and cold end, and hence the length of the imaginary piston varies slightly during the cycle. However, we can obtain an approximate analytic expression for the imaginary piston's length by assuming an incompressible oscillatory motion in the pulse tube. Under these assumptions, the length of the imaginary piston is given by

$$L_i = L - 2\frac{|V_{31}|}{A_{eff}} \tag{7.1.1}$$

where L is the length of the pulse tube, $|V_{31}|$ is half of the peak to peak volume amplitude of fluid executing a harmonic motion near the middle of the pulse tube, and A_{eff} is the effective cross sectional area of the pulse tube. A_{eff} is the cross sectional area of the pulse tube that is not blocked by the viscous boundary layer, so it is given approximately by

$$A_{eff} = \pi(D-2\delta_v)^2/4 \tag{7.1.2}$$

where δ_v is the thickness over which the fluid velocity becomes comparable to the free stream value. For a given volumetric displacement of fluid in the pulse tube, then, the length of the imaginary piston would decrease with increasing viscous boundary layer thickness. We expect the imaginary piston to disappear for large enough piston displacements. When this happens, part of the warm fluid that enters the pulse tube from the orifice would flow into the cold heat exchanger, thereby thermally loading the cold platform and reducing the measured cooling power.

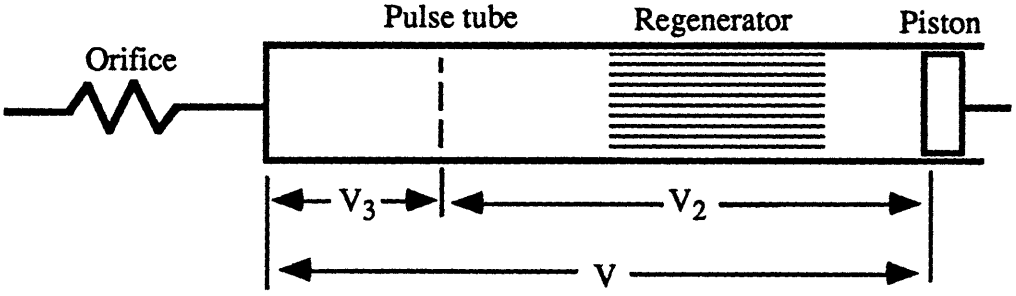

Figure 7.1. Fluid motion in the SOPTR.

We now find $|V_{31}|$ in order to evaluate Eq. 7.1.1. We follow the fluid particles indicated by the dashed vertical line in Fig. 7.1 executing a harmonic motion near the middle of the pulse tube, the amplitude of which is $|V_{31}|$. The volume of the fluid to the right of the dashed line will be called V_2, and the volume of the fluid to the left of the dashed line will be called V_3. Their sum is the total volume of the refrigerator. Our approach will be to find V_3 by subtracting V_2 from V. V_3 may be expressed as

$$V_3(t)= V(t)-V_2(t) \equiv V_{30}+\mathrm{Re}[V_{31}e^{i\omega t}]. \tag{7.1.3}$$

Even though we neglected the fluid's compressibility in deriving Eq. 7.1.1, we revert to compressible flow in order to evaluate $|V_{31}|$. Part of the fluid in the refrigerator behaves isothermally and part of it behaves adiabatically. However, we will model the entire fluid in the refrigerator as an isothermal volume of fluid and then use the effective volume discussed in Chapter 4 for the purposes of calculating the fluid's displacement amplitude. This model will enable us to analytically estimate the displacement amplitude of a fluid particle in the refrigerator with a minimum of mathematical tedium. Note also that $T_C/T_H=0.9$ in the measurements. Neglecting the difference between T_H and T_C in the model would result in error of the order of 10%.

With these assumptions and the ideal gas law, V_2 is

$$V_2(t)= \frac{n_2 RT}{p(t)} \tag{7.1.4}$$

where n_2, the number of moles of fluid in V_2, is constant, R is the universal gas constant, T is the temperature, and we use Eq. 6.1.10 to find p(t). Eq. 6.1.8 implies

$$V = V_0-V_1e^{i\omega t} \tag{7.1.5}$$

where V_1 is real. Combining Eqs. 7.1.3 through 7.1.5, we find

$$|V_{31}| = \sqrt{\left[\frac{V_1V_{20}/V_0}{1+1/(\omega R_o V_0)^2}\right]^2+\left[\frac{V_1V_{20}}{V_0}\frac{1/\omega R_o V_0}{1+1/(\omega R_o V_0)^2}\right]^2} \tag{7.1.6}$$

to first order in (V_1/V_0), where V_{20} is the time average of V_2 and R_o is the flow resistance of the orifice. Details of derivation of Eq. 7.1.6 are shown in Appendix L.

Next, we find δ_v, the boundary layer thickness in the pulse tube, from the equation of motion of fluid in order to evaluate Eq. 7.1.2. Consider the x-component of the equation of motion,[11] where x is parallel to the axis of a vertical pulse tube:

$$\frac{m^*}{m}\rho\left[\frac{\partial u_x}{\partial t}+(\mathbf{u}\cdot\nabla)u_x\right] =-\frac{\partial p}{\partial x}+\mu\nabla^2 u_x+\frac{\mu}{3}\frac{\partial}{\partial x}(\nabla\cdot\mathbf{u})+\rho f_x \tag{7.1.7}$$

where m* and m are the effective mass and true mass of a ^{3}He particle, ρ is the mass density of ^{3}He, u is the velocity of the ^{3}He component of the fluid, p is the pressure, μ is the viscosity of the mixture, and f_x is the net body force acting on the ^{3}He component. We have multiplied the inertial term by m*/m in order to account for the virtual mass effect of a ^{3}He particle in the background of ^{4}He. We assume a small, oscillatory motion. For simplicity, we assume that the pressure is essentially time-independent. Though this assumption contradicts the model in Fig. 7.1, pressure oscillations and the resultant density oscillations are spatially uniform and hence have no effect on the shape of the velocity profile. We also assume that the fluid has a negative thermal gradient dT/dx (fluid on top is colder than fluid on bottom). Finally, we assume that the temperature of a fluid particle is constant; we assume only convective heat transfer, and no diffusion heat transfer. Under these conditions, we have

$$\mathbf{u} = u_x\hat{x}+u_y\hat{y}+u_z\hat{z} = \mathrm{Re}[u_1(r)e^{i\omega t}]\hat{x}, \qquad u_y = u_z = 0 \tag{7.1.8a}$$

$$p = p_0+\mathrm{Re}[p_1e^{i\omega t}] \approx p_0 \tag{7.1.8b}$$

$$T = T_0+\mathrm{Re}[T_1e^{i\omega t}] \tag{7.1.8c}$$

$$\rho = \rho_0+\mathrm{Re}[\rho_1e^{i\omega t}] \tag{7.1.8d}$$

$$\frac{DT}{Dt} = \frac{\partial T}{\partial t}+u_x\frac{\partial T}{\partial x}+u_y\frac{\partial T}{\partial y}+u_z\frac{\partial T}{\partial z} = 0 \tag{7.1.8e}$$

where r is the radial coordinate. The effective body force acting on ^{3}He is found from the effective thermal expansion coefficient of a superfluid ^{3}He-^{4}He liquid mixture, defined as[13]

$$\beta_{\mathrm{eff}} = -\frac{1}{\rho_3}\left(\frac{\partial\rho}{\partial T}\right)_{p,\mu_4} \tag{7.1.9}$$

where ρ_3 and ρ are to the ^{3}He mass density and the total mass density, respectively, and μ_4 is the chemical potential of ^{4}He. Assuming an ideal gas behavior and neglecting the small change in the mixture's molar density with concentration, we find

$$\beta_{\mathrm{eff}} = -\frac{1}{3T}. \tag{7.1.10}$$

This is a third the magnitude and of opposite sign compared to that of a classical ideal gas. The minus sign comes from the fact that ^{3}He has a smaller mass density than ^{4}He.

Details of derivation of Eq. 7.1.10 are shown in Appendix L. The effective body force acting on ^{3}He is therefore

$$f_x = g_{eff} = \left(-\frac{1}{3}\right)(-g) = g/3 \tag{7.1.11}$$

where g is positive. With these results and the ideal gas approximation, we can expand Eq. 7.1.7 to first order and find:

$$i\omega\frac{m^*}{m}\rho_0 u_1 = \mu\nabla^2 u_1 + \frac{\rho}{3T}\frac{dT}{dx}\frac{u_1}{i\omega}g. \tag{7.1.12}$$

Usually, the gravitational term can be neglected, in which case Eq. 7.1.12 becomes

$$i\omega\frac{m^*}{m}\rho_0 u_1 = \mu\nabla^2 u_1 \approx \mu\frac{\partial^2 u_1}{\partial r^2}$$

$$u_1 \propto \exp\left[\pm(1+i)\frac{r}{\sqrt{\frac{2\mu}{\omega(m^*/m)\rho_0}}}\right]. \tag{7.1.13}$$

δ_v, the distance over which the fluid velocity becomes comparable to the free stream value, is given approximately by the distance over which the viscous term becomes comparable to the inertial term:

$$\delta_v = \sqrt{\frac{2\mu}{\omega(m^*/m)\rho_0}}. \tag{7.1.14}$$

However, the inertial term is negligibly small compared to the gravitational term in Eq. 7.1.12 in the superfluid pulse tube, so Eq. 7.1.12 becomes

$$\mu\nabla^2 u_1 = -\frac{\rho}{3T}\frac{dT}{dx}\frac{u_1}{i\omega}g$$

$$u_1 \propto \exp\left[\pm(1-i)\frac{r}{\sqrt{\frac{6\mu\omega T}{\rho g(-dT/dx)}}}\right]. \tag{7.1.15}$$

Note that the quantity inside the square root is positive because dT/dx is negative. We can define $\delta_{v,eff}$, the effective boundary layer thickness, as the boundary layer thickness in the presence of gravity. It is given approximately by the distance over which the viscous term becomes comparable to the gravitational term:

$$\delta_{v,eff} = \sqrt{\frac{6\mu\omega T}{\rho g(-dT/dx)}}. \tag{7.1.16}$$

We can substitute these results into Eq. 7.1.2 to find A_{eff}.

7.2 Procedure and Results

The refrigerator was operated with a 17% mixture at a fixed speed and with T_H and T_C maintained at 1.0 K and 0.9 K, respectively. V_{sw}, the peak to peak piston displacement volume, was varied by changing the setting of the cam driven by the drive motor. V_{sw} was measured with the linear position sensor. The maximum V_{sw} was limited to around 2 cm^3 in our apparatus. $|p_1|$ was measured from the readouts of pressure gauges. The maximum and minimum values of $\Delta p = p_{top} - p_{bot}$ during the refrigerator's cycle were recorded, and the difference between the two divided by two gave the pressure amplitude, since $|p_1|$ is half of the peak to peak amplitude. The phase between p_1 and V_1 was calculated from the data using the Fourier transform. T_C was actively controlled at 0.9 K by a feedback controller that delivered current to the heater mounted on the cold platform, and the heat delivered averaged over five to ten periods determined the cooling power $\dot{Q}_C$. $\dot{W}_P$, the average work done by the piston on the fluid per unit time, was calculated from $-\frac{1}{\tau}\int_0^\tau \Delta p \cdot dV$. The methods used to measure the cooling power and piston power of the SOPTR here are analogous to the methods used for the uniform temperature SSR measurements described in detail in Chapter 4. The results of the measurements are shown by the symbols in Figs 7.2 and 7.3, where we normalized V_{sw} by V_{pt}, the pulse tube volume.

For the conditions of Fig. 7.2, Eq. 7.1.14 gives δ_v = 1.8 mm where μ is[17] 1.5 $\times 10^{-6}$ kg/m-s and m*/m is[14] 2.6. Eq. 7.1.16 gives $\delta_{v,eff}$ = 10 μm.

L	6.8 cm
D	6.0 mm
V_0	5.0 cm^3
V_{20}	4.2 cm^3
V_{30}	0.8 cm^3
R_o	2.2 s/cm^3
V_{pt}	2.0 cm^3

Table 7.1. The refrigerator's parameters calculated from geometry

Table 7.1 shows the refrigerator's various parameters calculated from geometry. V_1 is half of the geometric piston swept volume. Geometric and effective volumes of various parts of the refrigerator are found in Chapter 6 and Appendix J. Using these values in Eqs. 7.1.1, 7.1.2, and 7.1.6, we can numerically find the piston swept volume where L_i, the length of the imaginary piston, becomes zero. The vertical dashed lines in Figs. 7.2 and 7.3 indicate the piston swept volumes where L_i would be zero if the viscous boundary layer given by Eq. 7.1.14 blocked the fluid in the pulse tube near the wall. The vertical solid line in Fig. 7.2 indicates the piston swept volume where L_i would be zero if δ_ν were replaced by $\delta_{\nu,eff}$ given by Eq. 7.1.16. For the conditions of Fig. 7.3, the solid line would be at $(V_{sw}/V_{pt})^2 = 1.7$.

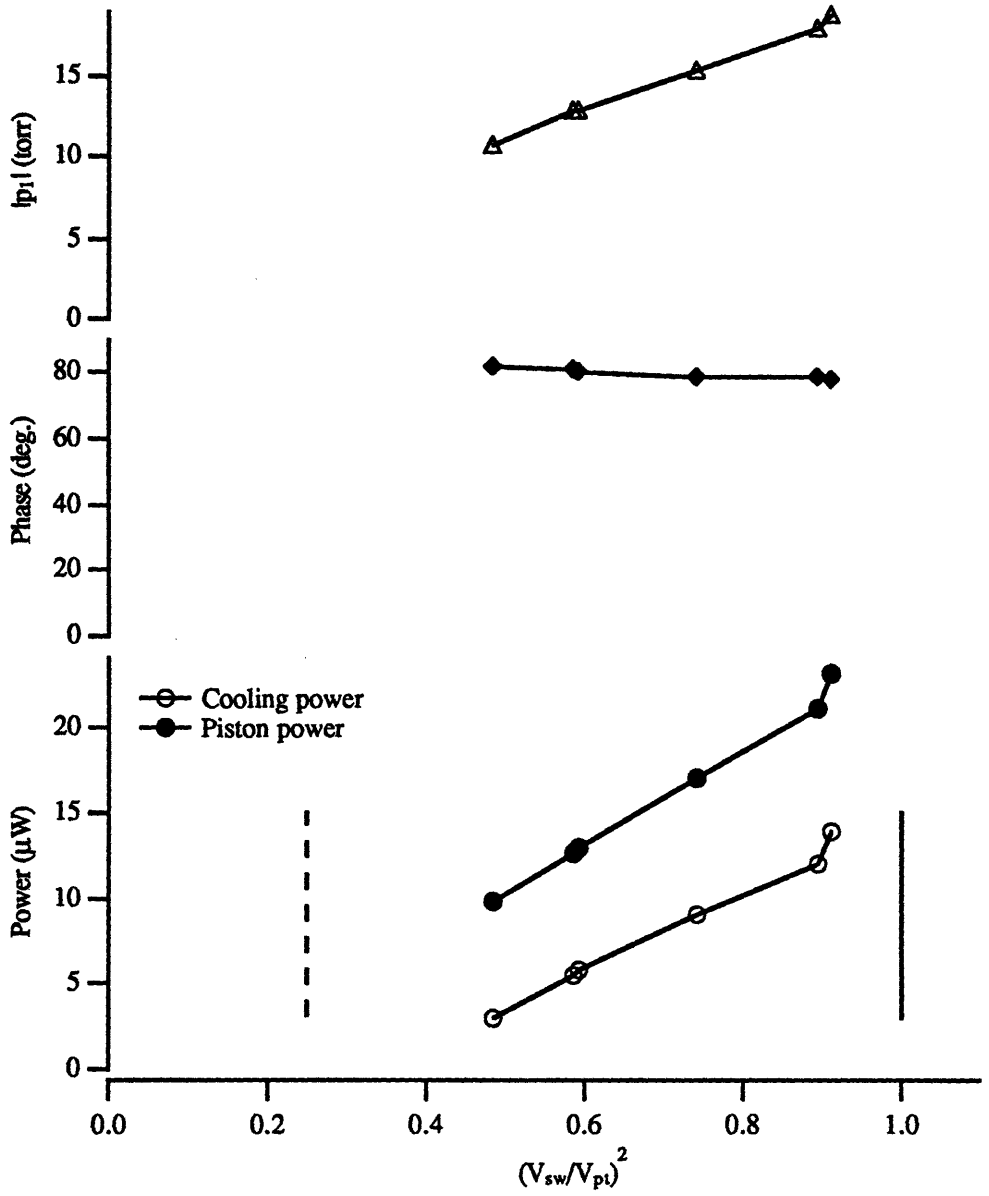

Figure 7.2. The SOPTR's pressure amplitude, phase between piston motion and pressure, cooling power, and piston power as a function of piston displacement volume. Here we normalize the peak to peak piston displacement volume V_{sw} by the pulse tube volume V_{pt}=2.0 cm^3. 17% mixture was used, T_H and T_C were 1.0 K and 0.9 K, respectively, and the period was 300 s. Lines are only guides to the eye. The vertical solid and dashed line indicates the piston swept volume above which the imaginary piston disappears in the presence and absence of gravity, respectively.

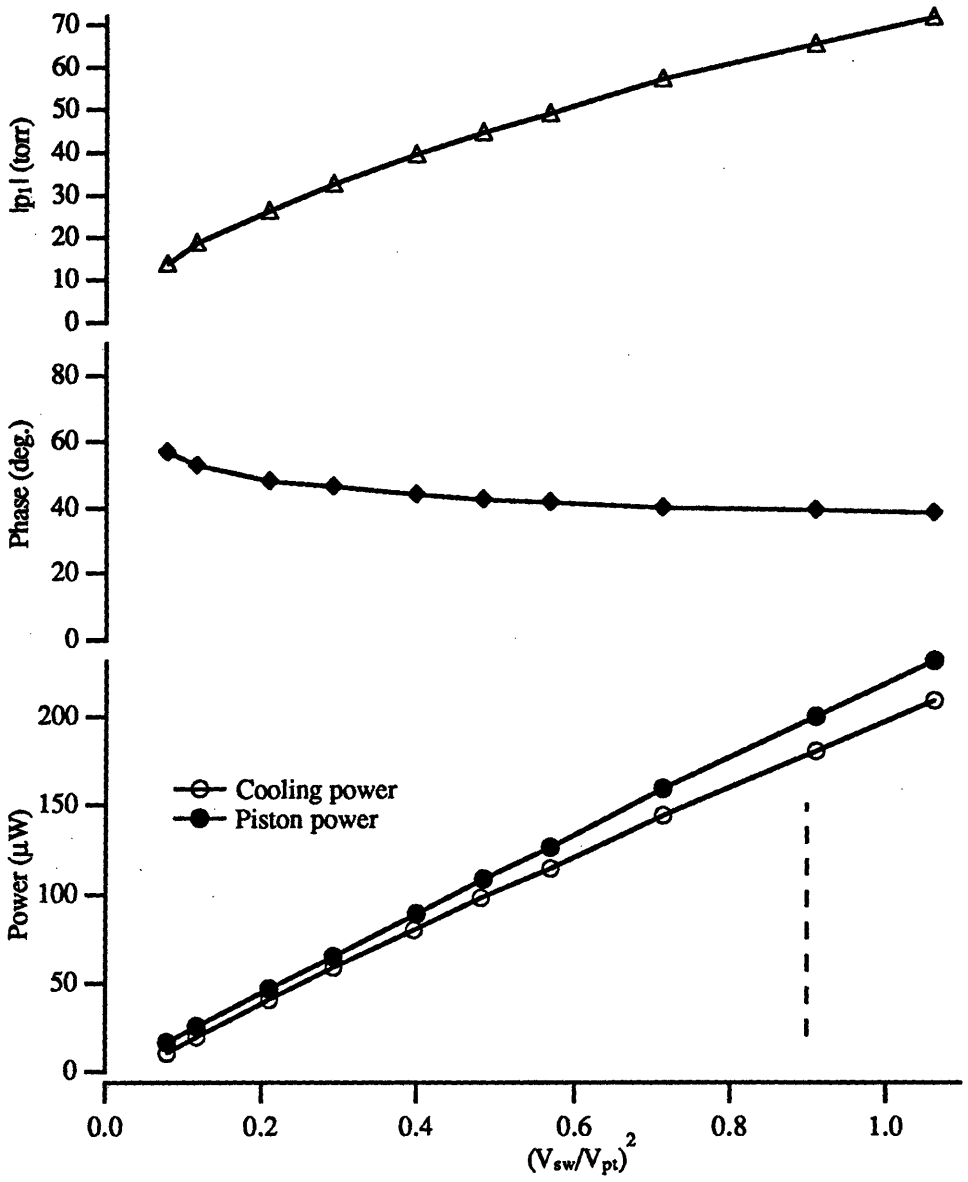

Figure 7.3. The SOPTR's pressure amplitude, phase between piston motion and pressure, cooling power, and piston power as a function of piston displacement volume. Here we normalize the peak to peak piston displacement volume V_{sw} by the pulse tube volume V_{pt}=2.0 cm^3. 17% mixture was used, T_H and T_C were 1.0 K and 0.9 K, respectively, and the period was 80 s. Lines are only guides to the eye.

7.3 Discussion

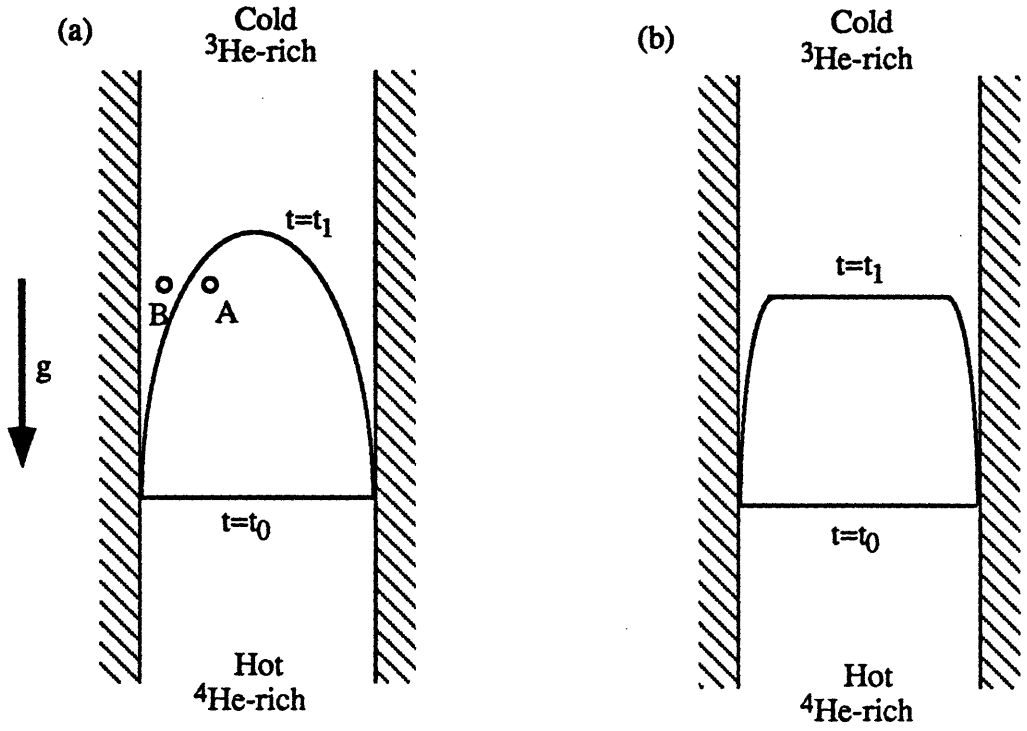

Figure 7.4. Oscillatory flow of ^{3}He-^{4}He mixture in a pipe

For the conditions of Fig. 7.2, Eqs. 7.1.14 and 7.1.16 show that the effective gravity acting on the ^{3}He component of the mixture reduces the viscous boundary layer thickness by two orders of magnitude, from 1.8 mm to 10 μm. We will now find a physical interpretation for this phenomenon. Consider an oscillatory motion of superfluid ^{3}He-^{4}He mixture in a vertical pipe with cold fluid on top and warm fluid on bottom, and consequently a higher ^{3}He concentration on top than on bottom. The fluid's total mass density would then be higher at the bottom than at the top, as ^{4}He has a higher mass density than ^{3}He. We first assume a classical parabolic flow profile shown in Fig. 7.4(a), where the velocity is given by $u=u_1(r)\sin \omega t$. We assume that the line of equal ^{3}He concentration is flat at $t=t_0$ and parabolic at $t=t_1$. Then, the pressure at point A at t_1 would be higher than that at point B because the greater mass density of the mixture above point A would result in a greater hydrostatic pressure. The pressure gradient would tend to accelerate the fluid particles to the left, resulting in the flow profile shown

in Fig. 7.4(b). Gravity coupled with thermal gradient thus flattens the velocity profile of an oscillating superfluid ^{3}He-^{4}He mixture.

Some indirect evidence of this flattening may be seen in Fig. 7.2. If the viscous boundary layer thickness were 1.8 mm as given by Eq. 7.1.14, part of the warm fluid that enters the pulse tube from the orifice would flow into the cold heat exchanger when the swept volume is above the dashed vertical line shown in Fig. 7.2. When this happens, the resultant thermal load on the cold platform would reduce the measured cooling power. The fact that there is an amount of cooling power comparable to the piston power where the piston swept volume is greater than that indicated by the dashed line suggests that the viscous boundary layer near the pulse tube walls is indeed thinned down by gravity.

The flattening of the velocity profile increases the viscous dissipation in the pulse tube by steepening the velocity gradient near the wall. This may be estimated as follows. The instantaneous power dissipated by viscous shear stress per unit surface area is given by

$$\dot{e} = \frac{\mu}{2}\int_0^\infty \left(\frac{du}{dr}\right)^2 dr = \frac{\mu U^2}{2\delta_{v,eff}} \tag{7.3.1}$$

where μ is the fluid's viscosity, Eq. 7.1.15 was used to evaluate u, and U is the free-stream velocity. Assuming[17] a μ of 1.5×10^{-6} kg/m-s, approximating U by fV_{sw}/A, where A is the cross sectional area of the pulse tube, and integrating over the surface area of the pulse tubes, Eq. 7.3.1 yields an average power dissipated by viscous shear stress of the order of 1 μW, which is negligibly small.

The flattening of the velocity profile also helps make this an essentially ideal pulse tube. The virtually flat velocity profile makes the imaginary piston model reasonably accurate. The strong stability enforced by gravity and the temperature gradient may also suppress flow separation and the resultant turbulent mixing of the fluid when it flows from the 3 mm diameter connecting tubes to the 6 mm diameter pulse tubes. This may eliminate the need for the flow straightening screens at the ends of the pulse tubes. This leaves ordinary conduction in the streamwise direction as the only significant loss mechanism in the pulse tube.

Fig. 7.3 shows the cooling power to be very nearly proportional to V_1^2. This is not unexpected since the pulse tube refrigerator should, to first approximation, behave as a Stirling refrigerator, and the Schmidt analysis presented in Chapter 5 predicts a Stirling refrigerator's cooling power to be proportional to the square of the piston swept volume. The cooling power increases linearly with V_{sw}^2 until the maximum piston displacement

without showing any signs of loss, in contrast to the frequency response of the cooling power in Chapter 6 where the cooling power started to drop at frequencies higher than around 30 mHz. The phase is near 45°, though we do not understand the observed decrease in the phase as V_{sw} increases.

7.4 Conclusion

Gravity couples with temperature gradient in the pulse tube to dramatically thin down the viscous penetration depth, resulting in a slug flow in the pulse tube and hence making the SOPTR behave as an ideal pulse tube. Consequently, the piston swept volume above which the insulating slug of fluid in the pulse tube disappears increases substantially, allowing a larger swept volume and a higher cooling power than in the absence of gravity. Viscous power dissipation in the thinned down viscous boundary layer is negligible.

Chapter 8

The SOPTR Cooling Power Measurements

In this chapter we present the SOPTR's cooling power as a function of temperature. Results from the previous chapters will be used as a guideline to select the various parameters in order to maximize the SOPTR's cooling power. A simple model based on a classical ideal gas will predict the gross cooling power, which is the expected cooling power in the absence of losses, and a loss mechanism will be discussed. Comparison with the SSR's cooling power will reveal the primary weakness of the SOPTR, and how to improve the SOPTR's design in order to minimize the weakness will be shown. Most of the data were taken with the pulse tube oriented cold side up, but one set of data with the pulse tube oriented cold side down will be shown.

8.1 Procedure and Results

The refrigerator was operated with a fixed speed and hot platform temperature, and the pressure's amplitude and phase, piston power, and cooling power were measured as a function of the cold platform temperature. V_{sw} is the peak to peak piston displacement volume. $|p_1|$, the pressure amplitude, was measured directly from the readings of pressure gauges. The maximum and minimum values of $\Delta p = p_{top} - p_{bot}$ during the refrigerator's cycle were recorded, and the difference between the two divided by two gave the pressure amplitude, since $|p_1|$ is half of the peak to peak amplitude. The phase between p_1 and V_{sw} was calculated from the data using the Fourier transform. T_C was actively controlled by a feedback controller that delivered current to the heater mounted on the cold platform, and the heat delivered averaged over five to ten periods determined the cooling

power $\dot{Q}_C$. $\dot{W}_p$, the work done by the piston on the fluid per unit time, was calculated from $-\frac{1}{\tau}\int_0^\tau \Delta p \cdot dV$. The methods used to measure the cooling power and piston power of the SOPTR here are analogous to the methods used for the uniform temperature SSR measurements described in detail in Chapter 4.

Fig. 8.1 shows the cooling power measured with the pulse tubes oriented cold side down before they were inverted to the cold side up configuration that was used to measure all the other data presented in Chapters 6 through 8. For this set of measurements, each pulse tube was approximately 11 cm long, corresponding to a pulse tube volume of 3.0 cm^3. The orifice was a single length of flow impedance 2.5 cm long as opposed to 16 of them being in parallel for the measurements with the pulse tube oriented cold side up. The refrigerator was operated with a 17% mixture.

The cooling power in Fig. 8.2 was measured near the SOPTR's natural frequency of 15 mHz as discussed in Chapter 6. Eq. 6.1.17 gives, for a lossless cycle with an ideal gas,

$$\dot{Q}_C = \frac{T_C}{T_H}\dot{W}_p, \tag{8.1.1}$$

where $\dot{Q}_C$ is the cooling power and $\dot{W}_p$ is the average work done by the piston on the fluid per unit time. Hence we expect the gross cooling power, which is the expected cooling power for an ideal lossless cycle with an ideal gas working fluid, to be $\frac{T_C}{T_H}\dot{W}_p$. The dashed lines in Fig. 8.2 is this expected gross cooling power. We also display in Fig. 8.2 Stirling refrigerator data taken before we replaced the cold pistons with the pulse tubes, for the same ^3He concentration and operating frequency. To account as well as possible for the slightly different piston stroke used in the earlier data, we multiplied the earlier cooling powers by 0.85 to bring them into agreement with the piston power at T_C=1 K.

Fig. 8.3 shows the result of measurements with optimum parameters in order to maximize the cooling power. It was shown in Chapter 6 that the maximum cooling power for a 17% mixture and T_H=1 K is achieved when the frequency is around 30 mHz. It was also discussed in Chapter 7 that the cooling power increases linearly with $(V_{sw})^2$ up to the maximum V_{sw} attainable with this refrigerator. Hence we operated the refrigerator with a frequency of 1/40 s = 25 mHz and a V_{sw} of 1.80 cm^3 in an attempt to maximize the SOPTR's cooling power with a 17% mixture and T_H=1 K.

The SOPTR's cooling power was also investigated at lower temperatures in order to find the ^{3}He evaporation refrigerator-SOPTR system's minimum temperature. A 6% mixture was chosen in order to avoid phase separation. It was indicated in Chapter 6 that the maximum cooling power is obtained when the refrigerator is run at a higher speed than the natural frequency, and that there is a loss mechanism at high frequencies. Though the loss mechanism is not fully understood, we chose for this set of measurements a frequency several times higher than the natural frequency in an attempt to maximize the cooling power. The pressure decay time constant after an abrupt change in piston position as the fluid flows out through the orifice, shown in Appendix K, is 50 s based on measurements. This gave us a natural period of 2π(50 s)=314 s. A period of 120 s was therefore chosen. Similarly, V_{sw} was set near the maximum at 1.60 cm^3 following the guidelines presented in Chapter 7. T_H was maintained at 0.374 K. The result is shown in Fig. 8.4.

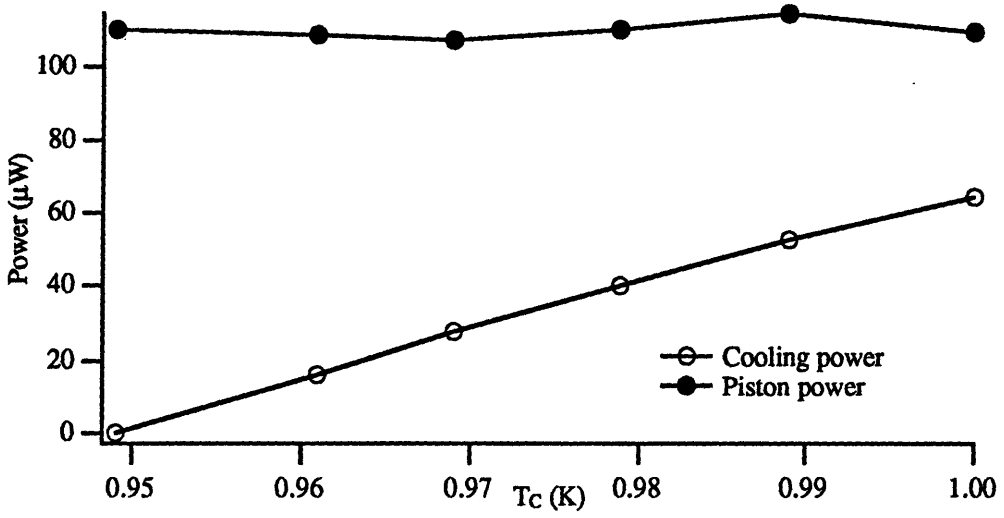

Figure 8.1. The SOPTR's cooling power and piston power with a 17% mixture , T_H of 1 K, a period of 84 s, and V_{sw} of 1.98 cm^3. This set of data was measured with the pulse tubes oriented cold side down. The lines are only guides to the eye.

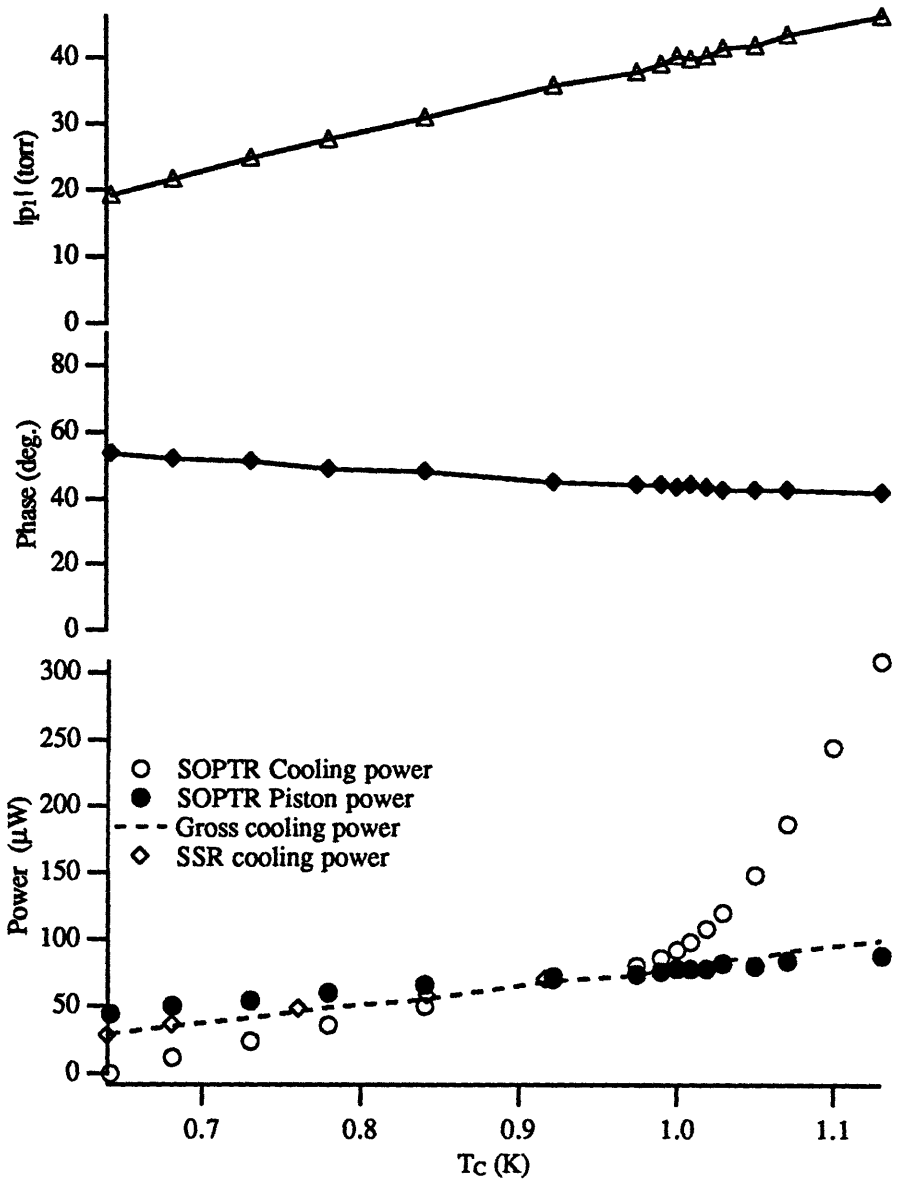

Figure 8.2. The SOPTR's pressure amplitude, phase between piston motion and pressure, cooling power, and piston power with a 17% mixture, T_H of 1 K, a period of 80 s, and V_{sw} of 1.12 cm^3. Diamonds are scaled cooling powers under similar operating conditions for conventional Stirling configuration. The solid lines are only guides to the eye. Dashed line is expected gross cooling power for a reversible machine calculated from the SOPTR piston power.

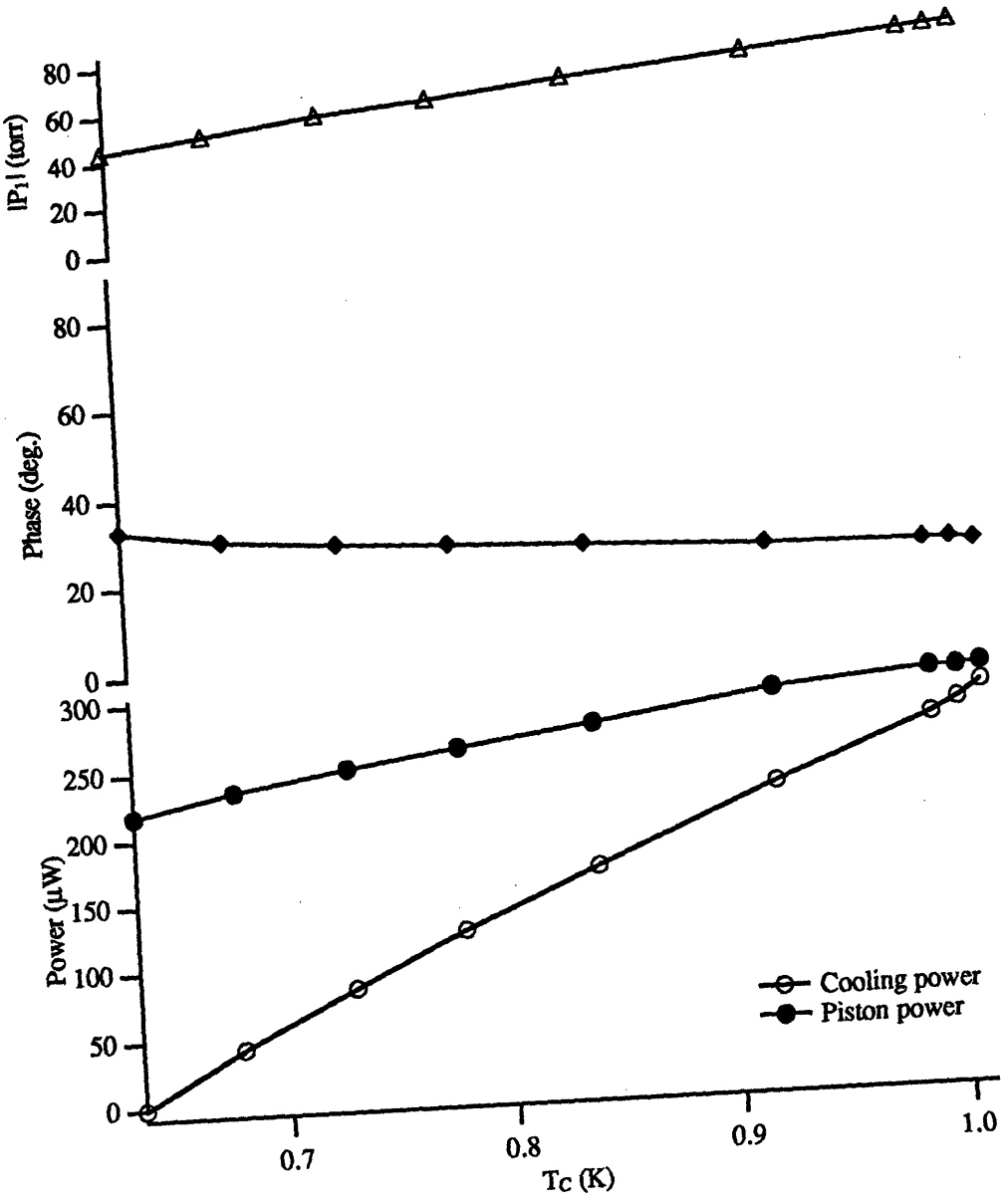

Figure 8.3. The SOPTR's pressure amplitude, phase between piston motion and pressure, cooling power, and piston power with a 17% mixture, T_H of 1 K, a period of 40 s, and V_{sw} of 1.80 cm^3. The lines are only guides to the eye.

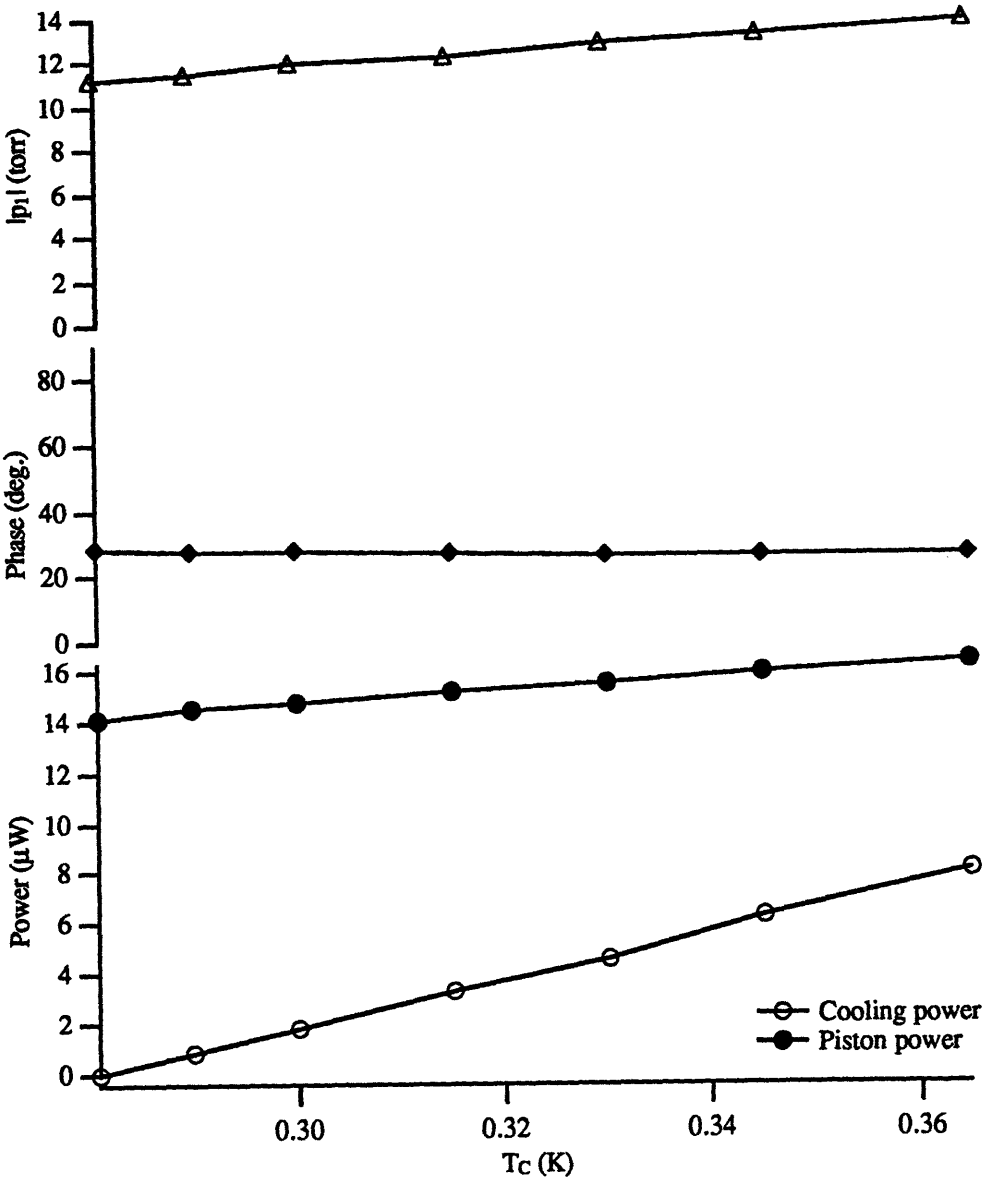

Figure 8.4. The SOPTR's pressure amplitude, phase between piston motion and pressure, cooling power, and piston power with a 6% mixture, T_H of 0.374 K, a period of 120 s, and V_{sw} of 1.60 cm^3. The lines are only guides to the eye.

8.2 Discussion

Fig. 8.1 shows that the refrigerator has only achieved a T_C of 0.95 K with the pulse tubes oriented cold side down. However, the fact that there is an amount of cooling power comparable to the piston power when both the hot and the cold platforms are near 1 K suggests that there is a significant amount of gross cooling power in the refrigerator. Fig. 8.1 also suggests that there is some form of loss mechanism that precludes the refrigerator from cooling below 0.95 K. We find the loss mechanism as follows. We can write

$$\dot{Q}_{measured} = \dot{Q}_{ideal} - \dot{Q}_{losses} \tag{8.2.1}$$

where $\dot{Q}_{measured}$ is the measured cooling power and $\dot{Q}_{losses}$ accounts for thermal loads on the cold platform due to loss mechanisms. Using Eq. 8.1.1 to approximate $\dot{Q}_{ideal}$, linear regression of data reveals $\dot{Q}_{losses} = 45.6+1120(T_H-T_C)$ [μW].

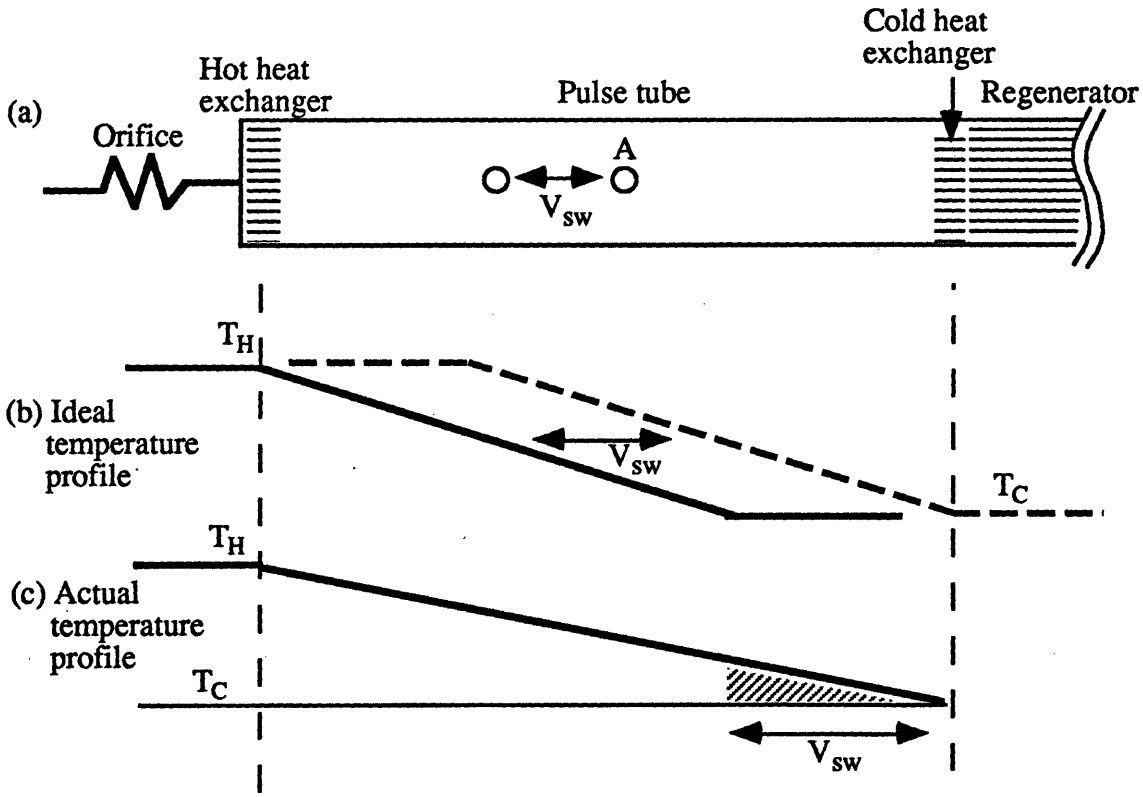

Figure 8.5. The fluid's temperature profile in the pulse tube. The heavy lines indicate the fluid's temperature in the pulse tube during the refrigerator's cycle.

The loss mechanism arises from turbulent mixing of the fluid in the pulse tube that destroys the insulating quality of the imaginary piston. Both the entrance of warm fluid into the cold heat exchanger as the fluid in the pulse tube executes an oscillatory motion and the convective heat transfer contribute to the heat load. We use the model shown in Fig. 8.5 to find the approximate magnitude of the former effect. Particle A in Fig. 8.5 (a) executes a harmonic motion inside the pulse tube with an amplitude of the order of the piston swept volume. Ideally, as shown in Fig. 8.5 (b), its temperature throughout the cycle is constant except for a slight variation due to adiabatic compression and expansion. The solid line and the dashed line indicate the fluid's temperature profile in the pulse tube during the leftmost and rightmost peaks of travel, respectively, ignoring the phase difference between the fluid motions across the length of the pulse tube. Ideally, the fluid particles that enter the orifice and the regenerator during the cycle remain at T_H and T_C, respectively, throughout the cycle. However, gravitational convection mixes the fluid in the pulse tube and hence the temperature profile indicated by the solid line in the ideal case, where the fluid is in the leftmost peak of travel, becomes approximately linear from the hot end to the cold end, as shown in Fig. 8.5 (c). As the fluid travels to the right, fluid near the right end of the pulse tube enters the cold heat exchanger and cools to T_C. The amount of enthalpy represented by the dashed area must therefore be absorbed by the cold platform during each cycle. This enthalpy is given approximately by $V_{sw}\rho C_p\overline{T}$, where ρ and C_p are the ^{3}He's density and specific heat, and $\overline{T}$ is the average temperature difference between the fluid in the dashed area and the cold platform. Multiplying by twice the operating frequency because there are two pulse tubes in this refrigerator, we obtain an expression for the heat load on the cold platform due to the mixing of fluid in the pulse tube:

$$\dot{Q}_{mixing} = fV_{sw}\rho C_p(V_{sw}/V_{pt})(T_H-T_C) \qquad (8.2.2)$$

where f is the frequency. For the operating conditions in Fig. 8.1, this expression yields $\dot{Q}_{mixing} = 1800\ \mu W/K\ (T_H-T_C)$ which is close to the observed loss inferred from Eq. 8.2.1.

It is of interest to calculate the Rayleigh number, which is the ratio of the fluid's buoyancy force to the viscous force:

$$R = \beta g \vartheta h^3 \rho^2 C_p/\mu\kappa \qquad (8.2.3)$$

where β is approximately -1/3T, g is the gravitational constant, ϑ is a temperature difference, h is a length scale, μ is the viscosity, and κ is the thermal conductivity. For a 17% mixture at 1 K, μ is[17] 1.5×10^{-6} kg/m-s, and κ is[12] 0.04 W/m-K. It is not certain whether the pulse tube's diameter or length should be used for the length scale, but |R| is around 10^6 for the former and 5×10^9 for the latter. This suggests that the buoyancy force far outweighs the viscous force in the pulse tube, thus leading to convective mixing of the fluid.

In Fig. 8.1, note that the cooling power is significantly lower than the piston power when the cold platform temperature is equal to the hot platform temperature. However, they would intersect if we extrapolated the cooling power to around 1.03 K. We believe that the hot end of the pulse tube is slightly warmer in reality than the hot platform on which the hot thermometer is mounted due to an imperfect thermal contact between the two parts. The heat dissipated in the orifice puts a thermal load on the hot heat exchanger of the pulse tube, and the imperfect thermal contact would result in the hot end of the pulse tube being slightly warmer than the hot platform. This imposes a thermal gradient in the pulse tube which results in a thermal load on the cold platform due to $\dot{Q}_{mixing}$ discussed above. A 30 mK of temperature difference would explain the disparity between the cooling power and the piston power when "$T_H=T_C$."

The cooling power in Fig. 8.2 was measured near the SOPTR's natural frequency of 15 mHz as discussed in chapter 6. The phase between the piston motion and the fluid's pressure remains near 45°, which is the expected phase of a Stirling refrigerator operating with $T_H=T_C$, isothermal compressions and expansions in the pistons, and a 90° phase between the hot and cold pistons. Using Eq. 8.1.1 and 8.2.1, linear regression of the data reveals $\dot{Q}_{losses} = -11.4+107(T_H-T_C)$ [μW] at T_C below 1 K. $\dot{Q}_{losses}$ at $T_H=T_C$, where the losses are predicted to be negligible, is non-zero because the working fluid and the refrigerator's cycle are non-ideal. This is the sum of the heat loads due to the pulse tube and the imperfect thermal contact in the regenerator. To estimate what fraction is due to the regenerator, we compare the SOPTR's cooling power with the SSR's cooling power measured under nearly identical operating conditions which are indicated by the diamonds in Fig. 8.2. These data fall much closer to the gross cooling power line than do the indicated cooling power of the pulse tube refrigerator, suggesting that the thermal losses through the regenerator are negligible compared to the thermal losses through the pulse tubes. Hence our data imply that the pulse tubes deliver a load of roughly (107 μW/K)(T_H-T_C) to the cold heat exchangers. This heat load must match the various loss mechanisms in the pulse tube. We estimate from thermal conductivity of the mixture that heat load on the cold platform due to ordinary thermal conduction through the pulse tubes

is 40 μW/K(T_H-T_C) for the conditions of Fig. 8.2, which is of the same order of magnitude as the observed loss.

Clearly, by using longer, thinner pulse tubes, it will be simple to reduce pulse tube losses by an order of magnitude in future superfluid orifice pulse tube refrigerators, while still keeping $\delta_{v,eff}$ much smaller than the pulse tube diameter and keeping viscous dissipation within $\delta_{v,eff}$ acceptably low. Hence, we expect that a ground-based superfluid pulse tube refrigerator can approximate the performance of a superfluid Stirling refrigerator, except for the added heat loads imposed on the heat sink at T_H by the dissipation in the orifice and the increased mechanical power input required to give the same amount of cooling power as that of a Stirling refrigerator.

Notice the dramatic increase of the "cooling power" when T_C>T_H. This is due to thermal convection in the pulse tube which tends to cool the "cold" platform through the mechanism shown in Fig. 8.5, thus enhancing the cooling power.

The cooling power shown in Fig. 8.3, as expected, increased to several times that shown in Fig. 8.2 due to the higher operating frequency and a larger piston swept volume. The cooling power at T_C=1 K, for instance, is 278 μW, which is about three times the cooling power of 92 μW under the same temperature in Fig. 8.2. The minimum temperature achieved, however, is virtually identical at 636 mK versus 642 mK for the earlier run, implying that the thermal losses have also increased proportionately.

Fig. 8.4 shows the cooling power measured with a 6% mixture. The SOPTR was only able to reach a minimum temperature of 0.281 K, which gives a T_C/T_H of 0.75, whereas the SSR with a 4.9% mixture and a period of 100 s reached a T_C/T_H of 168 mK/383 mK=0.44. The low efficiency of the SOPTR can be attributed to the heat conduction through the pulse tube, which is estimated based on thermal conductivity of the fluid to be 70 μW/K (T_H-T_C). This expression yields 6.5 μW for the coldest datum in Fig. 8.4, which is of the same order of magnitude as the observed heat loss.

The ^{3}He-^{4}He mixture's thermal conductivity at this concentration is significantly higher than that of a higher concentrated mixture,[12] while the gross cooling power to first approximation is proportional to concentration. A 6% mixture therefore yields a lower gross cooling power and a higher thermal load compared to a mixture of higher concentration, resulting in a significantly lower net cooling power. The SOPTR is therefore not suitable as a low temperature refrigerator unless the pulse tube's dimensions are altered significantly.

8.3 Conclusion

The SOPTR's net cooling power was found to be substantially lower than that of an SSR operating under similar conditions due to thermal conduction through the pulse tube. The use of a lower concentration mixture resulted in a lower gross cooling power and a higher thermal loss compared to a mixture of higher concentration, resulting in a significantly lower net cooling power. The use of longer, thinner pulse tubes would substantially lower the thermal conduction, though such pulse tubes would not work in a zero gravity environment. Operating the refrigerator with a positive thermal gradient in the pulse tube resulted in a substantial thermal load on the cold platform due to turbulent mixing of the fluid in the pulse tube.

Appendix A The ^{3}He pot's Cooling Power

The recirculating ^{3}He pot's cooling power was measured by applying a fixed voltage through the circuit shown in Fig. 4.1, measuring V_1 and V_2 to find $\dot{Q}=V_1V_2/R_2$ dissipated by the heater, and finding the temperature T where the ^{3}He platform settled down to. The steady-state cooling power versus temperature is shown in Fig. A.1. R_2 was 10,000 Ω. With no current applied to the heater, the temperature would slowly creep down to below 0.385 K, but we did not wait long enough for it to settle down. At $\dot{Q}$=3450 μW, the ^{3}He pot ran dry and the temperature rose rapidly.

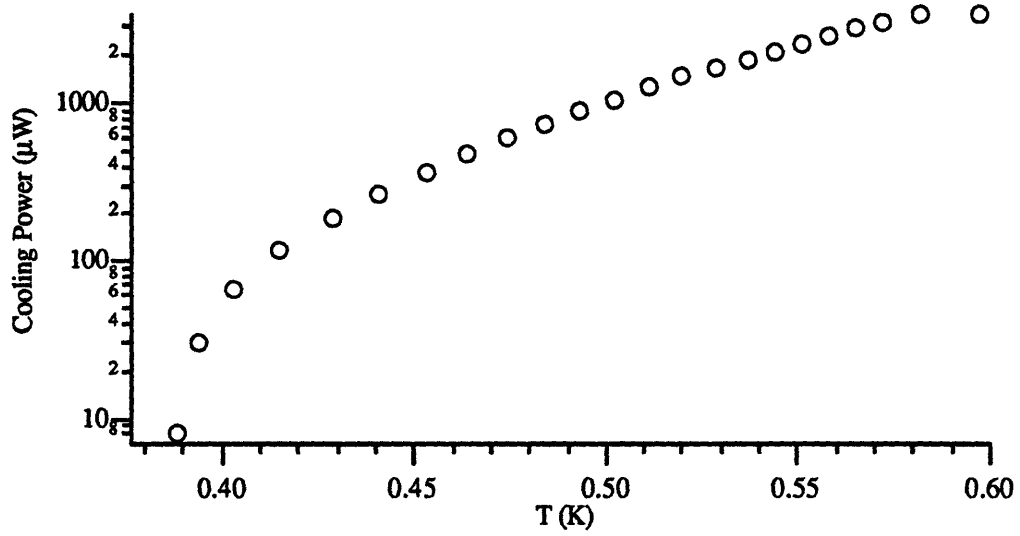

Figure A.1. The power delivered to the ^{3}He platform versus the temperature

Appendix B The SSR's Volume

The SSR's volume was found from the amount of mixture it took to fill the refrigerator. Neglecting the small volume (of the order of 0.1 cm^3) in the connecting tubes, the total amount of liquid ^3He-^4He mixture in the refrigerator is

$$V_{liq} = 2(V_{SSR}+V_{valve}) \tag{B.1}$$

where V_{SSR} is the closed volume of each half of the SSR when the pistons are held at the middle of their travel and V_{valve}, the volume within the valve used to seal the SSR's filling line which is outside the SSR's closed volume, is 0.29 cm^3. Chapter 3 discusses V_{valve} in more detail. The factor of two comes from the fact that there are two SSR's in parallel. V_{liq} may be calculated from the amount of mixture the refrigerator took from a tank at room temperature to fill the refrigerator. We assume an ideal gas for the room temperature tank:

$$pV=nRT \tag{B.2}$$

where p is the pressure of the mixture in the tank, V, the volume of the tank, is 22.9 liters, n is the number of moles of mixture in the tank, R is the universal gas constant, and T, the temperature of the gas in the tank, is 293 K. We can write

$$\begin{aligned} p_1V &= n_1RT \\ p_2V &= n_2RT \end{aligned} \tag{B.3}$$

where the subscripts 1 and 2 refer to before and after the refrigerator was loaded, respectively. During one filling, p_1 was 688 torr and p_2 was 267 torr, which means

$$(n_1-n_2) = (p_1-p_2)V/RT = 0.526 \text{ mol.} \tag{B.4}$$

The volume of liquid ^3He-^4He in the refrigerator corresponding to this amount is

$$V_{liq} = \rho\,(n_1-n_2) = (28.8 \text{ cm}^3/\text{mol})\,(0.526 \text{ mol}) = 15.1 \text{ cm}^3 \tag{B.5}$$

where ρ is given by Eq. D.4. Eq. B.1 then gives

$$V_{SSR} = V_{liq}/2\text{-}V_{valve} = 15.1\ cm^3/2 - 0.29\ cm^3 = 7.26\ cm^3. \quad (B.6)$$

From this we can find the volume of the piston. Assuming that the hot and the cold pistons have identical average volumes V_0, the SSR's average volume is given by

$$V_{SSR} = 2V_0 + V_r \quad (B.7)$$

where V_r is the volume of the regenerator. The latter is given by

$$V_r = NL\pi D^2/4 \quad (B.8)$$

where N, the number of tubes, is 119, L, the length of the regenerator, is 20.3 cm, and D is the inner diameter of the capillary. D is the capillary's outer diameter minus twice the wall thickness:

$$D = 0.305\ mm - 2\times 0.038\ mm = 0.229\ mm. \quad (B.9)$$

So Eq. B.8 gives $V_r = 1.00\ cm^3$. The dimensions of the regenerator are found in Ref. 4. Eq. B.7 then gives

$$V_0 = (V_{SSR} - V_r)/2 = 3.13\ cm^3. \quad (B.10)$$

As a check, we calculate V_0 from geometry.

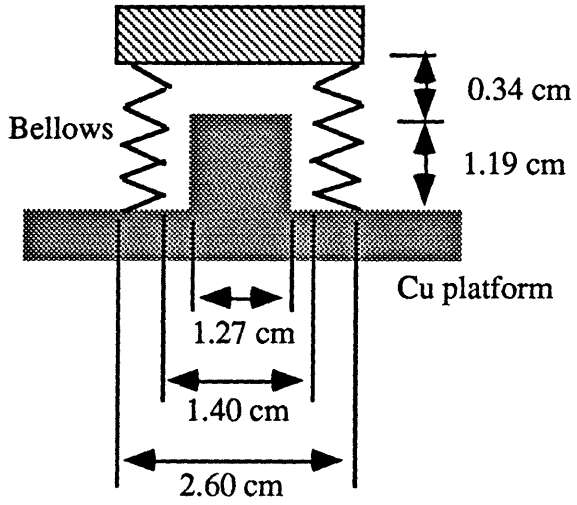

Figure B.1. The piston's geometry

Some of the dimensions are from the SSR's drawings, others are direct measurements. The effective area of the bellows[16] is 3.16 cm^2. V_0 is given by

$$V_0 = 3.16\ cm^2\ (1.19\ cm+0.34\ cm) - (\pi/4)(1.27\ cm)^2(1.19cm) = 3.32\ cm^3 \quad (B.11)$$

which shows a reasonable agreement with the value in Eq. B.10.

Appendix C The SSR's Background Heat

The friction generated by the bellows and other sources results in a background heat. The background heat was measured in order to find the total amount of heat absorbed by the fluid in the cold platform for the measurements in Chapter 4.

The procedure was as follows. The mixture in the SSR was removed and replaced by a small amount of ^{4}He. This created a thin ^{4}He film on the interior on the refrigerator which thermally linked the hot platform and the cold platform weakly. The hot platform was cooled with the ^{3}He pot and left overnight. The cold platform slowly cooled down due to the thermal link with the hot platform. T_H was raised with the heater mounted on the hot platform to match T_C on the following morning and the virtually empty SSR was operated with a period of 100 seconds and piston strokes identical to that used for the 4.9% constant temperature measurements. The friction generated by the bellows and other sources slowly raised T_C. T_H was manually controlled using the heater mounted on the hot platform to match T_C at all times in order to eliminate thermal conduction from one platform to the other. The background heat was calculated from the rate of temperature increase of the copper platform:

$$\dot{Q}_{background} = nC_p dT_C/dt \qquad (C.1)$$

where n is the number of moles of copper in the cold platform and C_p is the copper's specific heat. The volume of the cold platform was estimated from geometry as 240 cm^3, resulting in the number of moles of:

$$n = (240\ cm^3)\ (8.93\ g/cm^3)/(64 g/mol) = 33.4\ mol. \qquad (C.2)$$

The heat capacity of copper was approximated[12] as

$$C_p = 1.24\ T - 0.46 \qquad [mJ/mol\text{-}K] \qquad (C.3)$$

where T is in K. Fig. C.1 shows the result of several runs where each symbol corresponds to a run. The rate of heating is seen to increase with temperature, but this is suspected to be due to the change in the rate of heating with time. The block of brass attached to the top of the bellows is weakly linked to the copper platform via the bellows, possibly resulting in an RC time constant for the rate of heating of the copper platform.

In one run shown by the square symbols, the SSR was stopped at around 1.05 K. T_C kept rising after the SSR was stopped, though at a slower rate than when the SSR was running as shown by the black squares, supporting the above theory. This phenomenon is not completely understood. The background heat was determined to be

$$\dot{Q}_{background} = 2\pm1\ \mu W \tag{C.4}$$

where the uncertainty indicates two standard deviations. For the conditions of other measurements, we assume that the background heat is proportional to the frequency and the square of the piston swept volume,[1] so

$$\dot{Q}_{background} = (100\ s/\tau)\ (V_{sw}/1.55\ cm^3)^2\ (2\pm1\ \mu W) \tag{C.5}$$

where τ is the refrigerator's period.

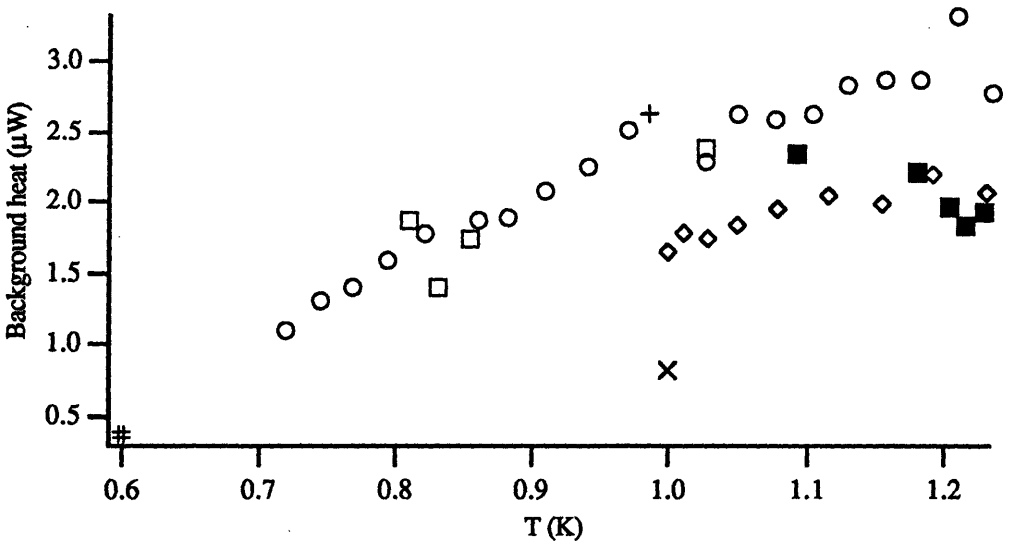

Figure C.1. The SSR's background heat calculated from the rate of heating of the cold platform. Each symbol corresponds to a run. The swept volume was 1.55 cm^3 and the period was 100 s.

Appendix D The Density of Liquid ^{3}He -^{4}He Mixtures

Radebaugh[14] gives the following formula for the conversion between the mixture's concentration and density:

$$1/\rho = 27.6/X + 7.6 + 1.65X^2 \qquad \text{(D.1)}$$

where ρ is in moles of mixture/m^3 and X is the ^{3}He molar concentration. However, this formula has the disadvantage of being difficult to invert. Hence we create the following simple model to find X from ρ.

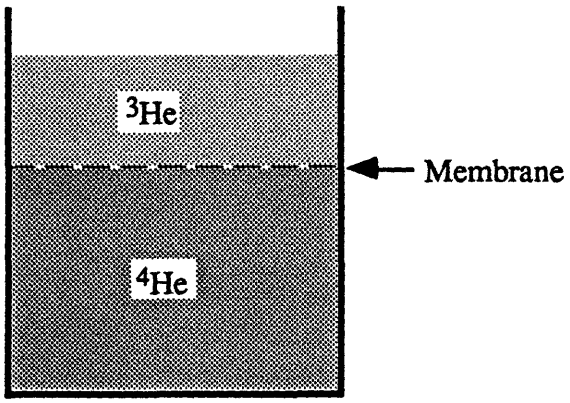

Figure D.1. Pure ^{3}He and pure ^{4}He in a container separated by a membrane

We assume that pure ^{3}He and pure ^{4}He are separated by a membrane in a container and that the total volume will remain unchanged when the membrane is broken and the two fluids mix together to from a homogeneous mixture. ^{3}He has a molar volume of[19]

$$v_3 = 36 \text{ cm}^3/\text{mole}. \qquad \text{(D.2)}$$

^{4}He has a molar volume of[19]

$$v_4 = (4 \text{ g/mole})/(0.145 \text{ g/cm}^3) = 27.6 \text{ cm}^3/\text{mole}. \qquad \text{(D.3)}$$

Assuming X mole of ^{3}He and (1-X) mole of ^{4}He, the volume occupied by ^{3}He is 36X cm^3 and the volume occupied by ^{4}He is 27.6(1-X) cm^3. The overall molar density is

$$\rho = \frac{1}{36X + 27.6(1-X)} mole/cm^3 = \frac{10^6}{27.6 - 8.4X} mole/m^3. \quad \text{(D.4)}$$

This formula is accurate to within ±1% of Eq. D.1 for X<0.8. Solving for X, we find

$$X = \frac{27.6 - 10^6/\rho}{8.4} = 3.28 - 1.19\times10^5/\rho \quad \text{(D.5)}$$

where ρ is the overall density in mole/m^3.

Appendix E Numerical Evaluation of Q_C/Wc

The normalized isothermal compressibility, $\frac{1}{\rho RT}\left(\frac{\partial p}{\partial c}\right)_{T,\mu_4}$, where ρ is the total mass density of the mixture, R is the gas constant per mass of ^{3}He, and c is the mass concentration of the mixture, is evaluated as follows. We first convert the expression to partial derivative at constant temperature and pressure, as Radebaugh's tables[14] list values at constant pressure. We can write

$$dp_{os} = \left(\frac{\partial p_{os}}{\partial c}\right)_{T,p} dc + \left(\frac{\partial p_{os}}{\partial T}\right)_{c,p} dT + \left(\frac{\partial p_{os}}{\partial p}\right)_{c,T} dp \tag{E.1a}$$

$$dp = \left(\frac{\partial p}{\partial c}\right)_{T,\mu_4} dc + \left(\frac{\partial p}{\partial T}\right)_{c,\mu_4} dT + \left(\frac{\partial p}{\partial \mu_4}\right)_{T,c} d\mu_4. \tag{E.1b}$$

Substituting Eq. E.1b into Eq. E.1a,

$$dp_{os} = \left[\left(\frac{\partial p_{os}}{\partial c}\right)_{T,p} + \left(\frac{\partial p_{os}}{\partial p}\right)_{T,c}\left(\frac{\partial p}{\partial c}\right)_{T,\mu_4}\right] dc + \left[\left(\frac{\partial p_{os}}{\partial T}\right)_{c,p} + \left(\frac{\partial p_{os}}{\partial p}\right)_{T,c}\left(\frac{\partial p}{\partial T}\right)_{c,\mu_4}\right] dT + \left(\frac{\partial p_{os}}{\partial p}\right)_{T,c}\left(\frac{\partial p_{os}}{\partial \mu_4}\right)_{T,c} d\mu_4. \tag{E.2}$$

Using the identity

$$\left(\frac{\partial p}{\partial c}\right)_{T,\mu_4} = \left(\frac{\partial p_{os}}{\partial c}\right)_{T,\mu_4}, \tag{E.3}$$

Eq. E.2 yields

$$\left(\frac{\partial p_{os}}{\partial c}\right)_{T,\mu_4} = \left(\frac{\partial p_{os}}{\partial c}\right)_{T,p} + \left(\frac{\partial p_{os}}{\partial p}\right)_{T,c}\left(\frac{\partial p_{os}}{\partial c}\right)_{T,\mu_4}$$

$$\left[1 - \left(\frac{\partial p_{os}}{\partial p}\right)_{T,c}\right]\left(\frac{\partial p_{os}}{\partial c}\right)_{T,\mu_4} = \left(\frac{\partial p_{os}}{\partial c}\right)_{T,p}. \tag{E.4}$$

However[3], $\left(\frac{\partial p_{os}}{\partial p}\right)_{T,c} << 1$, whereby Eq. E.4 becomes

$$\left(\frac{\partial p_{os}}{\partial c}\right)_{T,\mu_4} = \left(\frac{\partial p_{os}}{\partial c}\right)_{T,p}. \tag{E.5}$$

The normalized isothermal compressibility can then be evaluated by taking differences between entries in Radebaugh's tables. We take a 6.6% concentration mixture at 1.5 K as an example. P. 109 of Radebaugh's tables gives the osmotic pressure of 6.4% mole concentration mixture and 7.0% mole concentration mixture at 1.5 K as 207.9 torr and 226.7 torr, respectively. The mass concentration is related to the molar concentration as

$$c = \frac{3X}{3X+4(1-X)} = \frac{1}{1+\frac{4}{3}\left(\frac{1}{X}-1\right)} \tag{E.6}$$

so the mass concentrations of 6.4% and 7.0% mole concentration mixtures are 0.0488% and 0.0534%, respectively. The total mass density of the mixture is

$$\rho_{m,m} = \rho_{m,n} \cdot M_m \tag{E.7}$$

where the first subscript m refers to the total mixture and the second subscripts m and n refer to the mass and the mole densities, respectively. $\rho_{m,n}$ is given by Eq. D.4 while

$$M_m = [3X+4(1-X)]\cdot 10^{-3}. \qquad [\text{kg/mole}] \tag{E.8}$$

The normalized isothermal compressibility is therefore

$$\frac{1}{\rho RT}\left(\frac{\partial p}{\partial c}\right)_{T,\mu_4} = \frac{1}{139.8\frac{kg}{m^3}\frac{8.314 J/mol\cdot K}{0.003 kg/mol}1.5K}\frac{(226.7torr - 207.9torr)133\frac{Pa}{torr}}{0.0534-0.0488}$$
$$= 0.935. \tag{E.9}$$

The results for other concentrations and temperatures are displayed in Table E.1.

T (K)	X=5.9%	X=17%	X=20%
0.3	0.86439	0.301995	
0.4	0.86439	0.416353	
0.5	0.871266	0.501845	0.365036
0.6	0.880761	0.569942	0.453828
0.7	0.888947	0.621754	0.524298
0.8	0.8957	0.666165	0.579617
0.9	0.900407	0.700707	0.627028
1	0.908592	0.730561	0.664957
1.1	0.915289	0.754987	0.69868
1.2	0.916778	0.779043	0.726782
1.3	0.921815	0.795982	0.752079
1.4	0.926132	0.813673	0.773058
1.5	0.929874	0.829006	0.792555

Table E.1. Normalized isothermal compressibility using the equation of state by Radebaugh.

We now evaluate the heat absorbed at the cold platform divided by the work done by the fluid on the cold piston for a reversible cycle, which is given by Eq. 4.1.3 as

$$\frac{Q_C}{W_C} = -\rho c_0 \frac{(\partial h_{os}/\partial c)_{T,p}}{(\partial p_{os}/\partial c)_{T,p}} - \rho(1-c_0)\frac{(\partial \mu_4/\partial c)_{T,p}}{(\partial p_{os}/\partial c)_{T,p}} \tag{E.10}$$

where c is the mass concentration of the mixture, μ_4 is the chemical potential of ^{4}He, c_0 is the average mass density in of the mixture in the refrigerator, h_{os} is the osmotic enthalpy of the mixture. Eq. E.10 is evaluated as follows using a central difference formula. We use a 5.9% mixture at 1 K as an example. Eqs. E.6 and E.8 produce the following table:

X	c	M_m (kg/mol)
0.055	0.041825	0.003945
0.059	0.044526	0.003942
0.064	0.048780	0.003936

Table E.2. Conversion from molar to mass concentration

We first evaluate the osmotic enthalpy at X = 5.5%:

$$h_{os} = \mu_3 + TS/c \tag{E.11}$$

where μ_3 is the ^{3}He's chemical potential and S is the entropy of the total mixture. Radebaugh's tables gives the following, where the page numbers are indicated in the parenthesis.

$$\mu_3 = \mu_{3f} + \mu_3' \qquad \text{(p.11)}$$

$$= (-15.0630 \text{ J/mol} - 0.362685 \cdot 8.314 \text{ J/mol·K}) \frac{1}{0.003 kg/mol} \qquad \text{(pp.9, 98)}$$

$$= -6026.12 \frac{J}{kg \cdot {}^3He}, \qquad \text{(E.12a)}$$

$$S = 2.064 \frac{J}{mol \cdot K} \frac{1}{0.003945 kg/mol \cdot soln} \qquad \text{(p.117)}$$

$$= 523.2 \text{ J/kg·K of soln}, \qquad \text{(E.12b)}$$

$$h_{os} = -6026.12 \frac{J}{kg \cdot {}^3He} + \frac{1.0K \cdot 523.2 \frac{J}{kg \cdot K \cdot soln}}{0.041825 \frac{kg \cdot {}^3He}{kg \cdot soln}}$$

$$= 6483.0 \frac{J}{kg \cdot {}^3He}. \qquad \text{(E.12c)}$$

The chemical potential of ^{4}He and the osmotic pressure are

$$\mu_4 = -0.4471 \frac{J}{mol} \frac{1}{0.004 kg/mol} \qquad \text{(p.108)}$$

$$= -111.8 \frac{J}{kg \cdot {}^4He} \qquad \text{(E.13a)}$$

$$p_{os} = 118.8 \text{ torr} = 15790 \text{ Pa}. \qquad \text{(p.108)}$$

(E.13b)

Similar calculation at X=6.4% yields

$$h_{os} = 6401.6 \frac{J}{kg \cdot {}^3He}$$

$$\mu_4 = -128.8 \frac{J}{kg \cdot {}^4He}$$

$$p_{os} = 18250 \text{ Pa}. \qquad \text{(E.14)}$$

Substitution into Eq. E.5 yields

$$\frac{Q_C}{W_C} = -140.4 \frac{kg}{m^3} (1\text{-}0.044526) \frac{-128.8 \frac{J}{kg} - \left(-111.8 \frac{J}{kg}\right)}{18250 Pa - 15790 Pa}$$

$$-140.4\ \frac{kg}{m^3}\ 0.044526\ \frac{6401.6\frac{J}{kg} - 6483.0\frac{J}{kg}}{18250Pa - 15790Pa}$$
$$= 0.9270 + 0.2070$$
$$= 1.134. \qquad \text{(E.15)}$$

Results for other temperatures and concentrations are shown below. Q_C/W_C for the 36% mixture was linearly extrapolated from the values at 25% and 29%.

T (K)	X=5.9%	X=17%	X=20%	X=25%	X=29%	X=36%
0.3	0.973	2.28				
0.4	1.004	1.782				
0.5	1.029	1.527	1.999	5.904		
0.6	1.016	1.391	1.655	2.765		
0.7	1.029	1.294	1.468	2.060	3.116	4.96
0.8	1.047	1.234	1.35	1.730	2.209	3.05
0.9	1.072	1.193	1.278	1.543	1.795	2.24
1	1.136	1.181	1.240	1.428	1.580	1.85
1.1	1.248	1.207	1.228	1.378	1.450	1.58
1.2	1.446	1.237	1.259	1.362	1.390	1.44
1.3	1.715	1.328	1.315	1.393	1.379	1.355
1.4	2.116	1.458	1.429	1.455	1.415	1.345
1.5	2.652	1.648	1.575	1.570	1.494	1.361

Table E.3. Q_C/W_C using the equation of state by Radebaugh.

In Eq. 4.1.12, the thermal expansion coefficient,

$$\beta = \frac{1}{v}\left(\frac{\partial v}{\partial T}\right)_p, \qquad \text{(E.16)}$$

was numerically evaluated using approximate values of $p_3(\rho,T)$, which may be obtained by using the ideal Fermi gas equation of state in Huang.[7] The pressure is approximated as

$$p = kT\frac{g}{\lambda^3} f_{5/2}(z) \qquad \text{(E.17)}$$

where k is the Boltzmann's gas constant, g is degeneracy (2 for ^{3}He). λ, the DeBroglie wavelength, is

$$\lambda = \sqrt{\frac{2\pi\hbar^2}{mkT}} \qquad \text{(E.18)}$$

where $\hbar$ is Planck's constant. z, the fugacity, is found from

$$\frac{1}{v} = \frac{g}{\lambda^3} f_{3/2}(z). \tag{E.19}$$

The Fermi functions are defined as

$$\begin{aligned} f_{3/2}(z) &= z\frac{\partial}{\partial z} f_{5/2}(z) \\ f_{5/2}(z) &= \frac{4}{\sqrt{\pi}} \int_0^\infty x^2 (1 + ze^{-x^2}) dx. \end{aligned} \tag{E.20}$$

Appendix F The Uncertainty in Piston Power due to Phase Lag in Data Acquisition

There were time leads/lags among the various quantities (p_{top}, p_{bot}, V_H, V_C, etc.) measured and recorded by the PC, which resulted in uncertainties in the piston powers calculated. The uncertainties in time were estimated as follows. The SSR's drive motor turning the camshaft was suddenly stopped or re-started while the PC was acquiring the data, and the time at which the various quantities indicated by the data came to rest or started moving were recorded. Measurements were recorded every 0.35 second. This procedure was repeated several times over a course of about a week, with the results shown below:

1) V_H and V_C stopped at t = 15.1 s and 14.7 s, respectively.
2) p_{top}, p_{bot}, V_H, and V_C stopped at t = 1.4 s, 1.4 s, 1.8 s, and 1.2 s, respectively.
3) p_{top}, p_{bot}, V_H, and V_C stopped at t = 2.3 s, 2.4 s, 2.4 s, and 2.3 s, respectively.
4) p_{top}, p_{bot}, and V_H stopped at t = 2.7 s, 2.7 s, and 2.9 s, respectively.
5) V_H and V_C stopped at t = 10.3 s and 11.1 s, respectively.

It is seen that the phasing among the various quantities is a random and not a systematic effect. For instance, V_H lagged V_C in case 1) but V_H lagged V_C in case 5). It is therefore assumed that any two quantities recorded by the PC may be expected to be off by a certain amount of time in a direction that we cannot predict. Further, if the timing between V_H and V_C tend to be off by a certain amount, then we will assume that the timing between p and V will be expected to be off by the same amount in a random direction. We therefore calculate the standard deviation

$$\sigma_{n-1} = \sqrt{\frac{\sum_{i=1}^{n}(x_i - \bar{x})^2}{n-1}} \qquad \text{(F.1)}$$

of the timing in each case and take the average of the five standard deviations in order to find the time by which we can expect any two quantities recorded by the PC to be off by. σ_{n-1} for case 1 is found by substituting x_1 = 15.1 s and x_2 = 14.7 s into Eq. F.1, which yields a standard deviation of 0.28 s. Similarly, cases 2 through 5 yield standard deviations of 0.26 s, 0.06 s, 0.14 s, and 0.57 s, respectively. The average of the five

standard deviations is 0.26 s, resulting in the uncertainty in ϕ, the phase between the piston motion and the pressure, of

$$\Delta\phi = (0.26\ s/\tau)\cdot 360^\circ. \tag{F.2}$$

Eq. 6.1.13 suggests that the piston power is proportional to $\sin\phi$. The relative uncertainty in the piston power resulting from $\Delta\phi$ is therefore

$$\Delta\dot{W}/\dot{W} = [\sin(\phi+\Delta\phi)-\sin\phi]/\sin\phi \tag{F.3}$$

where the uncertainty in the timing between p_{top} and p_{bot} has been ignored for simplicity. ϕ is 45° for the SSR, and $\Delta\phi$ was doubled for the SSR constant temperature measurements in Chapter 4 in order to give two standard deviations.

Appendix G The Uncertainty in Q_C/W_C due to Uncertainty in Temperature

$|T_H-T_C|$ was as large as a five mK when the SSR constant temperature measurements were taken, which may lead to an uncertainty in the measured $\dot{Q}_C / \dot{W}_C$. In order to find the effect of T_H-T_C on $\dot{Q}_C / \dot{W}_C$, the refrigerator was operated with T_C deliberately set different form T_H and $\dot{Q}_C / \dot{W}_C$ was measured. T_H was set at 0.95 K and T_C was varied by as much as 20 mK above and below T_H. The result is shown below. Circles indicate the measured $\dot{Q}_C / \dot{W}_C$ and the line, which is a linear interpolation of the measurements, is

$$\dot{Q}_C / \dot{W}_C = 1.243 + 0.544/\mathrm{K}\ (T_H-T_C). \qquad \text{(G.1)}$$

The shift in $\dot{Q}_C / \dot{W}_C$ for T_H-T_C= 5 mK is therefore 0.0027 or 0.2%, which is negligible. The average of the absolute values of the difference between the measurements and the line, which is a measure of the scatter of data, is 0.005 or 0.4%, which is still quite small. The uncertainty in $\dot{Q}_C / \dot{W}_C$ that resulted from the uncertainty in T_H-T_C was therefore ignored.

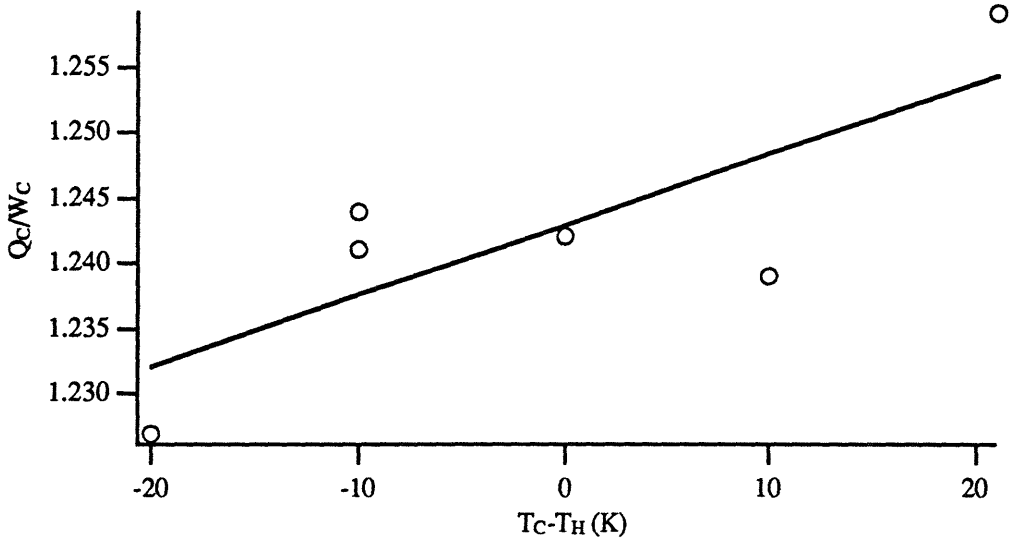

Figure G.1. The effect of T_H-T_C on $\dot{Q}_C / \dot{W}_C$. 17% mixture was used, and the refrigerator's period was 80 s. The hot and cold piston swept volumes were 1.02 cm^3 and 0.98 cm^3, respectively. The solid line is a linear interpolation of the measured values.

Appendix H The Schmidt Analysis

Schmidt analysis[18] shown below is based on ideal gas with sinusoidal piston motions. It assumes a constant thermal gradient in the regenerator, no temperature gradient in the pistons, no heat loss due to conduction from one platform to the other, and no frictional losses:

$$
\begin{aligned}
&W_C = Q_C = \pi V_{SWC} p_{mean} \sin\beta[(1-b^2)^{0.5}-1]/b \\
&p_{mean} \equiv nR/[s(1-b^2)^{0.5}] \\
&\tan\beta \equiv (V_{SWH}\sin\alpha/T_H)/[(V_{SWH}\cos\alpha/T_H)+(V_{SWC}/T_C)] \\
&c \equiv 0.5\times[(V_{SWH}/T_H)^2+2(V_{SWH}/T_H)(V_{SWC}/T_C)\cos\alpha+(V_{SWC}/T_C)^2]^{0.5} \\
&s \equiv (V_{SWC}/2T_C)+(V_{CLC}/T_C)+(V_h/T_H) \\
&\quad +V_r\ln(T_H/T_C)/(T_H-T_C)+(V_k/T_H)+(V_{CLH}/T_H)+(V_{SWH}/2T_H) \\
&b \equiv c/s \\
&V_H = V_{CLH}+V_{SWH}[1+\cos(\vartheta+\alpha)]/2 \\
&V_C = V_{CLC}+V_{SWC}(1+\cos\vartheta)/2
\end{aligned}
\qquad \text{(H.1)}
$$

where W_C is the work done on the cold piston by the fluid per cycle, Q_C is the heat removed from the cold platform per cycle, n is the number of moles of gas in the refrigerator, R is the universal gas constant, T_H is the hot platform temperature, T_C is the cold platform temperature, V_r is the regenerator volume, V_h is the volume between the hot piston and the regenerator, V_k is the volume between the cold piston and the regenerator, V_H is the hot piston volume, V_C is the cold piston volume, and ϑ is the crank angle. In our refrigerator, $\alpha = -90°$, $V_h = V_k = 0$, $b < 0.3$, and we assume

$$
\begin{aligned}
V_H &= V_0 + \frac{V_{sw}}{2}\sin\omega t \\
V_C &= V_0 + \frac{V_{sw}}{2}\cos\omega t
\end{aligned}
\qquad \text{(H.2)}
$$

where V_0 and V_{sw} are the average volume and the swept volume common to the hot and cold pistons. c, s, and $\sin\beta$ then become

$$
c = \frac{V_{sw}}{2}\sqrt{\frac{1}{T_H^2}+\frac{1}{T_C^2}}
$$

$$s = V_0\left(\frac{1}{T_H}+\frac{1}{T_C}\right)+V_r\frac{\ln\frac{T_H}{T_C}}{T_H-T_C}$$

$$\tan\beta = -\frac{V_{sw}/T_H}{V_{sw}/T_C} = -T_C/T_H$$

$$|\sin\beta| = \frac{1}{\sqrt{1+1/\tan^2\beta}}$$

$$\sin\beta = -\frac{1}{\sqrt{1+(T_H/T_C)^2}}. \qquad \text{(H.3)}$$

Expanding Q_C in Eq. H.1 to first order in b and V_{sw}/V_0, and multiplying by twice the operating frequency because our refrigerator consists of two Stirling cycles operating in parallel, we obtain

$$\begin{aligned}\dot{Q}_{Schmidt} &= 2fQ_C \\ &= 2f\frac{\pi V_{sw}nR}{s\sqrt{1-b^2}}\left[-\frac{1}{\sqrt{1+(T_H/T_C)^2}}\right]\frac{\sqrt{1-b^2}-1}{b} \\ &\approx \frac{2f\cdot\pi V_{sw}nR}{s}\left[-\frac{1}{\sqrt{1+(T_H/T_C)^2}}\right]\frac{-\frac{1}{2}b^2}{b} \\ &= \frac{f\pi V_{sw}nRc}{\sqrt{1+(T_H/T_C)^2 s^2}} \\ &= \frac{f\pi V_{sw}{}^2nR}{2V_0{}^2}\left[\frac{1}{\sqrt{1+\left(\frac{T_H}{T_C}\right)^2}}\frac{\sqrt{\frac{1}{T_H{}^2}+\frac{1}{T_C{}^2}}}{\left\{\frac{1}{T_H}+\frac{1}{T_C}+\frac{V_r}{V_0}\frac{\ln\frac{T_H}{T_C}}{T_H-T_C}\right\}^2}\right]. \qquad \text{(H.4)}\end{aligned}$$

The expression in the square brackets may be simplified using $\alpha = T_C/T_H$, whereby Eq. H.4 becomes

$$\dot{Q}_{Schmidt} = \frac{f\frac{\pi}{2}\left(\frac{V_{sw}}{V_0}\right)^2 nRT_H\left[\frac{\alpha}{1+\alpha}\right]^2}{\left[1-\frac{V_r}{V_0}\frac{\alpha\ln\alpha}{1-\alpha^2}\right]^2}. \qquad \text{(H.5)}$$

Appendix I Derivation of SOPTR's Frequency Response at Uniform Temperature

The pressure's amplitude and phase and the piston power for the SOPTR are derived as follows. Eq. 6.1.9 states

$$\frac{d(pV)}{dt} = -\frac{p-p_0}{R_o} \tag{I.1}$$

where R_0 is the resistive impedance of the orifice. Using

$$p(t)=p_0+\mathrm{Re}[p_1 e^{i\omega t}]$$
$$p(t)V(t) = n(t)RT \tag{I.2}$$

where p_1 is complex, n(t) is the number of moles of ^{3}He in the volume, and R is the universal gas constant, we find

$$p(t) = \frac{n(t)RT}{V(t)} = \frac{n(t)RT}{V_0}\frac{1}{1-\frac{V_1}{V_0}e^{i\omega t}} \tag{I.3}$$

where p(t) is the real part of Eq. I.3. Eq. I.1 then becomes

$$\frac{d(pV)}{dt} = \frac{d(nRT)}{dt} = -\frac{p-p_0}{R_o} = -\frac{1}{R_o}p_1 e^{i\omega t}$$
$$nRT = -\frac{\int p_1 e^{i\omega t}dt}{R_o} = -\frac{p_1}{i\omega R_o}e^{i\omega t} + \text{constant} = -\frac{p_1}{i\omega R_o}e^{i\omega t} + p_0V_0. \tag{I.4}$$

Eqs. I.3 and I.4 combine to give

$$p(t) = \frac{p_0V_0 - \frac{p_1}{i\omega R_o}e^{i\omega t}}{V_0}\frac{1}{1-\frac{V_1}{V_0}e^{i\omega t}} = p_0\left(1-\frac{p_1/p_0}{i\omega R_oV_0}e^{i\omega t}\right)\left(1+\frac{V_1}{V_0}e^{i\omega t}\right)$$
$$= p_0\left[1+\left(\frac{V_1}{V_0}-\frac{p_1/p_0}{i\omega R_oV_0}\right)e^{i\omega t}\right] = p_0+p_1e^{i\omega t} = p_0\left[1+\frac{p_0}{p_1}e^{i\omega t}\right]$$
$$\frac{p_1}{p_0} = \frac{V_1}{V_0}-\frac{p_1/p_0}{i\omega R_oV_0}$$

$$\frac{p_1}{p_0} = \frac{V_1}{V_0}\frac{1}{1+\dfrac{1}{i\omega R_0 V_0}} = \frac{V_1}{V_0}\frac{1}{1+\dfrac{1}{i\omega R_0 V_0}}\frac{1-\dfrac{1}{i\omega R_0 V_0}}{1-\dfrac{1}{i\omega R_0 V_0}} = \frac{V_1}{V_0}\frac{1}{1+\left(\dfrac{1}{\omega R_0 V_0}\right)^2}\left(1+\frac{i}{\omega R_0 V_0}\right)$$

$$|p_1| = p_0\frac{V_1}{V_0}\frac{1}{1+\left(\dfrac{1}{\omega R_0 V_0}\right)^2}\sqrt{1+\left(\frac{1}{\omega R_0 V_0}\right)^2} = p_0\frac{V_1}{V_0}\frac{1}{\sqrt{1+\left(\dfrac{1}{\omega R_0 V_0}\right)^2}} \qquad \text{(I.5a)}$$

$$\phi = \tan^{-1}\left(\frac{1}{\omega R_0 V_0}\right) \qquad \text{(I.5b)}$$

to first order in (p_1/p_0) and (V_1/V_0), where

$$p = p_0 + |p_1|\cos(\omega t+\phi). \qquad \text{(I.6)}$$

The work done by the piston on the fluid is the negative of the work done by the fluid on the piston. Using

$$p = p_0+p_1e^{i\omega t} = p_0 + |p_1|\cos(\omega t+\phi) = p_0\left[1+\frac{|p_1|}{p_0}\cos(\omega t+\phi)\right]$$

$$V = V_0-V_1 e^{i\omega t} = V_0-V_1\cos\omega t$$

$$dV = \omega V_1\sin\omega t\, dt, \qquad \text{(I.7)}$$

the piston power is

$$\begin{aligned}
\dot{W} &= -\frac{1}{\tau}\int_0^\tau p\,dV \\
&= -\frac{\omega V_1 p_0}{\tau}\int_0^\tau\left[1+\frac{|p_1|}{p_0}\cos(\omega t+\phi)\right]\sin\omega t\,dt \\
&= -\frac{\omega V_1 p_0}{\tau}\int_0^\tau \sin\omega t+\frac{|p_1|}{p_0}\sin\omega t\cos(\omega t+\phi)\,dt \\
&= -\frac{\omega V_1 p_0}{\tau}\frac{|p_1|}{p_0}\int_0^\tau -\sin\phi\sin^2\omega t+\cos\phi\sin\omega t\cos\omega t\,dt \\
&= \sin\phi\frac{\omega V_1 p_0}{\tau}\frac{|p_1|}{p_0}\frac{\tau}{2} \\
&= \pi f V_1|p_1|\sin\phi \\
&= \frac{1}{\sqrt{1+(\omega R_0 V_0)^2}}\frac{\omega V_1 p_0}{2}\frac{V_1/V_0}{\sqrt{1+(1/\omega R_0 V_0)^2}}
\end{aligned}$$

$$= \frac{(V_1/V_0)^2}{1+(1/\omega R_o V_0)^2}\frac{p_0}{2R} \tag{I.8}$$

where τ is the refrigerator's period.

The phase between p_1 and V_1 was calculated from the data using the Fourier transform. We first calculated ϕ_p, the pressure's phase, as follows:

$$p_1(t) \propto \cos(\omega t+\phi_p) = (-\sin\phi_p)\sin\omega t + (\cos\phi_p)\cos\omega t \equiv A\sin\omega t + B\cos\omega t$$

$$A= -\sin\phi_p,\ B= \cos\phi_p$$

$$\frac{A}{B} = -\tan\phi_p$$

$$\phi_p = -\tan^{-1}\left(\frac{A}{B}\right)$$

$$\int_0^\tau p_1(t)\sin\omega t\,dt \propto \int_0^\tau A\sin^2\omega t\,dt + \int_0^\tau B\sin\omega t\cos\omega t\,dt = A\frac{\tau}{2} + 0$$

$$\int_0^\tau p1(t)\cos wt\,dt \propto \int_0^\tau A\sin\omega t\cos\omega t\,dt + \int_0^\tau B\cos^2\omega t\,dt = 0 + B\frac{\tau}{2}$$

$$\phi_p = -\tan^{-1}\left(\frac{A}{B}\right) = -\tan^{-1}\frac{\int_0^\tau p_1(t)\sin\omega t dt}{\int_0^\tau p_1(t)\cos\omega t dt}. \tag{I.9}$$

We calculated ϕ_V, the phase of the piston displacement volume, in a similar fashion and then found

$$\phi = \phi_p - \phi_V. \tag{I.10}$$

Appendix J The Pulse Tubes' Volume

The top and the bottom pulse tubes had the following geometry.

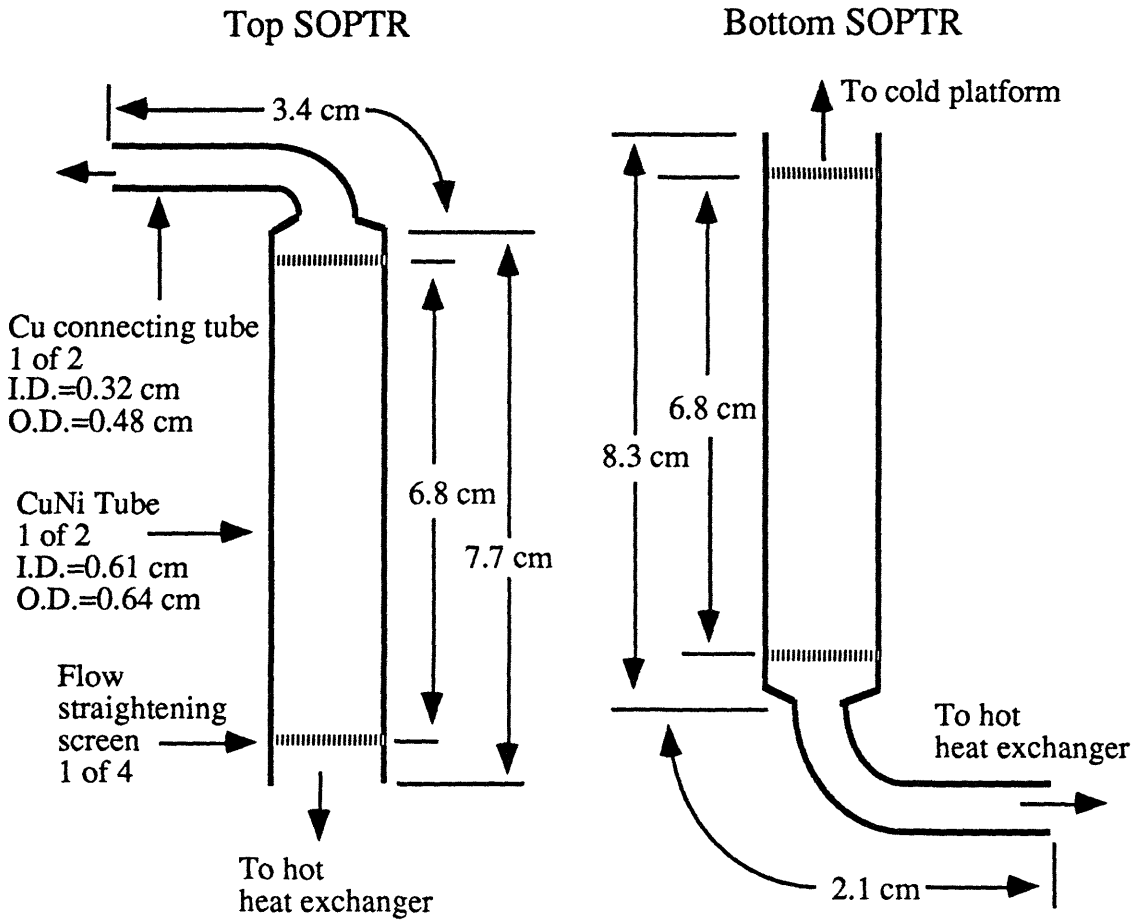

Figure J.1. The pulse tube's geometry

The top pulse tube had a total volume of

$$\pi/4[(0.32\text{ cm})^2(3.4\text{ cm}) + (0.61\text{ cm})^2(7.7\text{ cm})] = 2.5\text{ cm}^3 \qquad \text{(J.1)}$$

and the bottom pulse tube had a total volume of

$$\pi/4[(0.32\text{ cm})^2(2.1\text{ cm}) + (0.61\text{ cm})^2(8.3\text{ cm})] = 2.6\text{ cm}^3 \qquad \text{(J.2)}$$

yielding an average of 2.6 cm^3. In each pulse tube, the volume between the flow straightening screen

$$\pi/4(0.61\ cm)^2(6.8\ cm) = 2.0\ cm^3 \qquad (J.3)$$

will be defined as V_{pt}, the pulse tube volume, and the remaining 0.6 cm^3 will be defined as $V_{connecting\ tube}$, the connecting tube volume.

Appendix K The Pressure Decay Time Constant for the SOPTR's Orifice

R_o, defined as

$$\frac{d(pV)}{dt} = -\frac{p - p_0}{R_o}, \tag{K.1}$$

was found by measuring the pressure relaxation time constant after a sudden change in piston position. Since the piston is stationary after it is stopped,

$$\frac{d(pV)}{dt} = p\frac{dV}{dt} + V\frac{dp}{dt} = V\frac{dp}{dt}. \tag{K.2}$$

We let

$$\begin{aligned} p &= p_1 e^{-t/\tau_o} \\ dp/dt &= -(1/\tau_o)p_1 e^{-t/\tau_o} = -p/\tau_o \end{aligned} \tag{K.3}$$

where τ_o is the pressure decay time constant for the orifice. Combining Eqs. K.1 through K.3,

$$\begin{aligned} -Vp/\tau_o &= V\, dp/dt = d(pV)/dt = -(p-p_0)/R_o = -p/R_o \\ -Vp/\tau_o &= -p/R_o \\ R_o &= \tau_o/V. \end{aligned} \tag{K.4}$$

To find τ_o from the pressure decay curve, we assume it decays exponentially with a time constant of τ_o.

$$\begin{aligned} p &= p_1 e^{-t/\tau_o} \\ \ln(p/p_1) &= -t/\tau_o \\ \tau_o &= -t/\ln(p/p_1). \end{aligned} \tag{K.5}$$

We plot this quantity against the elapsed time, which is shown below. The pressure is labeled as Δp because it is actually the difference between the top and the bottom SOPTR's pressure readings. For a 17% mixture at 1 K, $\tau_o(t)$ decreases from 17 s at t=0 to

9 s at t≈25 s. The flow of superfluid ^{3}He-^{4}He in a capillary is apparently non-linear, as the rate of decay of pressure across a capillary changes with time. We choose τ_0 to be 11 s. For a 6% mixture at T_H=0.374 K and T_C=0.345 K, we choose τ_0 to be 50 s.

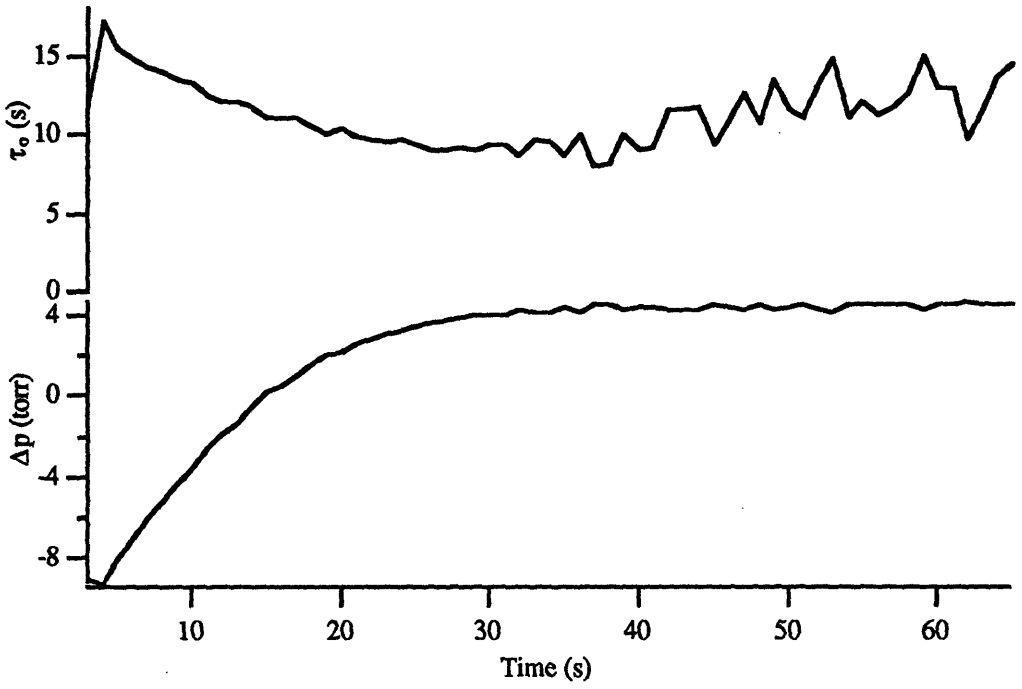

Figure K.1. The SOPTR's pressure reading after a sudden shift in piston position with a 17% mixture at 1 K. Δp does not decay to zero due to a shift in the calibration of pressure gauges. τ_o is the pressure relaxation time constant based on the measured pressure decay.

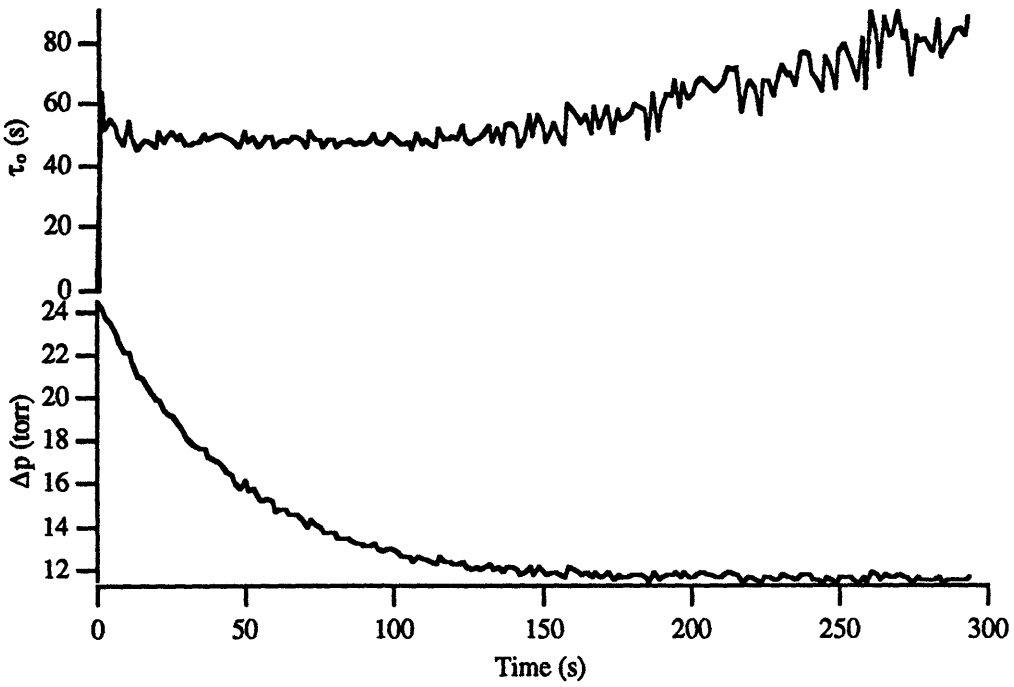

Figure K.2. The pressure reading after a sudden shift in piston position with a 6% mixture at T_H=0.374 K and T_C=0.345 K. Δp does not decay to zero due to a shift in the calibration of pressure gauges. τ_o is the pressure relaxation time constant based on the measured pressure decay.

Appendix L Derivation of the Length of Imaginary Piston in a Pulse Tube

$|V_{31}|$ is evaluated as follows. Eq. 7.1.3 states

$$V_3 = V\text{-}V_2 \tag{L.1}$$

where Eq. 6.1.8 implies

$$V = V_0\text{-}V_1 e^{i\omega t}. \tag{L.2}$$

The number of moles of fluid in V_2 is constant, which means

$$V_2 = \frac{n_2 RT}{p} = \frac{n_2 RT}{P_0\left(1+\frac{p_1}{p_0}e^{i\omega t}\right)} \approx \frac{n_2 RT}{P_0}\left(1-\frac{p_1}{p_0}e^{i\omega t}\right) \equiv V_{20}\left(1-\frac{p_1}{p_0}e^{i\omega t}\right) \tag{L.3}$$

where p is from Eq. 6.1.10 and V_{20} is the time average of V_2. Eqs. L.1 through L.3 then combine to give

$$V_3 = V_0\text{-}V_1 e^{i\omega t}\text{-}V_{20}\left(1-\frac{p_1}{p_0}e^{i\omega t}\right) = (V_0\text{-}V_{20})+\left(\frac{V_1 V_{20}/V_0}{1+1/i\omega R_0 V_0} - V_1\right)e^{i\omega t} \equiv V_{30}+V_{31}e^{i\omega t}$$

$$V_{31} = \frac{V_1 V_{20}/V_0}{1+1/i\omega R_0 V_0}\frac{1-1/i\omega R_0 V_0}{1-1/i\omega R_0 V_0} - V_1$$

$$= \left[\frac{V_1 V_{20}/V_0}{1+1/(\omega R_0 V_0)^2}\right] + i\left[\frac{V_1 V_{20}}{V_0}\frac{1/\omega R_0 V_0}{1+1/(\omega R_0 V_0)^2}\right]$$

$$\equiv [\mathrm{Re}]+i[\mathrm{Im}]$$

$$|V_{31}| = \sqrt{\mathrm{Re}^2+\mathrm{Im}^2}. \tag{L.4}$$

We now show the details of derivation of the viscous boundary layer thickness. Eqs. 7.1.8a through 7.1.8d are

$$\frac{m^*}{m}\rho\left[\frac{\partial u_x}{\partial t}+(\mathbf{u}\cdot\nabla)u_x\right] = \frac{\partial p}{\partial x}+\mu\nabla^2 u_x+\frac{\mu}{3}\frac{\partial}{\partial x}(\nabla\cdot\mathbf{u})+\rho f_x \tag{L.5}$$

$$\mathbf{u} = u_x\hat{x}+u_y\hat{y}+u_z\hat{z} = \mathrm{Re}[u_1(r)e^{i\omega t}]\hat{x}, \qquad u_y = u_z = 0$$

$$p = p_0+\mathrm{Re}[p_1 e^{i\omega t}] \approx p_0$$

$$T = T_0+\mathrm{Re}[T_1 e^{i\omega t}]$$

$$\rho = \rho_0 + \mathrm{Re}[\rho_1 e^{i\omega t}]$$

where r is the radial coordinate. ρ_1 can be approximated by the ideal gas relation:

$$\begin{aligned}
\rho &= M_3 \frac{p}{RT} \\
&= M_3 \frac{p}{RT_0\left(1+\frac{T_1}{T_0}e^{i\omega t}\right)} \\
&\approx M_3 \frac{p}{RT_0}\left(1-\frac{T_1}{T_0}e^{i\omega t}\right) \\
&= \rho_0\left(1-\frac{T_1}{T_0}e^{i\omega t}\right) \\
&= \rho_0 + \rho_1 e^{i\omega t} \\
\rho_1 &= -\rho_0 \frac{T_1}{T_0}.
\end{aligned} \tag{L.7}$$

T_1 is found as follows:

$$\begin{aligned}
\frac{DT}{Dt} &= \frac{\partial T}{\partial t} + u_x \frac{\partial T}{\partial x} + u_y \frac{\partial T}{\partial y} + u_z \frac{\partial T}{\partial z} = \frac{\partial T}{\partial t} + u_x \frac{dT}{dx} = 0 \\
\frac{\partial T}{\partial t} &= -u_x \frac{dT}{dx}.
\end{aligned} \tag{L.8}$$

Eqs. L.6 and L.8 combine to give

$$\begin{aligned}
i\omega T_1 e^{i\omega t} &= -u_1(r) e^{i\omega t} \frac{dT}{dx} \\
T_1 &= -\frac{u_1}{i\omega}\frac{dT}{dx}.
\end{aligned} \tag{L.9}$$

Substituting Eq. L.9 into Eq. L.7,

$$\rho_1 = \frac{\rho_0}{T_0}\frac{u_1}{i\omega}\frac{dT}{dx}. \tag{L.10}$$

Note that

$$(\mathbf{u}\cdot\nabla)u = (u_x\partial/dx)u_x = u_x\partial u_x/dx = 0$$
$$\nabla\cdot\mathbf{u} = \partial u_x/dx = 0. \qquad \text{(L.11)}$$

Substituting the above results into Eq. L.5, we find

$$\frac{m^*}{m}[\rho_0+\rho_1 e^{i\omega t}]i\omega u_1 e^{i\omega t} = \frac{\partial p_0}{\partial x}+\mu\nabla^2 u_1 e^{i\omega t}+\rho_0 g_{eff}-\rho_1 g_{eff}e^{i\omega t}. \qquad \text{(L.12)}$$

Using Eq. L.10 for ρ_1 and expanding to first order,

$$0 = -\frac{\partial p_0}{\partial x}-\rho_0 g_{eff}$$
$$i\omega\frac{m^*}{m}\rho_0 u_1 = \mu\nabla^2 u_1+\frac{\rho}{3T}\frac{dT}{dx}\frac{u_1}{i\omega}g. \qquad \text{(L.13)}$$

We now derive an expression for f_x by finding the thermal expansion coefficient. The effective thermal expansion coefficient of a superfluid ^{3}He-^{4}He liquid mixture is defined as[11]

$$\beta_{eff} = -\frac{1}{\rho_{3,m}}\left(\frac{\partial\rho_{m,m}}{\partial T}\right)_{p,\mu_4} \qquad \text{(L.14)}$$

where the first subscript of 3 and m refer to the ^{3}He component and the total fluid mixture, respectively, and the second subscript m refers to the mass density. The total mass density is given by

$$\rho_{m,m} = \rho_{m,n}M_m = \rho_{m,n}[M_3X+M_4(1-X)] = \rho_{m,n}[M_4+(M_3-M_4)X] \qquad \text{(L.15)}$$

where the second subscript n refers to the number density, M is the molecular mass, X is the mole fraction of ^{3}He, and the subscript 4 refers to the ^{4}He component. We use the ideal gas law to express X in terms of p and T:

$$pV = n_3RT$$
$$\frac{p}{n_m/V} = \frac{n_3}{n_m}RT$$
$$\frac{p}{\rho_{m,n}} = XRT$$

$$X = \frac{p}{\rho_{m,n} RT} \tag{L.16}$$

Substitution into Eq. L.15 yields

$$\rho_{m,m} = \rho_{m,n} M_4 + (M_3 - M_4)\frac{p}{RT}. \tag{L.17}$$

Neglecting the relatively small change in $\rho_{m,n}$ with temperature and concentration,

$$\left(\frac{\partial \rho_{m,m}}{\partial T}\right)_{p,\mu_4} = -(M_3 - M_4)\frac{p}{RT^2}. \tag{L.18}$$

The ^{3}He mass density is approximated by

$$\rho_{3,m} = \rho_{3,n} M_3 = \frac{p}{RT} M_3. \tag{L.19}$$

Combining Eqs. L.14, L.18, and L.19,

$$\beta_{eff} = \frac{(M_3 - M_4)\frac{p}{RT^2}}{\frac{p}{RT} M_3} = \frac{1}{T}\left(1 - \frac{M_4}{M_3}\right) = -1/3T. \tag{L.20}$$

Appendix M Tables of Data

V_1 (volt)	V_2 (volt)	$\dot{Q}=V_1V_2/R_2$ (μW)	T (K)
0.0832	0.964	8.02	0.388
0.1603	1.860	29.8	0.394
0.2369	2.745	65.0	0.403
0.3164	3.660	116	0.415
0.3966	4.592	182	0.429
0.4762	5.514	263	0.441
0.5546	6.420	356	0.453
0.6310	7.304	461	0.464
0.7122	8.243	587	0.474
0.7916	9.161	725	0.484
0.8669	10.03	870	0.493
0.9420	10.90	1030	0.502
1.022	11.83	1210	0.511
1.102	12.75	1410	0.520
1.182	13.67	1620	0.529
1.260	14.58	1840	0.537
1.336	15.46	2070	0.544
1.416	16.39	2320	0.551
1.493	17.27	2580	0.558
1.573	18.20	2860	0.565
1.652	19.12	3160	0.572
1.728	19.99	3450	0.582
1.728	19.99	3450	0.597

Table M.1. The power delivered to the ^{3}He platform versus the temperature. V_1 and V_2 are the voltages across the resistors shown in Fig. 4.1, $\dot{Q}$ is the heat dissipated in the heater mounted on the ^{3}He platform, and T is the temperature of the ^{3}He platform. R_2 was 10,000 Ω.

T (K)	V_{eff} (cm^3)	$\dot{Q}_C$ (μW)	$\dot{W}_H$ (μW)	$\dot{W}_C$ (μW)	$\dot{W}_{tot}$ (μW)
0.36	6.230677	9.6	-11.4	9.7	-3.5
0.42	6.435842	10.7	-12.5	10.6	-3.8
0.5	6.690144	12.1	-13.9	11.7	-3.7
0.55	6.730505	13.1	-14.9	12.8	-4.1
0.6	6.781264	14.1	-15.9	13.8	-3.9
0.7	6.864712	16.4	-18.2	15.9	-4.4
0.8	6.953167	18.7	-20.7	17.9	-4.9
0.9	6.88413	22.1	-23.4	20.6	-4.7
1	6.993842	25.4	-25.7	22.4	-4.7
1.1	6.97206	31.1	-29.1	25	-5.5
1.2	6.889334	40.4	-31.9	27.9	-5
1.3	6.804341	53.5	-35.3	31.2	-5.3
1.4	6.729158	73	-39.3	34.5	-6.3

Table M.2. *5.9%* SSR constant temperature measurements. The hot and the cold piston swept volumes were both 0.78 cm^3, and the refrigerator's period was 100 s. T is the common temperature of the hot and cold platforms, V_{eff} is the effective volume of the refrigerator, $\dot{Q}_C$ is the heat delivered to the heater mounted on the cold platform per unit time, $\dot{W}_H$ is the work done by the fluid on the hot piston per unit time, $\dot{W}_C$ is the work done by the fluid on the cold piston per unit time, and $\dot{W}_{tot}$ is the total work done by the fluid on the pistons per unit time.

T (K)	V_{eff} (cm^3)	$\dot{Q}_C$ (μW)	$\dot{W}_H$ (μW)	$\dot{W}_C$ (μW)	$\dot{W}_{tot}$ (μW)
0.425	5.006367	36.1	-66.6	35.6	-31
0.45	5.333896	47	-65.4	40.5	-25
0.46	5.103482	57.3	-70.2	47.1	-23.1
0.5	5.211548	75.3	-76.7	56.3	-20.4
0.55	5.363014	84.5	-85.3	62.4	-22.9
0.6	5.493057	93.1	-94.1	68.6	-25.5
0.65	5.795029	104.1	-98.7	73.5	-25.2
0.7	5.688197	110	-112.2	81.8	-30.4
0.8	5.824494	130.4	-131.8	97.5	-34.3
0.85	5.953823	136.9	-133.5	101	-32.9
0.9	5.943496	145.7	-143.1	109	-34.4
0.95	6.2301	160.7	-148	116	-32
1	6.054112	167.3	-158.2	124	-34.5
1.05	6.286614	184.7	-164.7	131	-33.6
1.1	6.194459	192	-170.3	139	-31
1.2	6.319887	222.7	-183.1	153	-30
1.25	6.307439	242.3	-191	161	-30
1.3	6.359518	264.8	-198	168	-30
1.35	6.376673	285.2	-204	173	-31
1.4	6.41833	316.2	-213	185	-28

Table M.3. 17% SSR constant temperature measurements. The hot and the cold piston swept volumes were 1.02 cm^3 and 0.98 cm^3, respectively, and the refrigerator's period was 80 s. T is the common temperature of the hot and cold platforms, V_{eff} is the effective volume of the refrigerator, $\dot{Q}_C$ is the heat delivered to the heater mounted on the cold platform per unit time, $\dot{W}_H$ is the work done by the fluid on the hot piston per unit time, $\dot{W}_C$ is the work done by the fluid on the cold piston per unit time, and $\dot{W}_{tot}$ is the total work done by the fluid on the pistons per unit time.

T (K)	V_{eff} (cm^3)	$\dot{Q}_C$ (μW)	$\dot{W}_H$ (μW)	$\dot{W}_C$ (μW)	$\dot{W}_{tot}$ (μW)
0.36	4.988197	6.08	-22.3	13.5	-8.8
0.38	5.175474	11.2	-23.7	14	-9.7
0.4	5.261814	13.9	-25.1	15.1	-9.9
0.425	5.343826	18.09	-26.8	17.1	-9.7
0.46	5.393618	28.2	-29	21.9	-7.1
0.5	5.539035	32.3	-32.2	24.1	-8
0.575	5.800965	38.4	-37.4	27.8	-9.6
0.825	6.200779	58.6	-56.6	42.9	-13.7
1.15	6.497395	92.1	-79.3	64.4	-14.9
1.275	6.532278	114.3	-89.3	74.5	-14.8
1.375	6.594033	138.8	-95.5	81	-14.5

Table M.4. 17% SSR constant temperature measurements. The hot and the cold piston swept volumes were 0.76 cm^3 and 0.82 cm^3, respectively, and the refrigerator's period was 100 s. T is the common temperature of the hot and cold platforms, V_{eff} is the effective volume of the refrigerator, $\dot{Q}_C$ is the heat delivered to the heater mounted on the cold platform per unit time, $\dot{W}_H$ is the work done by the fluid on the hot piston per unit time, $\dot{W}_C$ is the work done by the fluid on the cold piston per unit time, and $\dot{W}_{tot}$ is the total work done by the fluid on the pistons per unit time.

T (K)	$\dot{Q}_C$ (μW)	$\dot{W}_H$ (μW)	$\dot{W}_C$ (μW)	$\dot{W}_{tot}$ (μW)
0.675	10.15	-12	2.40909	-9.4
0.69	12.6	-12.8	3.49091	-8.9
0.7	24.4	-12.6	4.79091	-7.3
0.75	41.5	-17.8	8.72727	-8.2
0.8	41.1	-19.1	10.1364	-8
0.83	40.4	-20.9	11.0818	-8.7
0.87	45.8	-25.4	13.9364	-10
0.9	45.7	-25.2	14.8636	-8.9
0.95	48.1	-29.3	17.7545	-9.8
1	51.5	-31.1	19.7545	-9.4
1.08	55	-36	22.7727	-11
1.15	58.9	-39	26.4455	-9.9
1.2	61.6	-40	27.7545	-9.4
1.225	60.6	-41	28.9455	-9.1

Table M.5. 36% SSR constant temperature measurements. The hot and the cold piston swept volumes were 0.76 cm^3 and 0.80 cm^3, respectively, and the refrigerator's period was 300s. T is the common temperature of the hot and cold platforms, $\dot{Q}_C$ is the heat delivered to the heater mounted on the cold platform per unit time, $\dot{W}_H$ is the work done by the fluid on the hot piston per unit time, $\dot{W}_C$ is the work done by the fluid on the cold piston per unit time, and $\dot{W}_{tot}$ is the total work done by the fluid on the pistons per unit time.

τ (s)	T_H (K)	T_C (K)	$\dot{Q}_C$ (μW)
100	0.168	0.383	0
100	0.190	0.387	2.84
100	0.240	0.390	8.75
100	0.289	0.388	14.7
60	0.180	0.395	0
60	0.205	0.397	6.06
60	0.241	0.398	14.2
60	0.275	0.400	22.4
40	0.188	0.402	0
40	0.210	0.404	7.91
40	0.251	0.407	23.1
40	0.291	0.409	39.2
40	0.300	0.412	43.4
30	0.209	0.416	0
30	0.241	0.415	16.2
30	0.284	0.417	39.6
30	0.302	0.419	47.6
30	0.317	0.419	55
18	0.253	0.445	0
18	0.267	0.447	13.1
18	0.290	0.451	34.8
18	0.305	0.448	50.8
18	0.324	0.451	70.7
18	0.335	0.454	77.7

Table M.6. 4.9% SSR cooling power measurements. The hot and cold piston swept volumes were 1.53 cm^3 and 1.56 cm^3, respectively. τ is the refrigerator's period, T_H and T_C are the hot and the cold platform temperatures, respectively, and $\dot{Q}_C$ is the heat delivered to the heater mounted on the cold platform per unit time.

τ (s)	T_C (K)	$\dot{Q}_C$ (μW)
20	0.466	0
20	0.520	38.4
20	0.600	112.1
20	0.682	179.2
20	0.761	241.2
20	0.840	301.5
20	0.920	356.5
20	1.000	411.1
40	0.455	0
40	0.500	14.2
40	0.581	51.5
40	0.660	86
40	0.743	114.5
40	0.830	144.1
40	0.920	172.5
40	1.000	189.6
80	0.535	0
80	0.571	12
80	0.600	24.5
80	0.640	32.9
80	0.680	40.9
80	0.761	55.7
80	0.840	68.2
80	0.920	81.2
80	1.000	92.9

Table M.7. 17% SSR's cooling power measurements with the hot platform temperature held at 1 K. The hot and cold piston swept volumes were 0.763 cm^3 and 0.811 cm^3, respectively. τ is the refrigerator's period, T_C is the cold platform temperature, and $\dot{Q}_C$ is the heat delivered to the heater mounted on the cold platform per unit time.

τ (s)	T_C (K)	$\dot{Q}_C$ (μW)
22	0.865	0
22	0.880	273.6
22	0.900	512.5
22	1.000	747
40	0.871	0
40	0.880	115.3
40	0.890	208.1
40	0.900	309.7
40	0.910	392.6
40	0.920	409
40	0.940	434.8
40	0.960	453.8
40	1.000	495.8
75	0.883	0
75	0.890	50.9
75	0.900	113.9
75	0.910	170
75	0.917	203.3
75	0.920	208.7
75	0.930	217.7
75	0.950	231.8
75	0.970	243
75	1.000	254.6
150	0.895	0
150	0.900	22.9
150	0.910	57.8
150	0.917	77.7
150	0.920	82.3
150	0.930	95
150	0.940	95.5
150	0.960	103.8
150	0.980	109.9
150	1.000	111.5

Table M.8. 36% SSR cooling power measurements with the hot platform temperature held at 1 K. The hot and cold piston swept volumes were 0.767 cm^3 and 0.811 cm^3, respectively. τ is the refrigerator's period, T_C is the cold platform temperature, and $\dot{Q}_C$ is the heat delivered to the heater mounted on the cold platform per unit time.

τ (s)	T_C (K)	$\dot{Q}_C$ (μW)
30	0.782	0
30	0.792	165.2
30	0.800	222.4
30	0.820	339.2
30	0.900	585.7
40	0.793	0
40	0.798	71.6
40	0.800	108.3
40	0.805	134.9
40	0.810	162
40	0.820	257.2
40	0.830	351
40	0.840	377.4
40	0.860	408.7
40	0.880	430.1
40	0.900	453.3
75	0.808	0
75	0.815	51.6
75	0.822	110.4
75	0.830	153.3
75	0.835	183.5
75	0.840	189.9
75	0.851	201.4
75	0.866	211.5
75	0.885	222.3
75	0.900	225.8
150	0.822	0
150	0.828	38.9
150	0.835	64.9
150	0.840	76.4
150	0.855	87.8
150	0.870	93.2
150	0.885	98.1
150	0.900	99.9

Table M.9. 36% SSR cooling power measurements with a hot platform temperature held at 0.9 K. The hot and cold piston swept volumes were 0.767 cm^3 and 0.811 cm^3, respectively. τ is the refrigerator's period, T_C is the cold platform temperature, and $\dot{Q}_C$ is the heat delivered to the heater mounted on the cold platform per unit time.

τ (s)	f (mHz)	$\|p_1\|$ (torr)	ϕ (deg.)	$\dot{Q}_C$ (μW)	$\dot{W}_P$ (μW)
268	3.73	11.5	80.4	10.5	9.16
196	5.1	17.5	71.6	23.5	18.9
139	7.2	26.1	61.2	45.9	36.9
108	9.3	32.9	52.3	67.2	55.9
80	12.5	40	43.1	91.7	78.6
59	16.9	45.7	34.6	111	101.3
44	22.6	49.4	28.1	124	121.4
29.9	33.4	52.4	21	129	149.4
21.4	46.7	54.4	19	122	187.1
17.2	58.1	55.4	17.8	102.6	232.7

Table M.10. 17% SOPTR frequency response with both the hot and the cold platform temperatures held at 1 K. V_1, half of the piston swept volume, was 0.56 cm^3. τ and f are the refrigerator's period and frequency, respectively, $|p_1|$ is half of the observed peak to peak pressure amplitude, ϕ is the phase between the piston motion and the pressure, $\dot{Q}_C$ is the heat delivered to the heater mounted on the cold platform per unit time, and $\dot{W}_P$ is the work done by the piston on the fluid per unit time.

$\dot{Q}_C$ (μW)	$\dot{W}_P$ (μW)	ϕ (deg.)	$\|p_1\|$ (torr)	V_1 (cm^3)
10.3	16.5	56.5	13.9	0.279
19.8	25.7	53	18.5	0.343
40.9	47.3	48.2	26.5	0.458
57.9	65.5	46	32.7	0.54
97.5	108.2	42.4	44.4	0.63
80.3	89	43.8	39.4	0.70
114.1	125.8	41.7	48.8	0.76
145.4	160	39.6	56.7	0.85
181.6	201.1	38.6	65.3	0.96
209.5	231.6	38.1	71.6	1.03

Table M.11. 17% SOPTR cooling power as a function of piston displacement with the hot platform and the cold platform temperatures held at 1 K and 0.9 K, respectively, and a period of 80 s. $\dot{Q}_C$ is the heat delivered to the heater mounted on the cold platform per unit time, $\dot{W}_P$ is the work done by the piston on the fluid per unit time, ϕ is the phase between the piston motion and the pressure, $|p_1|$ is half of the observed peak to peak pressure amplitude, and V_1 is half of the piston swept volume.

$\dot{Q}_C$ (μW)	$\dot{W}_P$ (μW)	ϕ (deg.)	$\|p_1\|$ (torr)	V_1 (cm^3)
3.0	9.76	81.7	10.8	0.70
5.5	12.7	80.7	12.9	0.76
5.8	13	80.3	12.9	0.77
9.0	17	79.0	15.3	0.86
12.0	21	78.7	18.0	0.95
13.9	23	77.9	18.9	0.96

Table M.12. 17% SOPTR cooling power as a function of piston displacement volume with the hot and the cold platform temperatures held at 1 K and 0.9 K, respectively, and a period of 300 s. $\dot{Q}_C$ is the heat delivered to the heater mounted on the cold platform per unit time, $\dot{W}_P$ is the work done by the piston on the fluid per unit time, ϕ is the phase between the piston motion and the pressure, $|p_1|$ is half of the observed peak to peak pressure amplitude, and V_1 is half of the piston swept volume.

T_C (K)	$\dot{Q}_C$ (μW)	$\dot{W}_P$ (μW)
0.949	0	110.6
0.961	16.2	109.4
0.969	28.0	107.5
0.979	40.0	110.9
0.989	52.9	115.0
1.000	64.6	109.9

Table M.13. 17% SOPTR cooling power with the hot platform temperature held at 1 K. The refrigerator's period was 84 s, and V_1, half of the piston swept volume, was 0.99 cm^3. T_C is the cold platform temperature, $\dot{Q}_C$ is the heat delivered to the heater mounted on the cold platform per unit time, and $\dot{W}_P$ is the work done by the piston on the fluid per unit time. This set of data was measured with the pulse tube being cold side down.

T_C (K)	$\dot{Q}_C$ (μW)	$\dot{W}_P$ (μW)	ϕ (deg.)	$\lvert p_1 \rvert$ (torr)
0.642	0	44.2	54.3	19.2
0.681	12.2	49.1	52.3	21.5
0.730	23.1	54.4	50.9	24.9
0.780	35.1	60.2	48.9	27.6
0.841	49.1	65.2	47.5	30.8
0.920	69.3	72.8	44.9	35.6
0.975	80.2	74.4	44.0	37.7
0.990	85.5	76.4	43.4	39
1.000	91.7	78.6	43.1	40
1.010	97.5	77.0	43.4	39.6
1.019	107.5	78.7	42.9	40.2
1.030	120.4	80.9	42.3	41.3
1.050	147.1	80.5	42.4	41.7
1.070	185	84.3	42.1	43.3
1.099	243.5			
1.130	307.3	86.9	41.6	45.9

Table M.14. 17% SOPTR cooling power with the hot platform temperature held at 1 K. The refrigerator's period was 80 s, and V_1, half of the piston swept volume, was 0.56 cm^3. T_C is the cold platform temperature, $\dot{Q}_C$ is the heat delivered to the heater mounted on the cold platform per unit time, and $\dot{W}_P$ is the work done by the piston on the fluid per unit time, ϕ is the phase between the piston motion and the pressure, and $|p_1|$ is half of the observed peak to peak pressure amplitude.

T_C (K)	$\dot{Q}_C$ (μW)	$\dot{W}_P$ (μW)	φ (deg.)	$\|p_1\|$ (torr)
0.636	0	216.6	32.5	43.9
0.681	41.3	233.5	29.9	50
0.731	83.7	247	28.1	56.2
0.78	122.8	259.2	26.8	61.4
0.84	166.7	272.7	25.4	68.2
0.92	223	291.7	23.9	76.2
0.989	270	302.1	23.3	82.4
1.000	278	301.6	23.1	83.5
1.011	291	304.5	22.9	84.5

Table M.15. 17% SOPTR cooling power with the hot platform temperature held at 1 K. The refrigerator's period was 40 s, and V_1, half of the piston swept volume, was 0.90 cm^3. T_C is the cold platform temperature, $\dot{Q}_C$ is the heat delivered to the heater mounted on the cold platform per unit time, and $\dot{W}_P$ is the work done by the piston on the fluid per unit time, φ is the phase between the piston motion and the pressure, and $|p_1|$ is half of the observed peak to peak pressure amplitude.

T_C (K)	$\dot{Q}_C$ (μW)	$\dot{W}_P$ (μW)	φ (deg.)	$\|p_1\|$ (torr)
0.281	0	14.1	28.4	11.2
0.290	0.83	14.5	27.2	11.5
0.300	1.84	14.7	27.2	11.9
0.315	3.30	15.1	27.1	12.2
0.330	4.54	15.5	26.3	12.8
0.345	6.22	15.9	26.3	13.2
0.365	8.0	16.3	25.7	13.8

Table M.16. 6% SOPTR cooling power with the hot platform temperature held at 0.374 K. The refrigerator's period was 120 s, and V_1, half of the piston swept volume, was 0.80 cm^3. T_C is the cold platform temperature, $\dot{Q}_C$ is the heat delivered to the heater mounted on the cold platform per unit time, and $\dot{W}_P$ is the work done by the piston on the fluid per unit time, φ is the phase between the piston motion and the pressure, and $|p_1|$ is half of the observed peak to peak pressure amplitude.

References

1. J. G. Brisson and G. W. Swift, in Proceedings of the Seventh International Cryocoolers Conference, (Phillips Laboratory, Kirtland AFB, Albuquerque, NM 1992) p. 460.
2. J. G. Brisson and G. W. Swift, "A recuperative superfluid Stirling refrigerator", Adv. Cryogenic Eng. 39B, 1393 (1994).
3. J. G. Brisson and G. W. Swift, "High-temperature cooling power of the superfluid Stirling refrigerator", J. Low Temp. Phys. 93, 141 (1995).
4. J. G. Brisson and G. W. Swift, "Measurements and modeling of a recuperator for a superfluid Stirling refrigerator", Cryogenics 34, 971 (1994).
5. J. C. Fraser, Rev. Sci. Inst. 43, 1692 (1972).
6. E. P. Gyftopoulos, G. P. Beretta, Thermodynamics: Foundations and Applications, (Macmillan, New York), pp. 248, 305.
7. Huang, Statistical Mechanics, (Wiley, New York 1963), pp. 200, 228.
8. R. S. Kagiwada and I. Rudnick, J. Low Temp. Phys. 3, 113 (1970).
9. V. Kotsubo and G. W. Swift, in Proceedings of the Sixth International Cryocoolers Conference, edited by Geoffrey Green and Margaret Knox (David Taylor Research Center, Bethesda, MD 1991), V.2, p. 59.
10. V. Kotsubo and G. W. Swift, "Superfluid Stirling-cycle refrigeration below 1 Kelvin", J. Low Temp. Phys. 83, 217 (1991).
11. L. D. Landau and E. M. Lifshitz, Fluid Mechanics, (Pergamon Press, London), p. 45.
12. O. V. Lounasmaa, Experimental Principles and Methods Below 1 K, (Academic Press, New York 1974), pp. 31, 246, 253, 280
13. Y. Maeno, H. Haucke, R. E. Ecke, and J. C. Wheatley, "Oscillatory convection in a dilute ^{3}He-superfluid ^{4}He solution", J. Low Temp. Phys., 59:305 (1985).
14. R. Radebaugh, "Thermodynamic properties of ^{3}He-^{4}He solutions with applications to the ^{3}He-^{4}He dilution refrigerator", NBS Tech Note 362 (1967).
15. R. Radebaugh, "A review of pulse tube refrigeration", Adv. Cryogenic Eng., 35, 1191 (1990).
16. Senior Flexonics Inc. Metal Bellows Division catalog p. 6.
17. F. A. Staas, K. W. Taconis, and K. Fokkens, "Viscosity of liquid ^{3}He-^{4}He mixtures

in the Helium II region above 1 K", Physica 26, 669 (1960).
18. I. Urieli and D. M. Berchowitz, Stirling Cycle Engine Analysis, (Bristol 1984), p. 46.
19. J. Wilks, The Properties of Liquid and Solid Helium, (Clarendon, Oxford 1967), pp. 19, 27, 232, 476, 666.
20. J. C. H. Zeegers, R. G. K. M. Aarts, A. T. A. M. de Waele, and H. M. Gijsman, "Critical velocities in ^{3}He-^{4}He mixtures below 100 mK", Phys. Rev. B 45, 12442 (1992).